Vol. 294, No. 1, August 10, 1994

ISSN 0003-2670

ANALYTICA CHIMICA ACTA

An international journal devoted to all branches of analytical chemistry

ELSEVIER

ANALYTICA CHIMICA ACTA

Scope. *Analytica Chimica Acta* publishes original papers, rapid publication letters and reviews dealing with every aspect of modern analytical chemistry. Reviews are normally written by invitation of the editors, who welcome suggestions for subjects. Letters can be published within **four months** of submission. For information on the Letters section, see inside back cover.

Submission of Papers

Americas

Prof. Harry L. Pardue
Department of Chemistry
1393 BRWN Bldg, Purdue University
West Lafayette, IN 47907–1393
USA

Tel:(+1-317) 494 5320
Fax:(+1-317) 496 1200

Computer Techniques

Prof. J.T. Clerc
Universität Bern
Pharmazeutisches Institut
Baltzerstrasse 5, CH-3012 Bern
Switzerland

Tel:(+41-31) 6314191
Fax:(+41-31) 6314198

Prof. Sarah C. Rutan
Department of Chemistry
Virginia Commonwealth University
P.O. Box 2006
Richmond, VA 23284-2006
USA
Tel:(+1-804) 367 7517
Fax:(+1-804) 367 8599

Other Papers

Prof. Alan Townshend
Department of Chemistry
The University
Hull HU6 7RX
Great Britain

Tel:(+44-482) 465027
Fax:(+44-482) 466410

Prof. Willem E. van der Linden
Laboratory for Chemical Analysis
Department of Chemical Technology
Twente University of Technology
P.O. Box 217, 7500 AE Enschede
The Netherlands
Tel:(+31-53) 892629
Fax:(+31-53) 356024

Prof. Paul Worsfold
Dept. of Environmental Sciences
University of Plymouth
Plymouth PL4 8AA
Great Britain

Tel:(+44-752) 233006
Fax:(+44-752) 233009

Submission of an article is understood to imply that the article is original and unpublished and is not being considered for publication elsewhere. *Anal. Chim. Acta* accepts papers in English only. There are no page charges. Manuscripts should conform in layout and style to the papers published in this issue. See inside back cover for "Information for Authors".

Publication. *Analytica Chimica Acta* appears in 16 volumes in 1994 (Vols. 281–296). *Vibrational Spectroscopy* appears in 2 volumes in 1994 (Vols. 6 and 7). Subscriptions are accepted on a prepaid basis only, unless different terms have been previously agreed upon. It is possible to order a combined subscription (*Anal. Chim. Acta* **and** *Vib. Spectrosc.*).
Our p.p.h. (postage, packing and handling) charge includes surface delivery of all issues, except to subscribers in the U.S.A., Canada, Australia, New Zealand, China, India, Israel, South Africa, Malaysia, Thailand, Singapore, South Korea, Taiwan, Pakistan, Hong Kong, Brazil, Argentina and Mexico, who receive all issues by air delivery (S.A.L.–Surface Air Lifted) at no extra cost. For Japan, air delivery requires 25% additional charge of the normal postage and handling charge; for all other countries airmail and S.A.L. charges are available upon request.

Subscription orders. Subscription prices are available upon request from the publisher. Subscription orders can be entered only by calendar year and should be sent to: Elsevier Science B.V., Journals Department, P.O. Box 211, 1000 AE Amsterdam, The Netherlands. Tel: (+31-20) 5803 642, Telex: 18582, Telefax: (+31-20) 5803598, to which requests for sample copies can also be sent. Claims for issues not received should be made within six months of publication of the issues. If not they cannot be honoured free of charge. Readers in the U.S.A. and Canada can contact the following address: Elsevier Science Inc., Journal Information Center, 655 Avenue of the Americas, New York, NY 10010, U.S.A. Tel: (+1-212) 6333750, Telefax: (+1-212) 6333990, for further information, or a free sample copy of this or any other Elsevier Science journal.
Advertisements. Advertisement rates are available from the publisher on request.

US mailing notice – Analytica Chimica Acta (ISSN 0003-2670) is published 3 times a month (total 48 issues) by Elsevier Science B.V. (Molenwerf 1, Postbus 211, 1000 AE Amsterdam). Annual subscription price in the USA US$ 3035.75 (valid in North, Central and South America), including air speed delivery. Second class postage paid at Jamaica, NY 11431. *USA Postmasters*: Send address changes to Anal. Chim. Acta, Publications Expediting, Inc., 200 Meacham Av., Elmont, NY 11003. Airfreight and mailing in the USA by Publication Expediting.

ANALYTICA CHIMICA ACTA

An international journal devoted to all branches of analytical chemistry

(Full texts are incorporated in CJELSEVIER, a file in the Chemical Journals Online database available on STN International; Abstracted, indexed in: Aluminum Abstracts; Anal. Abstr.; Biol. Abstr.; BIOSIS; Chem. Abstr.; Curr. Contents Phys. Chem. Earth Sci.; Engineered Materials Abstracts; Excerpta Medica; Index Med.; Life Sci.; Mass Spectrom. Bull.; Material Business Alerts; Metals Abstracts; Sci. Citation Index)

VOL. 294 NO. 1 CONTENTS AUGUST 10, 1994

Chemiluminescence

Mechanism of terbium(III)-enhanced lyoluminescence of x-ray irradiated sodium chloride
S. Kulmala, E. Laine, A. Hakanen (Turku, Finland), P. Raerinne (Joensuu, Finland) and K. Haapakka (Turku, Finland) . 1

Terbium(III) lyoluminescence induced by the dissolution of UV-irradiated potassium peroxodisulfate in aqueous solutions
S. Kulmala and K. Haapakka (Turku, Finland) 13

Flow Analysis

Flow-injection chemiluminometric determination of some bile acids
I.M. Psarellis, N.T. Deftereos, E.G. Sarantonis and A.C. Calokerinos (Athens, Greece) 27

Chemiluminescent flow sensor for the determination of Paraoxon and Aldicarb pesticides
A. Roda (Bologna, Italy), P. Rauch (Prague, Czech Republic), E. Ferri, S. Girotti, S. Ghini (Bologna, Italy), G. Carrea and R. Bovara (Milan, Italy) 35

Continuous flow assay of ammonia in plasma using immobilized enzymes
R. Quiles (Toledo, Spain), J.M. Fernández-Romero (Córdoba, Spain), E. Fernández (Toledo, Spain) and M.D. Luque de Castro (Córdoba, Spain) 43

Flow-injection analysis with bulk extraction based optical sensor membranes
P.C. Hauser and J.C. Litten (Auckland, New Zealand) 49

Electrolysis

Purification of analytical reagents by constant-current electrodeposition of heavy metals at ultra-trace levels from highly concentrated salt solutions
K. Hoppstock, R.P.H. Garten, P. Tschöpel and G. Tölg (Dortmund, Germany) 57

Chromatography

Retention behaviour of metal chelates in ion-pair reversed-phase liquid chromatography as a function of mobile phase composition with methanol–water and acetonitrile–water mobile phases
C. Ohtsuka, K. Matsuzawa, H. Wada and G. Nakagawa (Nagoya, Japan) 69

Solvent study on the 9-substituted quinolizinocoumarins used as precolumn fluorescent and chemiluminescent reagents in liquid chromatography
F. Traoré, P. Prognon and G. Mahuzier (Châtenay-Malabry, France) 75

Chemometrics

Infrared sample preparation and interpretation using a knowledge based system
D.S. Moore, J.S. White and B.A. Harbin (Winston-Salem, NC, USA) 85

Atomic Absorption Spectrometry

Experimental design approach to the optimisation of the analysis of non-conducting materials using a glow discharge source
S.J. O'Gram, J.R. Dean, W.R. Tomlinson (Newcastle Upon Tyne, UK) and J. Marshall (Middlesbrough, UK) 95

Electroanalytical Chemistry

Copper–amine speciation: an electrochemical investigation of the selection of volatile amines for steam generator water
A.G. Kumbhar, S.V. Narasimhan and P.K. Mathur (Kalpakkam, India) 103

ANALYTICA CHIMICA ACTA
VOL. 294 (1994)

ANALYTICA CHIMICA ACTA

An international journal devoted to all branches of analytical chemistry
Revue internationale consacrée à tous les domaines de la chimie analytique
Internationale Zeitschrift für alle Gebiete der analytischen Chemie

Anal. Chim. Acta, Vol. 294 (1994)

ELSEVIER, Amsterdam–Lausanne–New York–Oxford–Shannon–Tokyo

0003-2670/94/$07.00

ELSEVIER

Analytica Chimica Acta 294 (1994) 1–11

ANALYTICA CHIMICA ACTA

Mechanism of terbium(III)-enhanced lyoluminescence of x-ray irradiated sodium chloride

S. Kulmala [a,*], E. Laine [b], A. Hakanen [b], P. Raerinne [c], K. Haapakka [a]

[a] *Department of Chemistry, University of Turku, FIN-20500 Turku, Finland*
[b] *Department of Physics, University of Turku, FIN-20500 Turku, Finland*
[c] *Department of Physics, University of Joensuu, FIN-80101 Joensuu, Finland*

(Received 9th November 1993)

Abstract

Dissolution of x-ray irradiated sodium chloride in aqueous solution produces a short-lived dynamic solid/solution interface which is able to raise the hydrated terbium(III) cation to its lowest excited state ($^5D_4$) and thus to induce the well-known $^5D_4 \rightarrow {}^7F$-multiplet peak emissions of terbium(III). This contribution points out that the lowest excited state $^5D_4$ of terbium(III) is attained by an intermolecular energy transfer from a lowest excited singlet state of a solid/solution interface-bound chloride anion which is generated by the recombination of a hydrated electron with the solid/solution interface-bound chlorine atom.

Key words: Chemiluminescence; Lyoluminescence; Sodium chloride; Terbium

1. Introduction

In our previous papers, we have demonstrated the versatility of an oxide-covered aluminium cathode as an electroluminescent probe for a variety of inorganic and organic trace analytes in aqueous solution [1–6]. The time-resolved electrogenerated terbium(III) luminescence with disposable luminescence generation cells especially seems to be of great practical value because of its feasibility for heterogeneous and homogeneous immunoassays [7,8]. To raise an electroluminophore to its excited singlet state at the oxide-covered aluminium cathode and to have a sufficiently intense electrogenerated luminescence response requires, however, the usage of a high cathodic potential and current density which results in a complex light-emitting oxide-covered electrode surface/electrolyte interface. So far, this complexity has prevented us to treat in detail the mechanisms of this cathodically induced electrogenerated luminescence processes.

The cathodic polarization of the oxide-covered aluminium electrode in an aqueous solution produces an energetic intermediate which may well be common to electrogenerated luminescence processes. It is tempting to propose that, depending on the solution pH, this intermediate is either a hydrogen atom or a hydrated electron or both. Different electrochemical pathways to generate these intermediates can be proposed: (i) the un-

* Corresponding author.

SSDI 0003-2670(94)00105-U

charged surface hydroxyl group of the oxide-covered electrode surface is reduced resulting in a hydrogen atom which is dissociated to give a hydrated electron, providing that the electrode surface is sufficiently alkaline [6], (ii) supposing that the applied voltage across the oxide layer is sufficiently high to fill the electron traps but too low to cause any electrical breakdown, the cathodically induced alkalization of the electrode surface dissolves the oxide layer and the hydration of the occupied electron trap produces a hydrated electron and/or a hydrogen atom [9], (iii) supposing that the applied voltage across the oxide layer is sufficiently high to cause local electrical breakdown, the hydration of the avalanching hot electron produces a hydrated electron and/or hydrogen atom [9].

It is well-known that x-ray irradiation generates trapped electrons and holes in solid sodium chloride [10]. The dissolution of x-ray irradiated sodium chloride in an aqueous solution produces a dynamic solid/solution interface where the occupied electron trap is hydrated to result in a hydrated electron and/or hydrogen atom which recombines immediately with a surface-bound chlorine atom initiating a chloride-specific emission, i.e., lyoluminescence of x-ray irradiated sodium chloride [11–13]. Providing that the aqueous sample solution contains additionally a luminophore, the dissolution of x-ray irradiated sodium chloride may initiate the luminophore-specific emission where the energetic hydrated electron and/or hydrogen atom participates in the light-emitting pathway on the following alternative bases [14–17]: first, it interacts directly with the luminophore producing the reduced luminophore in its excited state or secondly, its interaction with the surface-bound chlorine atom produces the excited surface-bound chloride anion which is followed by immediate intermolecular energy transfer to the excited singlet state of the luminophore.

As a final goal to solve whether the hydrogen atom and/or the hydrated electron has a universal role in cathodic electrogenerated luminescence processes at oxide-covered aluminium electrodes in aqueous solutions, studies on the mechanisms and analytical applicability of x-ray irradiated sodium chloride-induced lyoluminescence have been conducted. In this first alkali halide lyoluminescence study, the hydrated terbium(III) cation was used as the lyoluminophore, mainly because of its appropriate oxidation and reduction potentials and well-defined excited and ground state energy levels which produce the well-known $^5D_4 \rightarrow {}^7F$-multiplet peak emissions [18]. In the present investigation, a detailed mechanism of this terbium(III) lyoluminescence is presented.

2. Experimental

2.1. Apparatus

A detailed description of our lyoluminometer is presented elsewhere [19]. The lyoluminescence spectra were measured using our photon counter [20].

The absorption spectrum of the x-ray irradiated single crystal of sodium chloride was measured using a UV–visible Lambda 2 spectrometer (Perkin Elmer).

2.2. Reagents

Sodium chloride was a Suprapur product of Merck. Terbium(III) chloride hexahydrate (99.9%) was purchased from Aldrich. Hydrochloric acid, sodium hydroxide, sodium nitrate, potassium peroxodisulfate and hydrogen peroxide were analytical-grade products of Merck. Nitrogen (99.999%) was the purest grade available. All the solutions were made up in quartz-distilled water. All these reagents were used without further purification.

2.3. X-ray irradiation of sodium chloride

The x-ray source was a Siemens x-ray tube with a copper anode (40 kV, 16 mA) and the samples were irradiated in the primary beam 1 cm from the focus of the tube. In general, 500-mg quantities of white crystalline sodium chloride were irradiated with occasional turnover for 30 min at ambient temperature. The irradiated NaCl

was stored in a desiccator in the dark and afterglow was left to fade for one week. Irradiated NaCl was homogenised by vigorous shaking before use.

A 2.1-mm thick single crystal of sodium chloride, used to evaluate the efficiency of x-ray irradiation to produce trapped electrons and holes, was x-ray irradiated in an analogous manner.

2.4. Lyoluminescence procedure

A 15-mg aliquot of x-ray irradiated sodium chloride was weighed into a disposable test tube, which was transferred to the lyoluminescence cell compartment and the compartment was tightly closed. A 1-ml aliquot of terbium(III) sample solution adjusted to a desired pH and deaerated with nitrogen was injected into the test tube. The immediate dissolution of the sodium chloride induced the terbium(III) lyoluminescence which was registered on the photon counter after passing through a bandpass filter having maximum transmittance at 546 nm and bandwidth ca. 10 nm. The lyoluminescence integration time was always 2.0 s from the moment of injection.

3. Results and discussion

3.1. X-ray irradiation of solid sodium chloride

If a sodium chloride crystal is irradiated with high-energy x-rays, electrons escape from their original ions and equal numbers of trapped electrons and holes are formed [10], which are trapped at defects in the crystal lattice. A great multiplicity of absorption bands corresponding to the large number of resulting electron and hole centers can be observed in the absorption spectrum of an x-ray irradiated sodium chloride crystal. Fig. 1 displays the absorption spectra measured from a 0.21-cm thick sodium chloride crystal before and after 30 min of x-ray irradiation; the absorption bands peaking at 223, 458 and 725 nm can be assigned for the well-known hole trap denoted by a V_2-center and electron traps denoted by an F-center and an M-center, respectively [10].

The number of F-centers in 1 cm^3 of x-ray

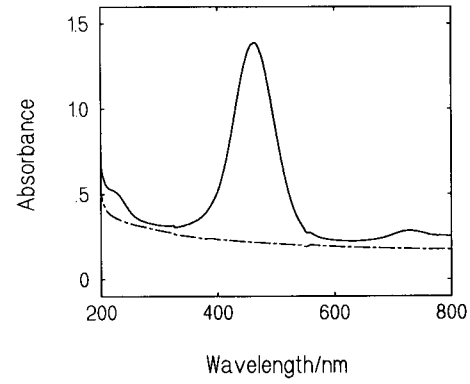

Fig. 1. Absorption spectrum of x-ray irradiated crystal of sodium chloride. (·–·–·) Before and (———) after the x-ray irradiation. Conditions: see text for details.

irradiated sodium chloride crystal (N) can be calculated from the Smakula equation [10]:

$$N = 1/f \times 0.87 \times 10^{17}\left[n/(n^2+2)^2\right]\alpha_{max}W \quad (1)$$

where f is the oscillator strength, i.e., the factor related to the probability of the optical transition producing the absorption, n is the refractive index of the crystal for the wavelength at the peak of the absorption band, α_{max} is the absorption coefficient in cm^{-1} at the peak of the absorption band and W is the half-width of the absorption band in eV. Accepting that f is 0.81 [10], n is 1.54 [21] and α_{max} is 12.5 cm^{-1} (measured from the absorption spectrum of x-ray irradiated sodium chloride shown in Fig. 1), the observed 0.54-eV half-width of the 458-nm absorption band in Fig. 1 points out that the F-center content, and thus also the V_2-center content, of this x-ray irradiated crystal is close to 6×10^{16} cm^{-3}.

The lyoluminescence experiments were, however, conducted using finely divided, analogously x-ray irradiated crystalline sodium chloride to attain a fast dissolution of the solid, which seems to be of utmost importance to initiate reproducible lyoluminescence response. Mainly because of a compression-induced fast recombination of F-centers and V_2-centers, no absorption spectrum could be measured from the tablet made of finely divided x-ray irradiated material. It is, however, assumed that the present x-ray irradiation produces rather similar amounts of F-centers in the

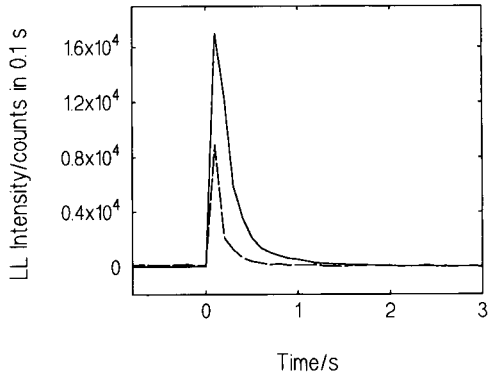

Fig. 2. Lyoluminescence (LL) of x-ray irradiated sodium chloride. (- - - - - -) Blank emission and (———) terbium(III)-enhanced emission. Conditions: 15 mg x-ray irradiated sodium chloride, 5.0×10^{-3} M terbium(III) chloride at pH 5.1, injection volume 1.0 ml, solutions deaerated with nitrogen.

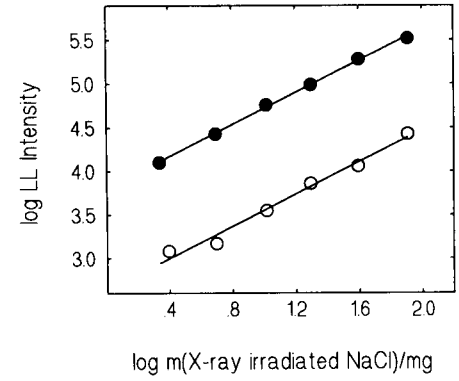

Fig. 3. Effect of amount of x-ray irradiated sodium chloride on the lyoluminescence intensity. (○) Blank emission and (●) terbium(III)-enhanced emission. Conditions: variable amount of x-ray irradiated sodium chloride, 1.0×10^{-2} M terbium(III) chloride, otherwise as in Fig. 2.

target in spite of whether it is a thin single crystal or finely divided crystalline material. On this basis, the 15-mg solid sample of x-ray irradiated sodium chloride used in the present work contained around 7×10^{-10} moles of F-centers and V_2-centers.

3.2. *Lyoluminescence of x-ray irradiated sodium chloride*

The dashed line in Fig. 2 displays lyoluminescence as a function of time after the onset of dissolution of a 15-mg solid sample of x-ray irradiated sodium chloride (i.e., around 7×10^{-10} moles of F-centers and V_2-centers) in an aqueous 1-ml sample solution adjusted to pH 5.2; this lyoluminescence flash reaches its maximum intensity in around 0.1 s, it decays to zero level in around 0.6 s and, as indicated in Fig. 3, its integrated intensity depends linearly on the amount of F-centers and V_2-centers at least up to around 4×10^{-9} moles (i.e., the dissolved sample of x-ray irradiated sodium chloride is 80 mg). Fig. 4 shows the spectrum of this lyoluminescence, which shows two distinct peak emissions at the wavelengths around 470 and 560 nm; this spectrum is in good agreement with those reported in the literature for this lyoluminescence [17].

On dissolution of x-ray irradiated sodium chloride, the V_2-centers (denoted by Cl_s to depict also all other hole centers, i.e., from the chemical point of view, chlorine atoms in different environments in the solid phase) can react either with water to produce a dichlorine radical ion through a hydroxyl adduct or with the dissolved chloride anion to produce the dichlorine radical ion:

$$Cl_s + H_2O \longrightarrow ClOH^- + H^+ \quad (2a)$$

$$ClOH^- + Cl^- \longrightarrow Cl_2^- + OH^- \quad (2b)$$

$$Cl_s + Cl^- \longrightarrow Cl_2^- \quad (3)$$

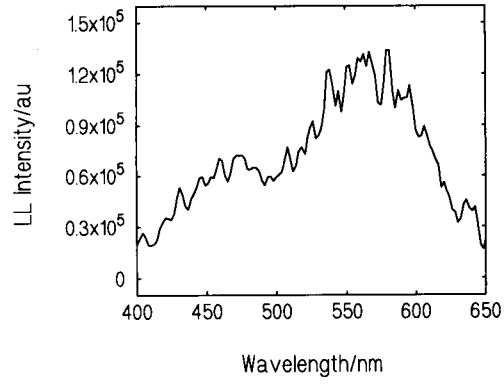

Fig. 4. Lyoluminescence spectrum of x-ray irradiated sodium chloride. Conditions: 500 mg x-ray irradiated sodium chloride, injection volume 10.0 ml, quartz distilled water, deaerated with nitrogen.

with pseudo first order rate constants of $k_{2a} = 2 \times 10^5$ s^{-1} [22], $k_{2b} = 2 \times 10^9$ s^{-1} [22], and taking into consideration that the concentration of the chloride ion in a thin light-emitting zone at the solid/solution interface has to be around 6 M (i.e., this zone is saturated in respect to chloride) with a pseudo first order rate constant of $k_3 = 3 \times 10^{10}$ s^{-1} [22]. The F-center, in turn, produces a hydrated electron:

$$\text{F-center} + H_2O \longrightarrow e^-_{aq} \quad (4)$$

which may react further either with water or with an impurity oxygen molecule. Note that the sample solutions were carefully deaerated with 99.999% nitrogen but their oxygen concentration may still be as high as 10^{-6} M,

$$e^-_{aq} + H_2O \longrightarrow H + OH^- \quad (5)$$

$$e^-_{aq} + O_2 \longrightarrow O_2^- \quad (6)$$

with pseudo first order rate constants of $k_5 = 1 \times 10^3$ s^{-1} [23] and $k_6 \approx 2 \times 10^4$ S^{-1} [23]; this high rate of hydrated electron scavenging by molecular oxygen lowers the intensity from air-equilibrated Tb(III) solutions. That of 0.01 M $TbCl_3$ at pH 5 increases by one order of magnitude after deoxygenation by the procedure used in this work.

It has been pointed out that the spectra of the lyoluminescence and afterglow (i.e., a chloride-specific emission which originates from an electron center/hole center recombination in the crystal) of x-ray irradiated sodium chloride are similar [24], which allows one to conclude that these luminescent processes have the same emitter. This means that the lyoluminescence is not induced in the solution but at the solid/solution interface. Hence, it has been postulated that the mechanism of the lyoluminescence of x-ray irradiated sodium chloride is as follows [24]:

$$Cl_{s,aq} + e^-_{aq} \longrightarrow Cl^{-*}_{s,aq} \quad (7)$$

$$Cl^{-*}_{s,aq} \longrightarrow h\nu + Cl^- \quad (8)$$

where $Cl_{s,aq}$ depicts a chlorine atom at the solid/solution interface. As described above, the hydrated electron is relatively stable and is transferred under these highly convective conditions to recombine with the chlorine atom at the solution/solid interface. On the basis of the equation [25]:

$$-\Delta H^\circ = (E^\circ_{Ox}) - (E^\circ_{Red}) - T\Delta S^\circ \quad (9)$$

where E°_{Ox} and E°_{Red} are the standard electrode potentials of oxidant and reductant, i.e, $Cl_{s,aq}$ and e^-_{aq}, respectively, and the other symbols have their usual meaning, the enthalpy of the recombination reaction (7) is ca. 5.3 eV, providing that E_{Ox} is 2.5 V [26] (all electrode potentials in this contribution are expressed vs. SHE; it is assumed that the standard electrode potentials of Cl/Cl^- and $Cl_{s,aq}/Cl^-$ redox couples are the same), E_{Red} is -2.9 V [23] and the entropy factor is 0.1 eV [25]; finally, this recombination enthalpy is sufficiently high to leave the resulting $Cl^-_{s,aq}$ in the excited state required to generate the emission at the wavelength range from 350 to 700 nm displayed in Fig. 4.

An alternative energy-sufficient recombination reaction for the generation of $Cl^{-*}_{s,aq}$ could be

$$Cl_{s,aq} + H \longrightarrow Cl^{-*}_{s,aq} + H^+ \quad (10)$$

where the hydrogen atom is produced by reaction (5); the electrode potential of the hydrogen atom is -2.3 V [23] and thus, the enthalpy of this recombination reaction is around 4.7 eV which is also sufficiently high to produce the aforementioned excited state. The hydrogen atom producing reaction is, however, relatively slow which makes us propose that the recombination reaction (10) is not of vital importance for the lyoluminescence generation but may occur in parallel with the recombination reaction (7).

All the experiments conducted so far in our laboratory have strongly supported the above mechanism of the lyoluminescence of x-ray irradiated sodium chloride.

3.3. *Terbium(III)-enhanced lyoluminescence of x-ray irradiated sodium chloride*

As the solid line in Fig. 2 points out, the intensity of the lyoluminescence of x-ray irradiated sodium chloride is enhanced if the injected 1.0-ml aqueous solution contains hydrated terbium(III); this enhanced lyoluminescence responds linearly both to the amount of F-centers

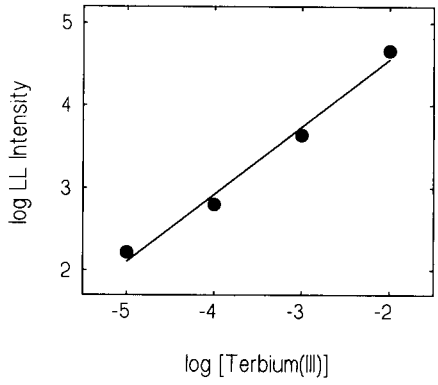

Fig. 5. Effect of terbium(III) on the lyoluminescence intensity of x-ray irradiated sodium chloride. Conditions: as in Fig. 2.

and V_2-centers in the dissolving x-ray irradiated sodium chloride as indicated in Fig. 3 and to the concentration of hydrated terbium(III), as shown in Fig. 5. Fig. 6 displays the spectrum of the lyoluminescence of x-ray irradiated sodium chloride in the presence of hydrated terbium(III) and, for comparison, the corresponding spectrum measured in the absence of terbium; the former lyoluminescence consists of four distinct peak emissions at around 490, 545, 585 and 625 nm and without doubt, originates from the well-known $^5D_4 \rightarrow {}^7F$-multiplet terbium(III) transitions [20].

Using nitrate, peroxodisulfate or hydrogen peroxide as hydrated electron scavenger, experiments were carried out in order to elucidate

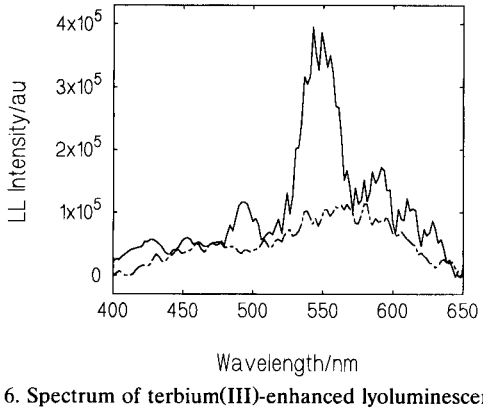

Fig. 6. Spectrum of terbium(III)-enhanced lyoluminescence of x-ray irradiated sodium chloride together with blank spectrum from Fig. 4. Conditions: as in Fig. 4 except 0.1 M terbium(III) chloride.

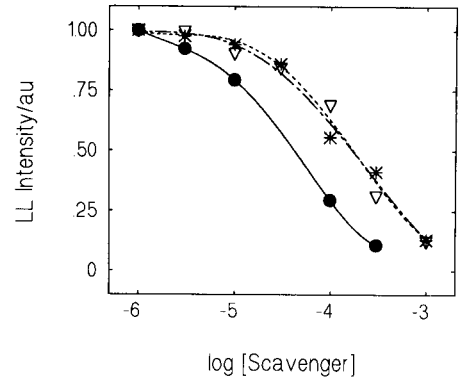

Fig. 7. Effect of hydrated electron scavengers on the terbium(III)-enhanced lyoluminescence of x-ray irradiated sodium chloride. (●) nitrate, (*) peroxodisulfate, (▽) hydrogen peroxide. Conditions: 0.1 M terbium(III) chloride, otherwise as in Fig. 2.

whether the generation of hydrated the electron as presented by the reaction (4) is an essential step in the terbium(III) lyoluminescence. These well-known one-electron scavenger reactions are:

$$e_{aq}^- + NO_3^- \longrightarrow NO_3^{2-} \quad (11)$$

$$e_{aq}^- + S_2O_8^{2-} \longrightarrow SO_4^- + SO_4^{2-} \quad (12)$$

$$e_{aq}^- + H_2O_2 \longrightarrow OH + OH^- \quad (13)$$

and the second order rate constants of these reactions are reported to be $k_{11} = 9.7 \times 10^9$ M^{-1} s^{-1}, $k_{12} = 1.2 \times 10^{10}$ M^{-1} s^{-1} and $k_{13} = 1.1 \times 10^{10}$ M^{-1} s^{-1}, respectively [23]. Fig. 7 displays the scavenger plots obtained, which demonstrate strong scavenger effects in all cases. In spite of the fact that the scavenger effects of peroxodisulfate and hydrogen peroxide are somewhat less than expected from these scavenger rate constants, which can be attributed to the terbium (III)-based luminescent interactions of the resulting energetic sulfate and hydroxyl radicals with the hydrated terbium(III) cation [6,19], these consistent scavenger plots make it possible to draw the conclusion that the hydrated electron plays a vital role in the terbium(III) lyoluminescence pathway. On this basis, the strong quenching of terbium(III) lyoluminescence in acidic solutions (Fig. 8) can be explained by the scavenger effect

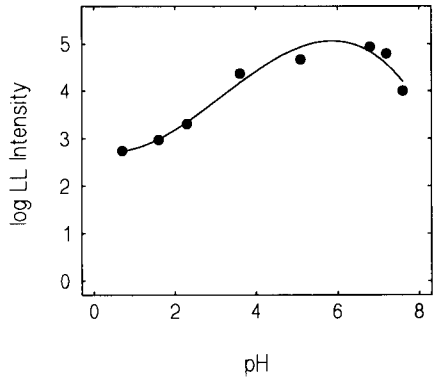

Fig. 8. Effect of pH on the terbium(III)-enhanced lyoluminescence of x-ray irradiated sodium chloride. Conditions: 1.0×10^{-2} M terbium(III) chloride, otherwise as in Fig. 2.

of the proton on the hydrated electron according to the reaction:

$$e_{aq}^- + H_3O^+ \longrightarrow H + H_2O \qquad (14)$$

with the second order rate constant $k_{14} = 2.3 \times 10^{10}$ M^{-1} s^{-1} [23]. Thus, reaction (10) seems to be too slow to occur and rather, the resulting hydrogen atoms recombine to form molecular hydrogen (the second order rate constant of this recombination reaction is reported to be 7.8×10^9 M^{-1} s^{-1} [23]). Quenching in slightly alkaline solutions is due to the precipitation of terbium(III) hydroxide.

Three reaction sequences, which involve the hydrated electron and are supplied with an enthalpy higher than the 2.55 eV required to leave the terbium(III) cation to its lowest excited state $^5D_4$, can be proposed for the generation of terbium(III) lyoluminescence, namely a terbium (IV)-intermediate pathway, a terbium(II)-intermediate pathway and an energy transfer pathway. The subsequent discussion evaluates in detail these terbium(III) lyoluminescence pathways.

3.4. Terbium(IV)-intermediate and terbium(II)-intermediate pathways

We have previously pointed out that the $^5D_4 \rightarrow {}^7F$ – multiplet emissions of terbium(III) can be attained through the reaction sequence which comprises the terbium(IV)-intermediate generated by the oxidation of terbium(III) with the sulfate radical [19]; the standard electrode potential of the SO_4^-/SO_4^{2-} redox couple is approximately 3.4 V [27] and the second order rate constant was determined to be ca. 5×10^6 M^{-1} s^{-1} [19]. In the present lyoluminescence process, the strong oxidizing agents are the surface-bound chlorine atom (the standard electrode potential of the $Cl_{s,aq}/Cl_{s,aq}^-$ couple is estimated to be around 2.5 V which is the same as that reported for the Cl/Cl^- couple [26]) and the dichlorine radical ion produced by reaction (3) (the standard electrode potential of $Cl_2^-/2Cl^-$ is reported to be 2.1 V [22,26]). The electrode potential of the terbium(IV)/terbium(III) couple is generally estimated to be at the range 2.7 – 3.7 V [28] although values down to 1.3 V (in 5.5 M potassium carbonate) have been reported in the same literature source. Assuming that under the present lyoluminescence conditions, the electrode potential of the terbium(IV)/terbium(III) redox couple is lower than that of the surface-bound chlorine atom or dichlorine radical ion, it is possible to propose the following terbium(IV)-intermediate pathway to generate the excited terbium(III) cation:

$$Cl_{s,aq} + Tb^{3+} \longrightarrow Cl_{s,aq}^- + Tb^{4+} \qquad (15a)$$

$$Cl_2^- + Tb^{3+} \longrightarrow 2Cl^- + Tb^{4+} \qquad (15b)$$

$$Tb^{4+} + e_{aq}^- \longrightarrow Tb^{3+*} \qquad (16a)$$

$$Tb^{4+} + H \longrightarrow Tb^{3+*} + H^+ \qquad (16b)$$

$$Tb^{4+} + H_2O \longrightarrow Tb^{3+*} + OH + H^+ \qquad (16c)$$

$$Tb^{3+*} \longrightarrow Tb^{3+} + h\nu \qquad (17)$$

Rapidly, the surface-bound chlorine atom oxidizes terbium(III) to terbium(IV). The oxidation of terbium(III) by the dichlorine radical can be disregarded because of its obvious sluggishness, e.g., it has been reported that the second order rate constant of the analogous cerium(III) oxidation is only approximately 1×10^4 M^{-1} s^{-1} [22]. The hydrated electron (or some other reducing agent present in the sample solution, e.g., a hydrogen atom) reduces the resulting terbium(IV) to terbium(III); assuming that the electrode potential of the terbium(IV)/terbium(III) couple is

ca. 2 V under these conditions, the enthalpy of this one-electron terbium(IV) reduction is as high as 4.9 eV, which indicates that even the upper excited states of terbium(III), e.g., $^5D_1$ which lies around 3.8 eV above the $^7F_6$ ground state [18], could easily be achievable in this terbium(IV) reduction; finally, after a fast radiationless internal conversion the resulting lowest excited state $^5D_4$ is reached which induces the characteristic terbium(III) peak emissions shown in Fig. 6.

It has been calculated that the standard electrode potential of the terbium(III)/terbium(II) couple should be ca. −3.7 V in an aqueous solution [28]. However, this value is only a theoretical estimation and the electrode potential is certainly influenced by changes in experimental conditions. Supposing that under the present experimental conditions the electrode potential of this redox couple is lowered below −2.9 V, the terbium(III) lyoluminescence could occur through a terbium(II)-intermediate as follows:

$$Tb^{3+} + e^-_{aq} \longrightarrow Tb^{2+} \quad (18)$$

$$Tb^{2+} + H_2O \longrightarrow Tb^{3+} + H + OH^- \quad (19a)$$

$$Tb^{2+} + Cl_{s,aq} \longrightarrow Tb^{3+*} + Cl^-_{s,aq} \quad (19b)$$

$$Tb^{2+} + Cl_2^- \longrightarrow Tb^{3+*} + 2Cl^- \quad (19c)$$

$$Tb^{3+*} \longrightarrow Tb^{3+} + h\nu \quad (20)$$

First, the hydrated electron reduces terbium(III) to terbium(II), which is immediately oxidized to terbium(III); possible oxidizing agents are the surface-bound chlorine atom, the dichlorine radical ion generated by reaction (3) and water. Assuming that the electrode potential of the terbium(III)/terbium(II) couple is around −2.6 V, Eq. 9 gives approximate enthalpies of 0.4 eV (the electrode potential of the H_2O/H couple is reported to be −2.3 V [23]), 5.1 eV and 4.9 eV for these terbium(II) oxidation reactions, respectively. On this basis, the oxidation of terbium(II) by water is not energy-sufficient to generate terbium(III) in its lowest excited state ($^5D_4$), while the other terbium(II) oxidation reactions are capable of leaving the resulting terbium(III) in its upper excited states. Even the highest $^5D_0$ excited state, which lies 3.88 eV above the $^7F_6$ ground state (see the energy diagram in Fig. 9) [18], should readily be achievable. Finally, the characteristic $^5D_4 \rightarrow {}^7F$ − multiplet terbium(III) emissions are induced, when the lowest excited state $^5D_4$ produced by the internal conversion of upper excited states is achieved.

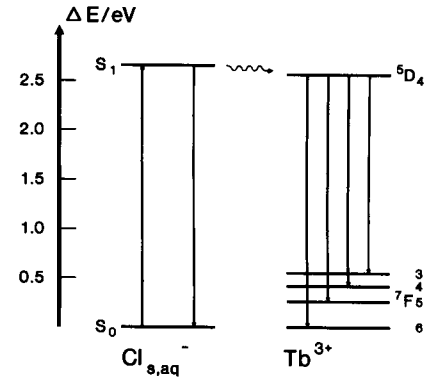

Fig. 9. Energy diagram for the generation of the terbium(III)-enhanced lyoluminescence of x-ray irradiated sodium chloride.

The dissolution of x-ray irradiated sodium chloride is a dynamic and partially convective process, which makes the detailed evaluation of these mechanistic proposals for terbium(III) lyoluminescence difficult. However, it is obvious that the rapid dissolution of a 15-mg sample of x-ray irradiated sodium chloride produces a short-lived light-emitting zone with a total volume of ca. 20 μl (density of sodium chloride is 2.2 g ml^{-1} [21] but it is estimated that the volume of the light-emitting zone has to be somewhat larger than the theoretical 7-μl volume). Taking into account that the 15-mg solid sample contains around 7×10^{-10} mol of F-centers and V_2-centers (see above), it is possible to estimate that the original concentrations of hydrated electron and surface-bound chlorine atoms or dichlorine radical ions in the light-emitting zone are close to 3×10^{-5} M.

In the proposed terbium(IV)-intermediate pathway, the decisive point is whether the surface-bound chlorine atom reacts in the light-emitting 20-μl zone with terbium(III) to generate terbium(IV) (see reaction 15a) or with the hydrated electron in reaction (7). Accepting that the $Cl_{s,aq}$ concentration is close to 3×10^{-5} M in the

reaction zone, the approximate pseudo first order rate constants for these competing reactions are $k_{15a} < 30\ s^{-1}$ (it is assumed that the second order rate constant of this terbium(III) oxidation is not greater than $10^6\ M^{-1}\ s^{-1}$ [22], and $k_7 > 3 \times 10^5\ s^{-1}$ (reduction of a chlorine atom is usually a diffusion controlled reaction, i.e., the second order rate constant of the reduction reaction is greater than $10^{10}\ M^{-1}\ s^{-1}$, e.g., $k(Cl + Fe^{2+}) = 1.3 \times 10^{10}\ M^{-1}\ s^{-1}$ [22]). In spite of its doubtfulness, the at least 10^4-fold difference in these pseudo first order rate constants to the advantage of the reaction (7) allows one to conclude that under these conditions, the aforementioned terbium(IV)-intermediate pathway cannot be the main pathway for the generation of terbium(III) lyoluminescence, even if the potential of the terbium(IV)/terbium(III) couple should be as low as 2.3 V.

In the proposed terbium(II)-intermediate pathway, the decisive point is whether the hydrated electron reacts in the light-emitting 20-μl zone with terbium(III) to generate terbium(II) (see reaction (18)) or with the surface-bound chlorine atom as presented by reaction (7). In addition, the recombination reaction of hydrated electrons occurs:

$$e^-_{aq} + e^-_{aq} \longrightarrow H_2 + 2OH^- \qquad (21)$$

with the second order rate constant of $6 \times 10^9\ M^{-1}\ s^{-1}$ [23]. As in the above discussion, the pseudo first order rate constants of these reactions are $k_{18} < 30\ s^{-1}$ (the second order rate constant of this terbium(III) reduction is less than $10^6\ M^{-1}\ s^{-1}$ [23]), $k_7 > 3 \times 10^5\ s^{-1}$ and $k_{21} = 2 \times 10^5\ s^{-1}$. In our opinion, the rate constants indicate that from these three competing reactions, the one-electron terbium(III) reduction is too slow to occur to any significant extent under these conditions and consequently, the terbium (II)-intermediate pathway has no essential role in the generation of terbium(III) lyoluminescence under these conditions.

3.5. Energy transfer pathway

The above terbium(III)-based charge transfer mechanisms cannot be used to explain the production of terbium(III) lyoluminescence under the present experimental conditions. Hence, it is postulated that intermolecular energy transfer from the excited surface-bound chloride anion (produced by reaction (7)) to the lowest excited level $^5D_4$ of terbium(III):

$$Cl^{-*}_{s,aq} + Tb^{3+} \longrightarrow Cl^-_{s,aq} + Tb^{3+*} \qquad (22)$$

$$Tb^{3+*} \longrightarrow Tb^{3+} + h\nu \qquad (23)$$

is responsible for the formation of the $^5D_4 \rightarrow {}^7F$-multiplet terbium(III) peak emissions, as displayed in the energy diagram in Fig. 9. An overlap integral of the emission spectrum of the energy donor and the absorption spectrum of the energy acceptor is a basic requirement for an intermolecular energy transfer [29]. Fig. 10 shows the absorption spectrum of the $^7F_6 \rightarrow {}^5D_4$ terbium(III) transition and, as concluded from the results in Fig. 4, this spectrum overlaps strongly with the 470-nm emission spectrum of the surface-bound-chloride anion, which gives a theoretical basis of the energy transfer mechanism of the terbium(III) lyoluminescence. In addition, the intermolecular non-radiative energy transfer depends strongly on the donor–acceptor distance; a short-range electron-exchange energy transfer occurs over approximately 2 nm, while a Coulombic energy transfer dominated by long-range dipole–dipole interactions may occur from the distance of ca. 10 nm. The excited surface-bound chloride anion and the hydrated terbium(III) cation must

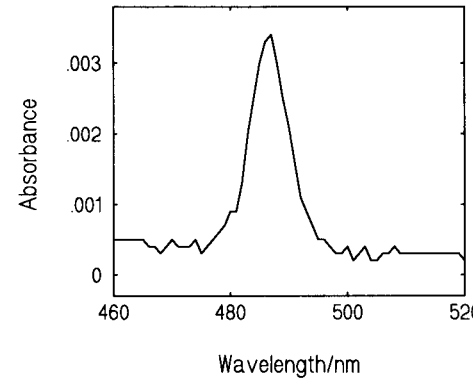

Fig. 10. Absorption spectrum of terbium(III). Conditions: 0.1 M terbium(III) chloride at pH 5.

therefore be sufficiently close to each other at the lyoluminescent solid/solution interface for efficient energy transfer to occur, at least in solutions where the terbium(III) concentration is high.

Especially in dilute terbium(III) solutions where the donor–acceptor distance may be too great to initiate efficient non-radiative energy transfer, radiative energy transfer may be of vital importance. This energy transfer depends also on the spectral overlap integral discussed above and it can be depicted by the following reactions:

$$Cl^{-*}_{s,aq} \longrightarrow Cl^{-}_{s,aq} + h\gamma_{470} \quad (24)$$

$$h\nu_{470} + Tb^{3+} \longrightarrow Tb^{3+*} \quad (25)$$

where the relaxation of an excited surface-bound chloride anion produces an emission at a peak wavelength of ca. 470 nm (see Fig. 4), which is sufficiently energetic to induce the $^7F_6 \rightarrow {}^5D_4$ terbium(III) excitation transitions. However, a detailed evaluation of these proposed energy transfer mechanisms is presently not appropriate.

The generation of terbium(III) lyoluminescence can be depicted using a simplified energy diagram presented in Fig. 9. Assuming that the 470-nm peak emission in Fig. 6 can be assigned to the lowest excited state (S_1)–lowest ground state (S_0) transition of the surface-bound chloride anion, this excited state is located 2.65 eV above the ground state; the diagram neglects (i) upper excited states of the surface-bound chloride anion (see below) and (ii) the 560-nm peak emission (see Fig. 4) which is presently unknown to us (it may be a sign for two independent emissive states of surface-bound chloride anion during the dissolution process or it may also be caused by the presence of impurities either in the x-ray irradiated sodium chloride or in the injected sample solution, e.g., it may arise from the hydrated copper(II) cation which is capable of generating an intense lyoluminescence at this wavelength [17]). The well-defined terbium(III) energy levels can be presented as follows: the $^7F_{5,4,3}$ multiplet ground states and lowest excited singlet state $^5D_4$ are located at 0.26 eV, 0.42 eV and 0.55 eV and 2.54 eV above the $^7F_6$ ground state, respectively [18].

The reaction of a hydrated electron with the surface-bound chlorine atom provides sufficient energy (see above) to raise the resulting surface-bound chloride anion even up to 5-eV excited singlet states. However, it is obvious that the upper excited states do not relax directly to the ground state S_0 but on a picosecond timescale by radiationless internal conversions to the lowest excited singlet state S_1 at 2.65 eV. This excited state of the surface-bound chloride anion is only ca. 0.1 eV above the lowest excited state $^5D_4$ of terbium(III) which makes the excitation energy transfer $S_1 \rightarrow {}^5D_4$ highly probable. In our opinion, the 2.65-eV excited state of the surface-bound chloride anion is relaxed in the present lyoluminescence conditions by two competing light-emitting pathways; firstly, the relaxation transition $S_1 \rightarrow S_0$ induces the chloride-characteristic emission peaking at 470 nm (see Fig. 4) and secondly, the intermolecular energy transfer $S_1 \rightarrow {}^5D_4$ excites the hydrated terbium(III) cation which is immediately deactivated by the radiative $^5D_4 \rightarrow {}^7$F-multiplet transitions, thus inducing the characteristic terbium(III) peak emissions at ca. 490, 545, 585 and 625 nm. A more detailed evaluation of these different relaxation pathways is presently not appropriate.

4. Conclusions

The original aim of the present work was to search for a new terbium(III) lyoluminescence pathway where the lowest excited state $^5D_4$ of terbium(III) is attained by the one-electron oxidation of a hydrated terbium(II) cation and which could shed light on the initial steps in the generation of cathodic electrogenerated luminescence at the oxide-covered aluminium electrode. The highly unstable hydrated terbium(II) intermediate produced by a one-electron reduction of terbium (III) by a hydrated electron was considered. However, the experimental results obtained so far indicate clearly that at least under the present conditions, the observed radiative terbium(III) $^5D_4 \rightarrow {}^7$F-multiplet transitions are not a consequence of a terbium(II)-intermediate in the lyoluminescence pathway but rather that the essential

step preceding these radiative transitions is the intermolecular energy transfer from an excited surface-bound chloride anion to the lowest excited state $^5D_4$ of terbium(III). A study of the terbium(II)-intermediate pathway of terbium(III) lyoluminescence continues in our laboratory and in this respect, some promising results has been obtained from the experiments using additively coloured sodium chloride to initiate the emissive $^5D_4 \rightarrow {}^7F$-multiplet transitions of terbium(III).

From the analytical point of view, the results obtained in this work are interesting; the terbium(III) lyoluminescence responds to terbium (III) down to around 10^{-5} M and, furthermore, preliminary experiments have clearly pointed out that this detection limit can be improved by a few decades using an appropriately chelated terbium(III). Taking into account that the instrumental set-up of the lyoluminescence method of measurement is not complicated and that the lyoluminescence measurement is easy to carry out, the present terbium(III) lyoluminescence can be regarded as the basis of a method which deserves further attention in developing new instrumentally simple trace analytical methods.

Acknowledgement

The assistance of Mr. Kai Rusi in the experimental work is gratefully acknowledged.

References

[1] K. Haapakka, J. Kankare and S. Kulmala, Anal. Chim. Acta, 171 (1985) 259.
[2] K. Haapakka, J. Kankare and O. Puhakka, Anal. Chim. Acta, 207 (1988) 195.
[3] K. Haapakka, J. Kankare and S. Kulmala, Anal. Chim. Acta, 209 (1988) 165.
[4] K. Haapakka, J. Kankare and S. Kulmala, Anal. Chim. Acta, 211 (1988) 105.
[5] S. Kulmala, J. Kankare and K. Haapakka, Anal. Chim. Acta, 252 (1991) 65.
[6] K. Haapakka, J. Kankare, S. Kulmala and K. Fälden, Anal. Chim. Acta, 256 (1992) 17.
[7] J. Kankare, K. Haapakka, S. Kulmala, V. Näntö and J. Eskola, Anal. Chim. Acta, 266 (1992) 205.
[8] S. Kulmala, J. Kankare, K. Haapakka, V. Näntö and J. Eskola, presented at the 44th ISE Meeting, Berlin, September, 1993.
[9] N. Klein and N. Albert, J. Appl. Phys., 53 (1982) 5840; and references cited therein.
[10] J. Schulman and W. Compton, Color Centers in Solids, Pergamon, Oxford, 1962.
[11] G. Ahnström and G. Ehrenstein, Acta Chem. Scand., 13 (1959) 855.
[12] T. Westermark and B. Grapengiesser, Nature, 188 (1960) 395.
[13] G. Ahnström, Acta Chem. Scand., 19 (1965) 300.
[14] N. Atari, J. Luminesc., 21 (1980) 387.
[15] F. Bolletta, Q. Mulazzani, M. Venturi, N. Serpone and V. Balzani, Gazz. Chim. Ital., 115 (1985) 137.
[16] C. Kalkar, Radiat. Phys. Chem. 34 (1989) 729.
[17] G. Reynolds, J. Luminesc., 54 (1992) 43.
[18] R. Reisfeld, J. Res. Natl. Bur. Stand., Sect. A, 76 (1972) 613.
[19] S. Kulmala and K. Haapakka, Anal. Chim. Acta, 294 (1994) 13.
[20] S. Pihlajamäki and J. Kankare, Anal. Instrum., 15 (1986) 171.
[21] R. Weast (Ed.), Handbook of Chemistry and Physics, 55th edn., The Chemical Rubber Company, Cleveland, OH, 1974.
[22] P. Neta, R. Huie and A. Ross, J. Phys. Chem. Ref. Data, 17 (1988) 1027.
[23] G. Buxton, C. Greenstock, W. Helman and A. Ross, J. Phys. Chem. Ref. Data, 17 (1988) 513.
[24] N. Atari, J. Luminesc., 21 (1980) 305.
[25] L. Faulkner, H. Tachikawa and A. Bard, J. Am. Chem. Soc., 94 (1972) 691.
[26] P. Wardman, J. Phys. Chem. Ref. Data, 18 (1989) 1637.
[27] R. Memming, J. Electrochem. Soc., 116 (1969) 785.
[28] W. Carnall, in K.G. Schneidner, Jr. and L. Eyring (Eds.), Handbook on the Physics and Chemistry of Rare Earths, Vol. 3, North-Holland, Amsterdam, 1979.
[29] A. Gilbert and J. Baggot, Essentials of Molecular Photochemistry, Blackwell, Oxford, 1991.

ELSEVIER

Analytica Chimica Acta 294 (1994) 13–25

ANALYTICA CHIMICA ACTA

Terbium(III) lyoluminescence induced by the dissolution of UV-irradiated potassium peroxodisulfate in aqueous solutions

S. Kulmala *, K. Haapakka

Department of Chemistry, University of Turku, FIN-20500 Turku, Finland

(Received 9th November 1993)

Abstract

The –O–O– bond of solid potassium peroxodisulfate can be ruptured by UV irradiation, which results in a solid solution of sulfate radicals in potassium peroxodisulfate. The dissolution of this irradiated solid in water produces a solid/solution interface rich in hydrated sulfate radicals, which can either recombine to form peroxodisulfate ions, or react with solvent or solutes in a sample solution. In terbium(III)-containing aqueous solutions, this dissolution produces the characteristic radiative $^5D_4 \rightarrow {}^7F$-multiplet transitions of terbium(III). This study points out that the light-emitting pathway of this terbium(III) lyoluminescence consists of the following steps: (i) hydrated sulfate radical oxidizes terbium(III) to terbium(IV), (ii) terbium(IV) is immediately reduced by water via a process that is sufficiently energetic to leave the resulting terbium(III) in its lowest excited state $^5D_4$ and finally, (iii) the relaxation of this excited $^5D_4$ state of terbium(III) induces the aforementioned transitions. Thus, this terbium(III) lyoluminescence can be also classified as chemiluminescence. In addition, x-ray irradiated potassium peroxodisulfate is capable of generating an analogous terbium(III) lyoluminescence, which is, however, investigated only on qualitative basis. Lyoluminescence generation of both irradiated materials can be used to determine hydrated Tb(III) down to the micromolar level in aqueous solutions.

Key words: Chemiluminescence; Lyoluminescence; Peroxodisulfate; Terbium

1. Introduction

An optical excitation can be used to raise the hydrated terbium(III) cation from its ground state $^7F_6$ to its lowest excited state $^5D_4$, where the energy gap between these states is 2.55 eV [1]. After this excitation transition, the deactivation transition $^5D_4 \rightarrow {}^7F$ multiplet occurs within the 4f electron shell of terbium(III). These 4f electrons are efficiently shielded by the outer shell electrons and as a result, they give rise to a number of discrete energy levels, which can be regarded as the principal reason for the exceptional properties of terbium(III) fluorescence, namely that it consists of narrow-band peak emissions and that its lifetime is relatively long in an aqueous solution, i.e., around 0.5 ms which depends to some extent on the surrounding medium [1].

However, the intra-f-orbital transition is forbidden, which makes the terbium(III) excitation transition weak and thus, the resulting fluores-

* Corresponding author.

SSDI 0003-2670(94)00106-V

cence of hydrated terbium(III) cation is not so intense. The $^5D_4$ excited state of terbium(III) can be attained considerably more efficiently using a chelated terbium(III) cation, provided that (i) the ligand of the terbium(III) chelate has a strong absorption at the UV range which raises the ligand to its excited singlet state, (ii) the energy difference between the singlet and triplet states of the ligand is small to provide an efficient intersystem crossing, (iii) the ligand has a relatively long-lived triplet state with the energy nearly equal to that of the lowest excited state of terbium(III) which allows an efficient intramolecular triplet energy transfer to the chelated terbium(III) cation and, finally, (iv) the chelating agent is capable of forming a multidentate terbium(III) chelate, which makes the lifetime of the excited $^5D_4$ state longer by excluding water from the coordination sphere of terbium(III) [2–6]. The resulting sensitized terbium(III) fluorescence with a time-resolved detection discriminates efficiently against the short-lived background fluorescence and has proved to be very sensitive to terbium(III) in aqueous solutions, which makes its use attractive for trace analysis [7].

In addition, the $^7F_6 \rightarrow {}^5D_4$ excitation transition of terbium(III) can be attained in non-aqueous and aqueous solutions by electrochemical means and the resulting terbium(III) emission is called electrogenerated terbium(III) luminescence. The cathodic polarization of a platinum electrode in terbium(III)-containing solvents such as dimethylformamide, dimethylsulphoxide and phosphorus oxychloride at high cathodic potentials is able to leave the terbium(III) cation in its excited $^5D_4$ state [8,9]. It has been proposed that this terbium(III) excitation transition is caused either by an inelastic collision of the terbium(III) cation with an electron injected from the cathode to the cathode/electrolyte interface [8] or by an electrical breakdown across an insulating gas-filled cavity produced by a local vaporization of solvent at the electrode surface during the electrode polarization [9]. In aqueous electrolytes, the efficient $^7F_6 \rightarrow {}^5D_4$ excitation transition of the surface-bound hydrated terbium(III) cation [10,11] and appropriately chelated terbium(III) [12] can be achieved at an oxide-covered aluminium cathode in the presence of hydrogen peroxide or potassium peroxodisulfate.

In the cathodic electrogenerated luminescence of the surface-bound hydrated terbium(III) cation, the excited $^5D_4$ state of terbium(III) is obviously generated as follows: hydrogen peroxide and potassium peroxodisulfate are reduced to hydroxyl and sulfate radicals, respectively; these radicals are sufficiently energetic to oxidize the surface-bound terbium(III) to the surface-bound terbium(IV) which is immediately reduced to the surface-bound terbium(III); this terbium(IV) reduction is sufficiently energetic to leave the hydrated terbium(III) in its excited $^5D_4$ state. As to the cathodic electrogenerated luminescence of the chelated terbium(III), the formation of the excited $^5D_4$ state seems to be analogous to that presented above for the sensitized terbium(III) fluorescence, with the exception that the ligand moiety of the terbium(III) chelate is raised to its excited singlet state via redox reactions and not by the optical excitation. The electrochemically produced excited $^5D_4$ state is also long lasting enough for an efficient discrimination against the cathodic background electroluminescence on time-resolved basis and so far, the time-resolved terbium(III) electroluminescence at the oxide-covered aluminium electrode has been applied successfully in our laboratory for immunochemical analysis [13].

Lyoluminescence is defined as a process where the dissolution of a solid material induces light emission. Perhaps the most well-known lyoluminescent process is the light-emitting dissolution of γ-ray or x-ray irradiated sodium chloride in an aqueous solution alone or in the presence of a wide variety of luminescent compounds, e.g., fluorescein, tris(2,2′-bipyridine)ruthenium(II), thallium(I) cations, etc. [14–20]. The exposure of a sodium chloride crystal to the γ-ray or x-ray irradiation generates trapped electrons and equivalent amount of holes in the solid. The dissolution of the irradiated sodium chloride produces a solid/solution interface which contains hydrated electrons and surface-bound chlorine atoms, which are sufficiently energetic to initiate light-emitting pathways at least on the following basis: (i) by a recombination mechanism where the in-

teraction of hydrated electrons with surface-bound chlorine atoms leave the resulting chloride anion in its excited state thus producing the chloride-specific emission, (ii) by an energy transfer mechanism where the excited chloride anion generated as presented above transfers its excitation energy to a luminophor deliberately added into the aqueous sample solution, which produces the luminophor-specific emission and, finally, (iii) by an electron transfer mechanism where the interaction of a luminophor either with the chlorine atom and/or with the hydrated electron leaves the luminophor in its excited state which in relaxing to its ground state produces the luminophor-specific emission.

In the present study, we describe the lyoluminescence of hydrated terbium(III). It has been observed that the –O–O– bond of solid potassium peroxodisulfate can be ruptured by UV or x-ray irradiation, which results in the formation of a stable solid solution of sulfate radicals in potassium peroxodisulfate. The dissolution of this solid solution in an aqueous solution containing either hydrated terbium(III) or appropriately chelated terbium(III) initiates an intense emission which in both cases can be assigned to the terbium(III) $^5D_4 \rightarrow {}^7F$ multiplet transition. This paper evaluates the mechanism of the lyoluminescence arising from the hydrated terbium(III) cation and proposes its usage as an instrumentally simple basis for the terbium(III) detection in aqueous solutions. A detailed treatment of the lyoluminescence of chelated terbium(III) is presented later.

So far, lyoluminescence has been utilized only in dosimetry and mechanistical studies [20]. It is proposed in this and subsequent papers considering more practical applications of this phenomenon, that lyoluminescence can be the basis for extremely sensitive analytical methods.

2. Experimental

2.1. Instrumentation

A block diagram of the lyoluminometer is presented in Fig. 1. The photomultiplier, the high

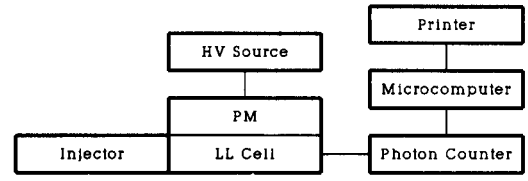

Fig. 1. Block diagram of lyoluminometer.

voltage source of the photomultiplier, the photon counter and spectrometer have been described in detail elsewhere [12,21].

Fig. 2 shows the lyoluminescence cell compartment. The transferable upper part of the compartment, which contains the head-on type pho-

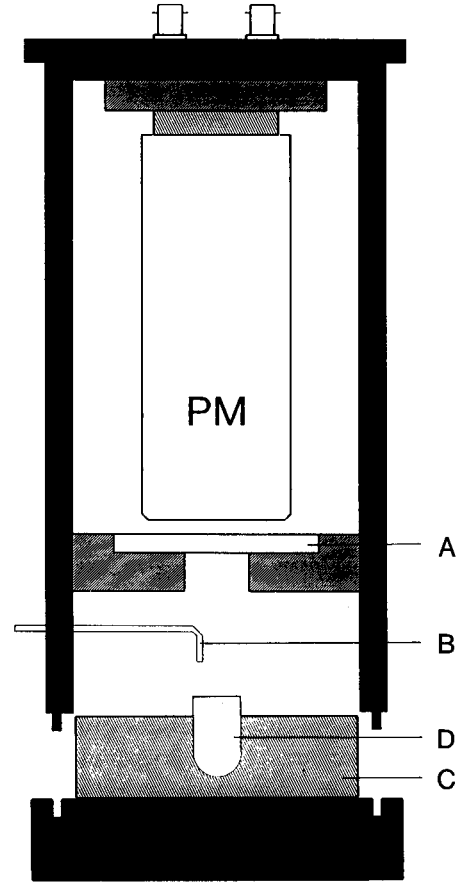

Fig. 2. Cell compartment of the lyoluminometer. (A) Exchangeable interference filter, (B) tubing for injections (C) light scattering support for test tubes, (D) plastic disposable test tube.

tomultiplier (Hamamatsu Model R580), the 546-nm interference filter (A) (bandpass ca. 10 nm, transmittance at 546 nm ca. 50% and diameter 54 mm) and the 2-mm diameter PTFE tubing (B) for the injections of sample solutions by the conventional plastic injection syringe. The support for the disposable plastic test tubes made of white PTFE (C). Plastic test tubes (D) (length 17 mm and diameter 12 mm), which contained the appropriate amount of the solid solution of sulfate radicals in potassium peroxodisulfate, was placed in the lower part of the PTFE compartment as shown in the figure. In addition, the disposable test tube was furnished with a small notch at the upper end to set the PTFE sample tube in its proper place in the test tube.

2.2. Reagents

Potassium peroxodisulfate, sodium hydroxide, nitric acid, sodium thiocyanate and sodium bromide were analytical-reagent grade products of Merck. Terbium(III) nitrate hexahydrate (99.999%) was purchased from Aldrich. All these chemicals were used without further purification. Nitrogen (99.999%) was of purest grade available. All solutions were prepared in quartz-distilled water.

2.3. Preparation of solid solutions of sulfate radicals in potassium peroxodisulfate and the determination of sulfate radicals liberated by the dissolution process

The solid solutions of sulfate radicals in potassium peroxodisulfate were produced by UV or x-ray photolysis. The UV source was a Philips HPLR/125W mercury lamp, which was placed in a polished $30 \times 30 \times 30$ cm aluminium box where the mercury lamp was located around 10 cm above an approximately monogranular layer of the solid sample of potassium peroxodisulfate; proper ventilation was achieved by lifting the aluminium box approximately 1 cm above the sample disc during irradiation. The x-ray source was a Siemens x-ray tube with copper anode (40 kV and 16 mA) and the samples were irradiated in primary beam at a distance of 1 cm from the focus of the tube. In general, 0.5-g quantities of white crystalline potassium peroxodisulfate were irradiated with occasional turnovers for 30 min at ambient temperature.

The UV irradiation produced a white solid solution of sulfate radicals in potassium peroxodisulfate. The sulfate radical content of this solid solution was determined using a method modified from the conventional iodometric method for peroxodisulfate [22]. The reduction of peroxodisulfate by iodide is slow at pH 7 at low iodide concentrations without added catalysts (reaction 1) [22].

$$S_2O_8^{2-} + 3I^- \longrightarrow 2SO_4^{2-} + I_3^- \quad (1)$$

$$S_2O_8^{2-} + I^- \longrightarrow SO_4^- + SO_4^{2-} + I \quad (1a)$$

$$SO_4^- + I^- \longrightarrow SO_4^{2-} + I \quad (1b)$$

$$I + I^- \longrightarrow I_2^- \quad (1c)$$

$$I_2^- + I_2^- \longrightarrow I_3^- + I^- \quad (1d)$$

The first one-electron reduction step of this overall reaction is rate determining (1a), whereas, the second one-electron reduction step (1b) occurs probably close to the diffusion controlled rate. An accurate value for the rate constant k_{1b} is presently not available, but other reduction reactions of SO_4^- are very fast, e.g., the second order rate constant for the reaction of sulfate radicals with bromide ions is reported to be 4×10^9 l mol^{-1} s^{-1} [23]. Diiodine radical ion formation is fast ($k_{1c} = 1.2 \times 10^{10}$ l mol^{-1} s^{-1} [23]), as is the diiodine radical disproportionation reaction ($k_{1d} = 3.2 \times 10^9$ l mol^{-1} s^{-1} [23]). Hence, it is concluded that the presence of hydrated sulfate radicals in an iodide ion solution leads to the fast overall reaction:

$$2SO_4^- + 3I^- \longrightarrow 2SO_4^{2-} + I_3^- \quad (2)$$

Spectrophotometric detection of triiodide ions immediately after dissolution of irradiated potassium peroxodisulfate in dilute iodide ion solution will offer a way to determine the amount of sulfate radicals liberated by the dissolution process. Therefore, it is accepted that at the wavelength where triiodide ion absorbs, the absorbance of the sample cell (which contains the amount of solid solution of sulfate radical in

potassium peroxodisulfate) compared to the reference cell (which contains the same amount of non-irradiated potassium peroxodisulfate) immediately after the dissolution of these solid samples in an appropriate potassium iodide solution, is linearly proportional to the original amount of irradiation-generated sulfate radical in the sample.

The procedure is as follows: 10.0-mg quantities of non-irradiated and carefully homogenized UV irradiated potassium peroxodisulfate were weighed into the reference and sample cells, respectively; 3.00-ml aliquots of the 0.010 M phosphate buffer at pH 6.9, which were additionally 1.00×10^{-3} M in potassium iodide, were added simultaneously to the cells; the cells were vigorously shaken to ensure the complete dissolution of the solid (this step lasted around 10 s); finally, the absorbance of the sample cell against the reference cell was measured at 355 nm where the triiodide anion has a strong absorption band (i.e., $\epsilon_{355} = 28600$ l mol^{-1} cm^{-1} [22]).

When the increase of triiodide ion concentration was thus recorded spectrophotometrically as a function of time the observed linear absorbance vs. time plots had the same slope irrespective of the original sample absorbance and thus the original sulfate radical amount, indicating that the slow reaction between peroxodisulfate and iodide was progressed steadily after the instantaneous reaction between sulfate radicals and iodide. On this basis, Fig. 3 displays the effect of UV irradiation time on the formation of sulfate radicals in a 10-mg solid sample of potassium peroxodisulfate. These results show that UV irradiation can be used to prepare a solid solution of sulfate radicals in potassium peroxodisulfate with the radical content at least up to around 3×10^{-8} mol per 10 mg of irradiated potassium peroxodisulfate, which under the present irradiation conditions corresponds to an irradiation time of 20 h. Mainly from a practical point of view, the terbium(III) lyoluminescence experiments were conducted using a radical content of 2×10^{-9} mol per 10 mg of irradiated potassium peroxodisulfate, (i.e., the irradiation time was only 60 min). All these solid solutions were found to be stable for at least six months.

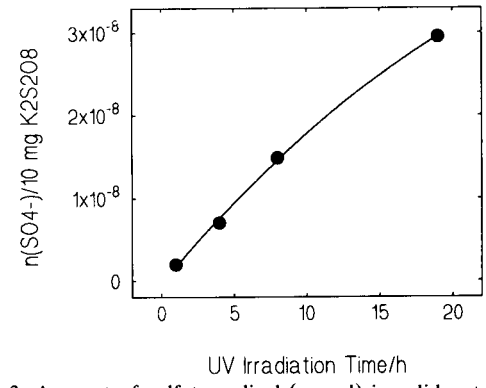

Fig. 3. Amount of sulfate radical (n mol) in solid potassium peroxodisulfate as a function of UV irradiation time.

X-ray irradiation produced a light purple solid solution of sulfate radicals in potassium peroxodisulfate where the colour can be attributed to the presence of electron and hole centres in the irradiated solid [24]. When this x-ray irradiated solid is dissolved in aqueous solutions electron centres generate highly energetic hydrated electrons at the solid/solution interface:

$$\text{trapped electron} + \text{water} \longrightarrow e^-_{aq} \qquad (3)$$

which, in turn, react readily with peroxodisulfate anions to produce sulfate radicals,

$$S_2O_8^{2-} + e^-_{aq} \longrightarrow SO_4^- + SO_4^{2-} \qquad (4)$$

The rate constant of this reaction is reported to be 1.1×10^{10} l mol^{-1} s^{-1} [25]. Thus, both radiation-induced O–O bond rupture and electron centre generation should, on dissolution, produce highly oxidizing conditions. However, energetic x-ray irradiation may introduce a variety of hole centres and other transformations into the solid, hence various radical species can be formed in the solid and be effective during the dissolution process.

2.4. Lyoluminescence monitoring procedure

An appropriate amount of sulfate radicals in potassium peroxodisulfate (generally 10 mg) was weighed to the disposable test tube, which was transferred to the lyoluminescence cell compartment and the compartment was tightly closed. A

1.00-ml aliquot of terbium(III) sample solution, adjusted to the desired pH and deaerated with nitrogen, was injected into the test tube. The immediate dissolution of the potassium peroxodisulfate induced the terbium(III) lyoluminescence which was registered on the photon counter. Photons were counted using a time window of 0.100 s, and for the measurement of lyoluminescence intensity, the integral of photon counts within 10.00 s from the moment of injection was chosen. This integral was calculated from the lyoluminogram at the screen after each measurement with using the SR465 program purchased with the photon counter.

3. Results and discussion

3.1. Generation of terbium(III) lyoluminescence

The solid line in Fig. 4 demonstrates that a 1.00-ml injection of a nitrogen-deaerated aqueous terbium(III) solution (pH 5) onto finely divided, UV irradiation-produced sulfate radicals in potassium peroxodisulfate induces an emission which lasts for ca. 10 s, and which is directly

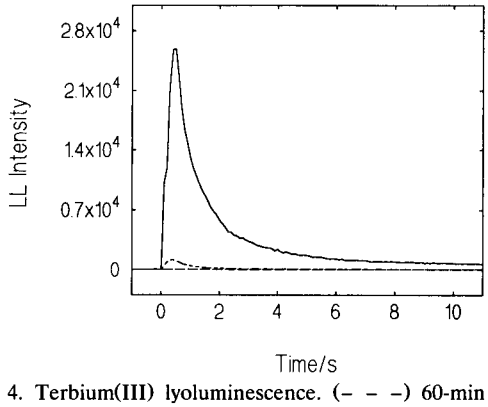

Fig. 4. Terbium(III) lyoluminescence. (– – –) 60-min UV-irradiated potassium peroxodisulfate without terbium(III), (– - - - –) non-irradiated potassium peroxodisulfate with terbium(III), (solid line) 60-min UV-irradiated potassium peroxodisulfate with terbium(III) (LL = lyoluminescence intensity). Conditions: 10.0-mg sample of solid potassium peroxodisulfate, 1.0-ml injection of deaerated quartz-distilled water either with or without 3.0×10^{-3} M terbium(III) nitrate at pH 5.1, no interference filter.

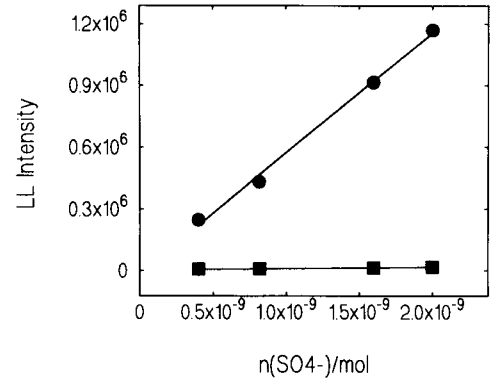

Fig. 5. Effect of the amount of UV-irradiation produced sulfate radical (n mol) on the terbium(III) lyoluminescence intensity. (■) background lyoluminescence, (●) terbium(III) lyoluminescence. Conditions: 2.0, 4.1, 8.0 and 10.0 mg samples of 60-min UV-irradiated or non-irradiated potassium peroxodisulfate, 1.0-ml injection of deaerated quartz-distilled water containing 1.0×10^{-2} M terbium(III) nitrate at pH 5.1, no interference filter.

proportional to the amount of sulfate radicals in the irradiated potassium peroxodisulfate as displayed in Fig. 5. For comparison, Fig. 4 also shows corresponding lyoluminescence responses obtained from the injection of a blank solution onto the sulfate radicals–potassium peroxodisulfate solution (Fig. 5 shows how this response is unaffected by sulfate radical concentration) and of terbium(III) solution onto a non-irradiated potassium peroxodisulfate. These results allow one to conclude that non-irradiated potassium peroxodisulfate is able to initiate only extremely weak lyoluminescence although the injected solution contains hydrated terbium(III) cations, which can be attributed to sulfate radicals produced thermally or by ambient light in the unirradiated potassium peroxodisulfate. The sulfate radicals in potassium peroxodisulfate are also capable of generating a weak background lyoluminescence in the blank solution, which is probably caused by the presence of luminescent impurities either in the chemicals or in the test tube.

The dissolution of x-ray irradiated potassium peroxodisulfate in nitrogen-deaerated terbium (III) solutions stimulates peak emissions similar to those presented in Fig. 4. As displayed in Fig. 6, the lyoluminescence response in the presence

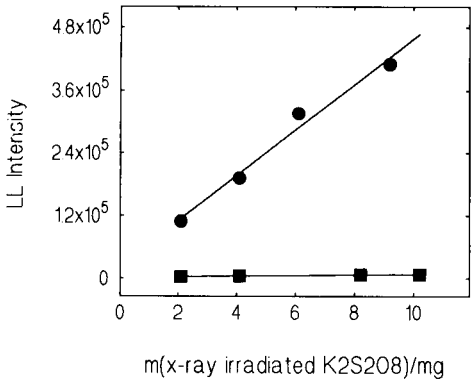

Fig. 6. Effect of the 30-min x-ray irradiated potassium peroxodisulfate sample mass (m) on the terbium(III) lyoluminescence intensity. (■) background lyoluminescence, (●) terbium(III) lyoluminescence. Conditions: as in Fig. 5.

of terbium increases linearly as a function of the amount of 30-min x-ray irradiated potassium peroxodisulfate. Again, a weak luminescence is also produced in the absence of terbium. However, because of the wider possible spectrum of generated radical species, only some qualitative studies were performed with this more complex lyoluminescent material.

Fig. 7 shows a spectrum of terbium lyoluminescence produced by dissolution of UV irradiated potassium peroxodisulfate; under these conditions, the background lyoluminescence proved to

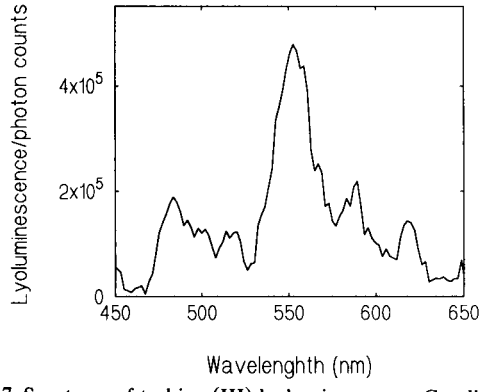

Fig. 7. Spectrum of terbium(III) lyoluminescence. Conditions: 200-mg sample of 5-h UV-irradiated potassium peroxodisulfate, 20-ml injection of nitrogen deaerated quartz-distilled water containing 1.0×10^{-2} M terbium(III) nitrate at pH 5.1, measured with the instrument described in [21].

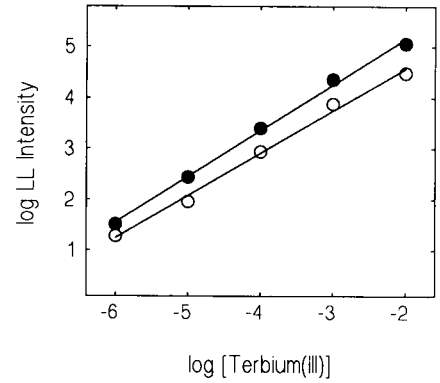

Fig. 8. Calibration graphs for terbium(III) (546-nm interference filter, bandpass = 10 nm). (●) 60-min UV-irradiated potassium peroxodisulfate, (○) 30-min x-ray irradiated potassium peroxodisulfate. Conditions: 10.0-mg sample of irradiated potassium peroxodisulfate, 1.0-ml injection of deaerated quartz-distilled water containing an appropriate concentration of terbium(III) at pH 5.1.

be too weak for spectral measurement. The spectrum shows relatively clear peak emissions at 490, 550, 585 and 625 nm and without any doubt, these peak emissions can be assigned to the well-known terbium(III) transitions $^5D_4 \rightarrow {}^7F_6$, $^5D_4 \rightarrow {}^7F_5$, $^5D_4 \rightarrow {}^7F_4$ and $^5D_4 \rightarrow {}^7F_3$. Hereafter, this lyoluminescence is called terbium(III) lyoluminescence.

The terbium(III) lyoluminescence was practically pH-independent over the pH range 1–7 but in alkaline solutions its intensity was sharply decreased, mainly because of the precipitation of terbium(III) hydroxide. Fig. 8 shows the terbium (III) lyoluminescence response as a function of the terbium(III) concentration for both UV and x-ray irradiated potassium peroxodisulfate. The results indicate that this lyoluminescence responds linearly to the terbium(III) concentration over four decades; the lower limit of detection is below 10^{-6} M.

3.2. Mechanism of terbium(III) lyoluminescence

As in the liquid phase [26–29], UV irradiation of solid potassium peroxodisulfate ruptures its –O–O– bond:

$$^-O_3S\text{–}O\text{–}O\text{–}SO_3^- \longrightarrow 2SO_4^- \qquad (5)$$

and produces a solid solution of sulfate radicals in potassium peroxodisulfate. The UV irradiation did not change the original white colour of potassium peroxodisulfate, which indicates that this irradiation is not capable of significant production of trapped electrons in the solid, unlike to x-ray irradiation. Hence, it is postulated that in the UV irradiated material, the sulfate radical is the only species supplied with the energy required to initiate terbium(III) lyoluminescence.

The sulfate radical is a powerful oxidizing agent in aqueous solutions (i.e., the electrode potential of the SO_4^-/SO_4^{2-} couple should be close to 3.4 V [30]; note that all electrode potentials in this paper are expressed against standard hydrogen electrode) and it may initiate at least the following reactions when the UV irradiation product is dissolved in the aqueous sample solutions under the present experimental conditions:

$$SO_4^- + H_2O \longrightarrow SO_4^{2-} + OH + H^+ \quad (6)$$

$$SO_4^- + SO_4^- \longrightarrow S_2O_8^{2-} \quad (7)$$

$$SO_4^- + S_2O_8^{2-} \longrightarrow SO_4^{2-} + S_2O_8^- \quad (8)$$

$$SO_4^- + NO_3^- \longrightarrow SO_4^{2-} + NO_3 \quad (9)$$

where the reduction potentials are known only for the OH/H_2O and NO_3/NO_3^- redox couples (ca. 2.2 V (pH 5.0) and 2.5 V, respectively) [31]. Utilizing published second-order rate constants [23], the pseudo first order rate constants of these sulfate radical reactions under the present conditions are as follows: $k_6 = < 3 \times 10^4\ s^{-1}$, $k_7 = 2 \times 10^3\ s^{-1}$, $k_8 = 4 \times 10^4\ s^{-1}$ and $k_9 = 7 \times 10^4\ s^{-1}$, respectively. These calculated rate constants show that the sulfate radical is rather stable under these experimental conditions, which allows one to infer that if this aqueous solution also contains hydrated terbium(III) cations, their interaction with sulfate radicals to generate terbium(III) lyoluminescence is quite possible, notwithstanding that the estimated standard electrode potential of the terbium(IV)/terbium(III) couple is reported to be as high as 3.1 ± 0.5 V [32]. Therefore it is proposed that the sulfate radical oxidizes the hydrated terbium(III) cation to the hydrated terbium(IV) cation at the interface between the solid material containing the sulfate radical and the aqueous terbium(III) solution:

$$SO_4^- + Tb^{3+} \longrightarrow SO_4^{2-} + Tb^{4+} \quad (10)$$

and that this one-electron terbium(III) oxidation is the initiating step for the generation of the terbium(III) lyoluminescence under the present conditions.

The hydrated terbium(IV) cation formed by reaction (10) is known to have only a transient existence in aqueous solutions [33] and the terbium(IV) reduction may occur competitively:

$$Tb^{4+} + NO_3^- \longrightarrow Tb^{3+} + NO_3 \quad (11)$$

$$Tb^{4+} + H_2O \longrightarrow Tb^{3+} + OH + H^+ \quad (12)$$

either nitrate or water acting as the reducing agent. Under the present conditions, the electrode potentials of NO_3/NO_3^- and OH/H_2O couples are 2.5 and 2.2 V, respectively [31] but the rate constants for these reactions are not available. From these terbium(IV) reduction alternatives, the nitrate-based reduction pathway, however, cannot be of vital importance for the formation of terbium(III) lyoluminescence, because an increase in nitrate concentration up to at least 0.1 M had no measurable effect on the terbium(III) lyoluminescence. Replacing nitrate as the counter anion in the terbium(III) salt with chloride (the standard potential of the Cl/Cl^- couple is reported to be approximately 2.5 V [31]) decreased the observed terbium(III) lyoluminescence intensity 3-fold, which can be explained by the scavenging effect of chloride on the reaction of the sulfate radical with the hydrated terbium (III) cation. Unlike nitrate (reaction 9), chloride reacts with the sulfate radical

$$SO_4^- + Cl^- \longrightarrow SO_4^{2-} + Cl \quad (13)$$

sufficiently fast (the pseudo first order rate constant under the present conditions is $k_{13} = 9 \times 10^6\ s^{-1}$ [23]) to compete with reaction (10), which creates partially scavenging conditions for the terbium(III) lyoluminescence pathway. On the other hand, Faraggi and Feder [34] have pointed out that the rate constant of the one-electron reduction of praseodymium(IV) to praseodymium(III) by water (solution adjusted to pH 5.0) is

8×10^7 l mol^{-1} s^{-1}. Taking into account the generally accepted analogy between praseodymium and terbium, e.g., the electrode potential of the praseodymium(IV)/praseodymium(III) couple is also 3.1 ± 0.5 V [32], the aforementioned results demonstrate that the water-based reduction of terbium(IV) occurs readily under the present conditions and that this reduction is an essential step in the terbium(III) lyoluminescence pathway.

The enthalpy of this light-emitting terbium (IV)/terbium(III) reduction process can be evaluated from Eq. 14 [35]:

$$-\Delta H = E(Tb^{4+}/Tb^{3+}) - E(R/R^-) - T\Delta S \quad (14)$$

where $E(Tb^{4+}/Tb^{3+})$ and $E(R/R^-)$ denote the electrode potentials for the two half reactions comprising the redox processes, and the remaining symbols have their usual meaning. Supposing that the electrode potentials of the terbium(IV)/terbium(III) and OH/H_2O couples are 3.1 and 2.2 eV (pH 5.0), respectively [31], and that the entropy term in Eq. 14 is 0.1 eV [35], the enthalpy of the water-based reduction of terbium(IV) is only approximately 0.8 eV, which is far less than the enthalpy of 2.55 eV required to generate the hydrated terbium(III) cation in its lowest excited state ($^5D_4$) [1].

Accepting that, like the hydrated terbium(III) cation [36], the hydrated terbium(IV) cation has nine water molecules in its inner coordination sphere, it is proposed that the energy-sufficient decomposition of the hydrated terbium(IV) cation to induce the radiative $^5D_4 \rightarrow {}^7F$-multiplet transitions under the present aqueous conditions occurs as follows:

$$(H_2O)_9Tb^{4+} \longrightarrow (H_2O)_8Tb^{4+}(OH^-) + H^+ \quad (15a)$$

$$(H_2O)_8Tb^{4+}(OH^-) \longrightarrow \left[(H_2O)_8Tb^{3+}(OH)\right]^{(*)} \quad (15b)$$

$$(H_2O)_8Tb^{3+}(OH) + SO_4^- \longrightarrow (H_2O)_8Tb^{4+}(OH) + SO_4^{2-} \quad (15c)$$

$$(H_2O)_8Tb^{4+}(OH) \longrightarrow (H_2O)_7Tb^{4+}(OH,OH^-) + H^+ \quad (15d)$$

$$(H_2O)_7Tb^{4+}(OH,OH^-) \longrightarrow \left[(H_2O)_7Tb^{3+}(H_2O_2)\right]^* \quad (15e)$$

$$\left[(H_2O)_7Tb^{3+}(H_2O_2)\right]^* \longrightarrow (H_2O)_7Tb^{3+}(H_2O_2) + h\nu \quad (15f)$$

Assuming that the acid dissociation constant pK_{a1} of the hydrated terbium(IV) cation is approximately 0, i.e., close to that reported for the hydrated cerium(IV) cation [37], the hydroxy-aqua-terbium(IV) cation is the prevailing species of terbium(IV) under the lyoluminescence conditions, i.e., in the solutions adjusted to pH 5; pK_{a1} for terbium(III) is 8.2 [37], hence unprotonated hydrated terbium(III) ions are the prevailing species before oxidation. After fast deprotonation of hydrated terbium(IV), an "intramolecular" hydroxide ion-to-terbium(IV) electron transfer results in formation of a hydroxyl radical-aqua-terbium(III) cation; providing that the enthalpy of this reaction is high enough it may produce terbium(III) cations in their lowest excited state $^5D_4$. However, if the electrode potential of the terbium-coordinated OH/OH^- couple is close to the value for the hydrated OH/OH^- couple, this reaction is not energy-sufficient for the excitation, and subsequent reactions are needed to explain the observed emission.

In the next step, the hydroxyl radical-aqua-terbium(III) cation is oxidized by the sulfate radical to generate a hydroxyl radical-aqua-terbium(IV) cation which is immediately dissociated to a hydroxyl ion-hydroxyl radical-aqua-terbium(IV) cation. An "intramolecular" electron transfer from the coordinated hydroxyl radical or hydroxide ion to terbium(IV) results in formation of a hydrogen peroxide-aqua-terbium(III) cation and, taking into account that the electrode potential of the hydrated $OH,OH^-/H_2O_2$ redox couple is around 0.4 eV at pH 5 [25], the enthalpy of this terbium(IV) reduction is around 2.6 eV, which is sufficiently high to leave the resulting terbium(III) cation in its lowest excited state ($^5D_4$). Finally,

the radiative relaxation of this excited terbium(III) cation induces the well-known $^5D_4 \rightarrow {}^7F$-multiplet transitions of terbium(III).

3.3. Evaluation of the rate constant of terbium(III) oxidation by the sulfate radical

An attempt to evaluate the rate constant of the one-electron oxidation of terbium(III) by the sulfate radical was made by a competition method, where a scavenger (denoted by Sca) was added into the terbium(III) sample solution to compete with the hydrated terbium(III) cation for the sulfate radical on the following basis:

$$Tb^{3+} + SO_4^- \longrightarrow Tb^{4+} + SO_4^{2-} \quad (16)$$

$$Sca + SO_4^- \longrightarrow Sca^+ + SO_4^{2-} \quad (17)$$

In this method, it is assumed that the terbium(III) oxidation reaction is an essential part of the reaction sequence generating the terbium(III) lyoluminescence as presented above, while the scavenger reaction is not capable of inducing any lyoluminescence. Providing that the scavenger reaction is fast, that the scavenger or its oxidation product do not play any essential role in the terbium(IV) reduction, and that the scavenger or its oxidation product do not interact with the excited ($^5D_4$) hydrated terbium(III), the following intensity expressions can be written for the terbium(III) lyoluminescence in the absence of the scavenger (I_o) and in the presence of an appropriate scavenger concentration (I_{Sca}):

$$I_o \propto k_{Tb}[Tb^{3+}][SO_4^-] \quad (18)$$

$$I_{Sca} \propto k_{Tb}[Tb^{3+}][SO_4^-] - k_{Sca}[Sca][SO_4^-] \quad (19)$$

where k_{Tb} and k_{Sca} denote the rate constants for reactions (16) and (17), and $[Tb^{3+}]$, $[SO_4^-]$ and [Sca] the concentrations of hydrated terbium(III) cation, sulfate radical and scavenger in the sample solution. At the point where the competing terbium(III)–sulfate radical (16) and scavenger–sulfate radical (17) reactions occur at an equal rate, i.e., $I_{Sca} = I_o/2$, k_{Tb} can be obtained on the following basis:

$$k_{Tb}[Tb^{3+}][SO_4^-] = k_{Sca}[Sca]_{1/2}[SO_4^-] \quad (20)$$

and thus

$$k_{Tb} = k_{Sca}[Sca]_{1/2}/[Tb^{3+}] \quad (21)$$

where $[Sca]_{1/2}$ denotes the scavenger concentration required to decrease the terbium(III) lyoluminescence intensity to one half of its original value. Consequently, the determination of $[Sca]_{1/2}$ from the scavenger plot I_{Sca} vs. [Sca] makes it possible to estimate the rate constant of the one-electron oxidation of terbium(III) by the sulfate radical under the terbium(III) lyoluminescence conditions, providing that k_{Sca} and $[Tb^{3+}]$ are exactly known.

In these experiments, thiocyanate and bromide anions were utilized as scavengers for the following reasons: (i) their reactions with sulfate radical

$$SCN^- + SO_4^- \longrightarrow SCN + SO_4^{2-} \quad (22)$$

$$Br^- + SO_4^- \longrightarrow Br + SO_4^{2-} \quad (23)$$

are fast (see below), (ii) the resulting thiocyanate and bromide radicals are not sufficiently strong oxidizing agents to interact with the hydrated terbium(III) cation, i.e., the standard electrode potentials of the SCN/SCN^- and Br/Br^- couples are reported to be approximately 1.6 and 1.9 V [31], respectively, (iii) on the basis of the fast reaction of terbium(IV) with water (the analogy with praseodymium(IV)) and of the low scavenger concentrations required to reduce the terbium (III) lyoluminescence intensity, these scavengers cannot play a role of great importance in the reduction of terbium(IV) and, finally, (iv) our photoluminescence experiments under the lyoluminescence conditions did not unveil any quenching interactions of these scavengers with the excited $^5D_4$ state of terbium(III).

On the basis of the scavenger plots displayed in Fig. 9, the $[Sca]_{1/2}$ values for the thiocyanate and bromide anions in the sample solutions containing 1.0×10^{-2} M terbium(III) are 8.3×10^{-6} M and 1.7×10^{-5} M, respectively. Taking into account that the rate constants of the sulfate radical scavenging reactions for SCN^- and Br^- are 5.2×10^9 and 3.5×10^9 l mol^{-1} s^{-1}, respectively [23], Eq. 21 gives values for k_{Tb} of 4.3×10^6 and 6.0×10^6 l mol^{-1} s^{-1}, respectively, with these two scavengers. These k_{Tb} values are reasonable

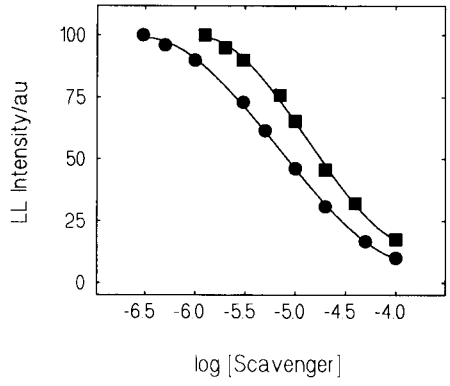

Fig. 9. Effect of sulfate radical scavengers on terbium(III) lyoluminescence. (■) Bromide, (●) thiocyanate. Conditions: 10.0-mg sample of 60-min UV-irradiated potassium peroxodisulfate, 1.0-ml injection of deaerated quartz-distilled water containing 1.0×10^{-2} M terbium(III) nitrate at pH 5.1.

for terbium(III) oxidation by sulfate radicals (reaction 16), but the assumption above (that terbium(IV) will not have any significant interactions with thiocyanate or bromide ions) can be questioned at least on a thermodynamic basis, hence, bromide or thiocyanate may offer a non-luminescent pathway for terbium(IV) to be reduced, so that the value of k_{Tb} obtained by this procedure can be regarded only as the lowest limit of this reaction rate constant. Thus, without extensive studies, it can be only concluded that $k(SO_4^- + Tb^{3+}) > 4 \times 10^6$ l mol^{-1} s^{-1}.

3.4. Terbium(III) lyoluminescence with x-ray irradiated potassium peroxodisulfate

To test the effect of more energetic radiation on solid peroxodisulfate, some preliminary terbium(III) lyoluminescence experiments were carried out using x-ray irradiated potassium peroxodisulfate (see Fig. 6). As already described above, the dissolution of this potassium peroxodisulfate is likely to produce energetic hydrated electrons (the electrode potential of this strong reducing agent is reported to be around −2.9 V [25]) at the solid/electrolyte interface, which may react under the present lyoluminescence conditions at least in the following ways:

$$e_{aq}^- + H_3O^+ \longrightarrow H + H_2O \quad (24)$$

$$e_{aq}^- + NO_3^- + H_2O \longrightarrow NO_2 + 2OH^- \quad (25)$$

$$e_{aq}^- + S_2O_8^{2-} \longrightarrow SO_4^- + SO_4^{2-} \quad (26)$$

Using the second-order rate constants from [25], the pseudo first order reaction rate constants for these reactions are $k_{24} = 2 \times 10^5$ s^{-1}, $k_{25} = 3 \times 10^8$ s^{-1} and $k_{26} = 4 \times 10^8$ s^{-1}. From these hydrated electron reactions, the proton reaction (24) is not significant under these conditions, while the nitrate reaction (25) is fast enough to compete with the peroxodisulfate reaction (26) but the resulting nitrite radical is only a relatively weak oxidizing agent (i.e., the electrode potential of the NO_2/NO_2^- redox couple is 1.0 V [31]) and is not able to initiate the terbium(III) lyoluminescence pathway via the one-electron oxidation of the hydrated terbium(III) cation. Accepting that, as with UV irradiation, x-ray irradiation produces a solid solution of sulfate radicals in potassium peroxodisulfate by rupturing the –O–O– bond, it is obvious that the dissolution of x-ray irradiated potassium peroxodisulfate in the aqueous terbium(III)-containing solution induces the terbium(III) lyoluminescence according to the mechanism presented above but where the reaction (26) provides, however, an additional source of sulfate radical.

The UV-irradiated potassium peroxodisulfate, therefore, produces a less complicated lyoluminescence-generating solid/solution-interface than x-ray irradiated potassium peroxodisulfate, and so is a more promising material for analytical methods utilizing oxidative lyoluminescence, and also for other difficult oxidations in aqueous solutions, because it is easily obtained in every laboratory equipped with a UV-radiation source.

4. Conclusions

The UV and x-ray photolysis of solid potassium peroxodisulfate provides a feasible means of preparing solid solutions of the sulfate radical in

potassium peroxodisulfate, where the content of sulfate radical can easily be regulated by the duration of irradiation. These stable solid solutions can be utilized as the source of sulfate radical in chemical processes where a strong oxidizing agent is required in aqueous solutions, providing that the aqueous solution does not contain any compound capable of efficiently scavenging the sulfate radicals. The sulfate radical may be an active oxidizing agent or its role may be the generation of a secondary oxidizing agent with some specific property, e.g. by the oxidation of the hydroxide anion to the hydroxyl radical (the rate constant of this reaction is reported to be around 8×10^7 l mol^{-1} s^{-1}) which could replace the use of Fenton's reagent in the cleavage of DNA [38]; and analogously halide and pseudohalide radicals can be easily generated.

In the present contribution, it is pointed out that the solid solution of sulfate radicals in potassium peroxodisulfate can be used to produce the terbium(III) lyoluminescence where the light-emitting pathway contains the terbium(IV) intermediate which is formed in the one-electron oxidation of terbium(III) by the sulfate radical; as estimated on the basis of scavenger experiments with terbium(III) lyoluminescence, the second order rate constant of this terbium(III) oxidation reaction is greater than 4×10^6 l mol^{-1} s^{-1}. This lyoluminescence responds to terbium(III) down to concentrations around 10^{-6} M, but this detection limit could, however, be considerably lowered, because (i) the generation of the sulfate radical by the photolysis of solid potassium peroxodisulfate can be made considerably more efficient (the UV-emission intensity of the Philips HPLR/125W mercury lamp used in this work proved to be very low, below 300 nm, where peroxodisulfate has its absorption bands) and (ii) as in the conventional terbium(III) photoluminescence and electrogenerated terbium(III) luminescence at the oxide-covered aluminium electrode, an appropriate multidentate chelation of the hydrated terbium(III) cation sensitizes the terbium-(III)-based emission. A paper on sensitized terbium(III) lyoluminescence will be presented in the near future.

The method of lyoluminescence measurement is simple, and the lyoluminometer introduced in this paper can be used for extremely sensitive determinations of various analytes excitable in lyoluminescent processes of various solid materials. The high sensitivity and versatility of lyoluminescence methods will be shown in subsequent papers.

Acknowledgement

The authors thank Mr. Arvi Hakanen and Mr. Kai Rusi for their assistance with the experimental work.

References

[1] R. Reisfeld, J. Res. Natl. Bur. Stand. U.S., Sect. A, 76 (1972) 613.
[2] G. Crosby, R. Whan and J. Freeman, J. Phys. Chem., 66 (1962) 2493.
[3] R. Whan and G. Grosby, J. Mol. Spectrosc., 8 (1962) 315.
[4] G. Crosby, Mol. Cryst., 1 (1966) 37.
[5] A. Sinha, Spectrosc. Inorg. Chem., 2 (1971) 255.
[6] E. Soini and T. Lövgren, CRC Crit. Rev. Anal. Chem., 18 (1987) 105; and references cited therein.
[7] I. Hemmilä, Anal. Chem., 57 (1985) 1676.
[8] A. Heller, K. French and P. Hauhsjaa, J. Phys. Chem., 55 (1972) 2368.
[9] K. Doblhofer and H. Gerischer, J. Electroanal. Chem., 65 (1975) 101.
[10] S. Kulmala, J. Kankare and K. Haapakka, Anal. Chim. Acta, 252 (1991) 65.
[11] E. Meulenkamp, J. Kelly and G. Blasse, J. Electrochem. Soc., 140 (1993) 84.
[12] J. Kankare, K. Fälden, S. Kulmala and K. Haapakka, Anal. Chim. Acta, 256 (1992) 17.
[13] J. Kankare, K. Haapakka, S. Kulmala, V. Näntö and J. Eskola, Anal. Chim. Acta, 266 (1992) 205.
[14] G. Ahnström and G. Ehrenstein, Acta Chem. Scand., 13 (1959) 855.
[15] T. Westermark and B. Grapengiesser, Nature, 188 (1960) 395.
[16] G. Ahnström, Acta Chem. Scand., 19 (1965) 300.
[17] N. Atari, J. Lumin., 21 (1980) 387.
[18] F. Bolletta, Q. Mulazzani, M. Venturi, N. Serpone and V. Balzani, Gazz. Chim. Ital., 115 (1985) 137.
[19] C. Kalkar, Radiat. Phys. Chem., 34 (1989) 729.
[20] G. Reynolds, J. Luminol., 54 (1992) 43.
[21] S. Pihlajamäki and J. Kankare, Anal. Instrum., 15 (1986) 171.
[22] N. Frigerio, Anal. Chem., 35 (1963) 412.
[23] P. Neta, R. Huie and A. Ross, J. Phys. Chem. Ref. Data, 17 (1988) 1027.

[24] J. Schulman and W. Compton, Color Centers in Solids, Pergamon, Oxford, 1962.
[25] G. Buxton, C. Greenstock, W. Helman and A. Ross, J. Phys. Chem. Ref. Data, 17 (1988) 513.
[26] R. Crist, J. Am. Chem. Soc., 54 (1932) 3939.
[27] L. Heidt, J. Mann and H. Schneider, J. Am. Chem. Soc., 70 (1948) 3011.
[28] M.-S. Tsao and W. Wilmarth, J. Phys. Chem., 63 (1959) 346.
[29] L. Dogliotti and E. Hayon, J. Phys. Chem., 71 (1967) 2511.
[30] R. Memming, J. Electrochem. Soc., 116 (1969) 785.
[31] P. Wardman, J. Phys. Chem. Ref. Data, 18 (1989) 1637.
[32] W. Carnall, in K. Gschneidner, Jr. and L. Eyring (Eds.), Handbook on the Physics and Chemistry of Rare Earths, Vol. 3, North-Holland, Amsterdam, 1979.
[33] K. Nash and J. Sullivan, in K. Gschneidner, Jr. and L. Eyring (Eds.), Handbook on the Physics and Chemistry of Rare Earths, Vol. 3, North-Holland, Amsterdam, 1979.
[34] M. Faraggi and A. Feder, J. Chem. Phys., 56 (1972) 3294.
[35] L. Faulkner, H. Tachikawa and A. Bard, J. Am. Chem. Soc., 94 (1972) 691.
[36] W. Horrocks, Jr. and D. Sudnick, Acc. Chem. Res., 14 (1981) 384.
[37] D. Perrin (Ed.), Ionisation Constants of Inorganic Acids and Bases in Aqueous Solutions, Pergamon Press, Oxford, 1982.
[38] R. Macgregor, Jr., Anal. Biochem., 204 (1992) 324.

ELSEVIER

Analytica Chimica Acta 294 (1994) 27–34

ANALYTICA CHIMICA ACTA

Flow-injection chemiluminometric determination of some bile acids [1]

Ioannis M. Psarellis, Nikolaos T. Deftereos, Evangelos G. Sarantonis, Antony C. Calokerinos *

Laboratory of Analytical Chemistry, University of Athens, Panepistimiopolis, Zografou, 157 71 Athens, Greece

(Received 6th December 1993; revised manuscript received 9th February 1994)

Abstract

The chemiluminometric oxidation of sulphite by cerium(IV), permanganate, bromate and dichromate is sensitized by various bile acids. Each reaction is investigated by flow-injection chemiluminometric analysis and conclusions are drawn about the effectiveness of each oxidant. The reaction with cerium(IV) allows the measurement of 2.00–20.0 μg ml^{-1} cholic acid, 2.00–50.0 μg ml^{-1} ursodeoxycholic acid and 3.00–30.0 μg ml^{-1} chenodeoxycholic and deoxycholic acids with limits of detection of ca. 1 μg ml^{-1}.

Key words: Chemiluminescence; Flow injection; Sensitized chemiluminescence; Bile acids; Sulphite

1. Introduction

Chemiluminescence (CL) can be achieved by direct reactions or by energy-transfer mechanisms. Direct CL reactions, such as the oxidation of morphine by potassium permanganate [1], paracetamol by cerium(IV) [2] or rifampicin by *N*-bromosuccinimide [3] are continuously being developed. Nevertheless, chemi-excitation by energy-transfer is more widely used since it is based on the vast knowledge of spectrofluorimetry. The most well-established energy-transfer system is the peroxyoxalate CL reaction [4]. Fluorophores like dipyridamole [5], dansyl amino acids [6], amines labelled with luminarine 1 [7] and thyroxine labelled with fluorescamine [8] have been determined with limits of detection equal or less than 1×10^{-9} M.

Inorganic redox systems have also been used for chemi-excitation but in most cases the analyte is the reductant or oxidant and not the fluorophore. Hence, the fluorophore acts as a sensitizer since it amplifies the emission intensity. Typical examples are fluorescein and rhodamine B which sensitize the CL reaction between sulphide and hypochlorite [9] and fluorescein for the reaction of β-nitrostyrene with dissolved oxygen [10] or the reaction of alkaline cyanide with didodecyldimethylammonium bromide [11]. Other ex-

* Corresponding author.

[1] Presented at the *fifth International Symposium on Quantitative Luminescence Spectrometry in Biomedical Sciences, Ghent, Belgium, May 25–27, 1993*. The majority of papers presented at this symposium was published in *Anal. Chim. Acta*, Vol. 290/1–2, 1994.

SSDI 0003-2670(94)00117-5

amples are riboflavin and brilliant sulfaflavine for the oxidation of sulphite by permanganate [12] and rhodamine B for the oxidation of triethylamine by hypochlorite [13].

Bile acids were found to enhance the emission intensity from the chemiluminogenic oxidation of sulphite. The observation was further investigated since simple chemiluminescing reactions with bile acids are limited. One procedure involves derivatization with aminobutylethylisoluminol (ABEI) before the reaction with hydrogen peroxide [14] and another involves derivatization with dansyl hydrazine before liquid chromatographic separation with peroxyoxalate detection [15]. CL from sulphite was generated by the reactions of cerium(IV), potassium permanganate, bromate and dichromate in order to establish the most sensitive redox system.

2. Experimental

2.1. Apparatus

The flow manifold used (Fig. 1) was similar to that used previously [16] and consisted of a peristaltic pump (Ismatec Mini-S 820) which pumped both reagent solutions at equal flow rates (6.0 ml min^{-1}) through PTFE flow tubes, a low-pressure PTFE injection valve (Rheodyne Model 5020, Anachem) manually operated and provided with a 500-μl sample loop through which the sample was injected into the stream of sulphite, and a Y-shaped mixing element for mixing the two streams, positioned in front of the flow cell inlet.

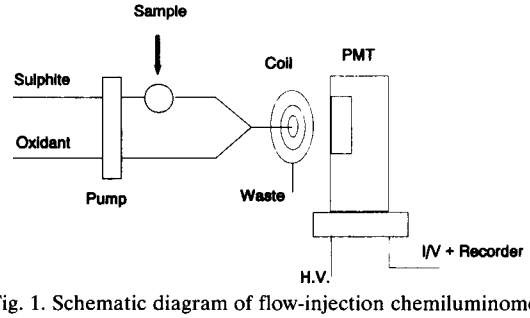

Fig. 1. Schematic diagram of flow-injection chemiluminometer (not to scale).

The detector consisted of a glass coil with 3.5 turns of glass tubing (2 mm i.d.) with a total height of 22 mm accommodated in a Heath sample cell module (EU-701-11). The coil was placed 2 mm from the photomultiplier tube (PMT) window and was backed by a mirror for maximum light collection by the photomultiplier. The PMT (RCA 931A, S-4 response) was housed in a Heath photomultiplier module (EU-701-30) and was operated at −700 V. The output was fed to a current-to-voltage (I/V) converter based on an RCA CA 3140 operational amplifier. Damping was provided by inserting an RC circuit between the converter and the multi-speed variable-span recorder (Perkin-Elmer Model 56).

2.2. Reagents

All solutions were prepared from analytical-reagent grade materials in deionized, distilled water.

A 1.00×10^{-2} M stock solution of sulphite was prepared daily by dissolving 0.630 g of sodium sulphite (Merck) in water and diluting to 500 ml.

Stock solutions (1.00×10^{-2} M) of cerium(IV) and bromate were prepared by dissolving 6.320 g of ammonium cerium(IV) sulphate (Merck) and 1.509 g of sodium bromate (Carlo Erba) in 0.50 M sulphuric acid and diluting to 1 l with the same acidic solution. Stock solutions (1.00×10^{-3} M) of permanganate and dichromate were prepared by dissolving 0.1580 g of potassium permanganate (Ferak) and 0.2942 g of potassium dichromate (Malinckrodt) in 0.10 M sulphuric acid and diluting to 1 l with the same acidic solution.

Stock solutions (100.0 μg ml^{-1}) of cholic and deoxycholic acid, sodium salt (Serva) and chenodeoxycholic acid, sodium salt (Sigma) were prepared by dissolving 0.1000 g of each compound in water and diluting with water to 1 l. Ursodeoxycholic acid (Sigma) was dissolved in 0.010 M sodium hydroxide and diluted to 1 l with the same alkaline solution. More dilute solutions were prepared from the stock solutions by appropriate dilution with water.

2.3. Procedure

The appropriate concentration of each oxidant and sulphite were continuously pumped into the manifold. Volumes of 500 μl of solutions of each bile acid were injected into the stream of sulphite.

3. Results and discussion

Excited sulphur dioxide has been proposed as the emitting species during the oxidation of sulphite by potassium permanganate [17] and cerium(IV) [18]. The mechanism proposed by Meixner and Jaeschke [19] for the CL reaction with permanganate is:

$$HSO_3^- + MnO_4^- \longrightarrow HSO_3 + MnO_4^{2-}$$

$$2HSO_3 \longrightarrow S_2O_6^{2-} + 2H^+$$

$$S_2O_6^{2-} \longrightarrow SO_4^{2-} + SO_2^*$$

$$SO_2^* \longrightarrow SO_2 + h\nu$$

Thus, sulphite acts as the reductant and the energy released from the chemical reaction chemiexcites sulphur dioxide, which emits radiation at wavelengths > 300 nm [20].

Recently, the chemiluminogenic oxidation of sulphite has been used as the energy transfer reaction for a plethora of fluorophoric analytes.

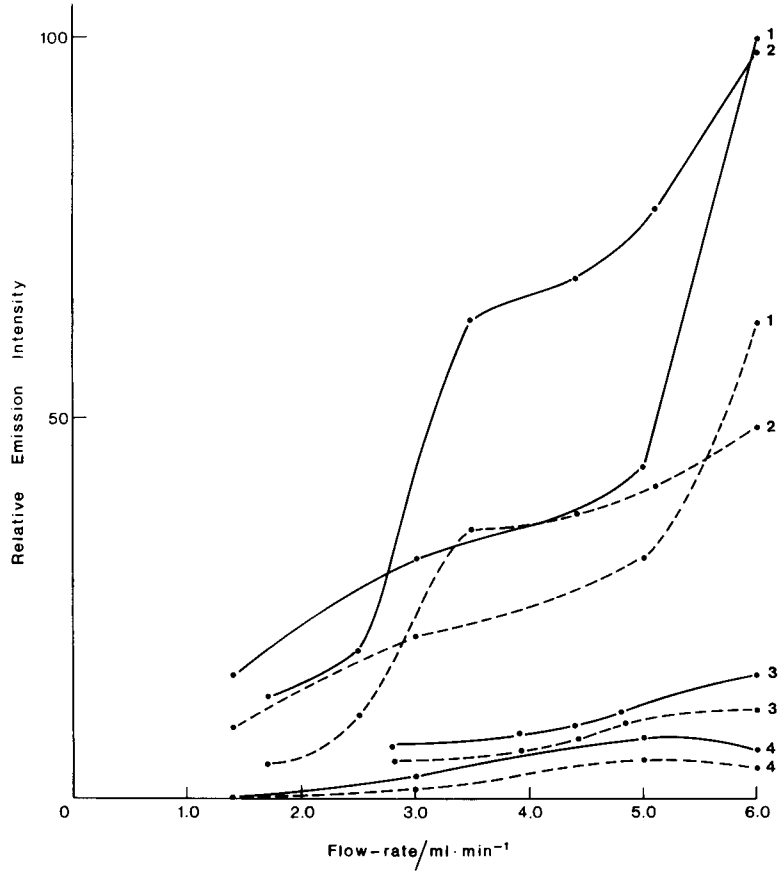

Fig. 2. Effect of flow rate of 1.00×10^{-3} M sulphite and (1) 4.00×10^{-4} M permanganate in 0.10 M sulphuric acid and (2) 5.00×10^{-4} M cerium(IV), (3) 5.00×10^{-3} M bromate and (4) 1.00×10^{-3} M dichromate in 0.50 M sulphuric acid on the emission intensity in the presence of 10.0 (dashed line) and 20.0 (solid line) μg ml^{-1} cholic acid.

These are quinine and quinidine [21], corticosteroids [22] and cyclamate [16] by the action of cerium(IV). Steroids have also been determined by the action of bromate [23] or cerium(IV) in organic solvents [24].

Intriguing examples of sensitizers are also known. These compounds do not fluoresce but are capable of amplifying the intensity of the chemiluminogenic oxidation of sulphite. 3-Cyclohexylaminopropane sulphonic acid (CAPS) is a non-fluorophore which sensitizes the CL from the oxidation of sulphite from permanganate; the limit of detection is lower than when riboflavin is used [25]. CAPS [26] and similar compounds with cyclohexyl groups [27] also sensitize the oxidation of sulphite by cerium(IV).

Bile acids increase the weak radiation emitted during the CL oxidation of sulphite by some common oxidants in sulphuric acid medium. The two reactants are continuously mixed and introduced into the flow cell and the weak CL radiation emitted from this reaction is continuously recorded as the baseline. When a bile acid is injected into the sulphite stream, the intensity is enhanced in proportion to its concentration.

In order to compare cerium(IV), permanganate, bromate and dichromate as chemiluminogenic reactants for sulphite, the experimental

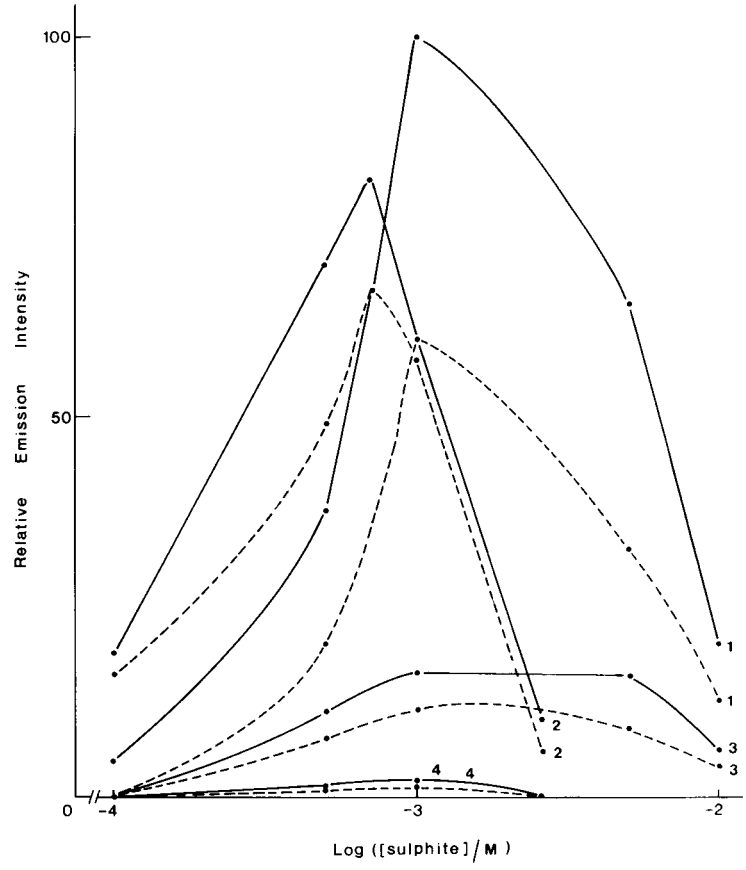

Fig. 3. Effect of sulphite concentration on the emission intensity from (1) 4.00×10^{-4} M permanganate in 0.10 M sulphuric acid, (2) 1.00×10^{-3} M cerium(IV) in 0.10 M sulphuric acid, and 1.00×10^{-3} M (3) bromate and (4) dichromate in 0.50 M sulphuric acid in the presence of 10.0 (dashed line) and 20.0 (solid line) μg ml^{-1} cholic acid.

conditions (flow rate, oxidant, sulphuric acid and sulphite concentration) used were optimised with cholic acid for each oxidant.

3.1. Effect of flow rate

The solutions of oxidant and sulphite were introduced into the manifold at equal flow rates. The effect of flow rate on the emission intensity is shown in Fig. 2. High flow rates were required for the increased sensitivity for cerium(IV), permanganate and bromate and it was decided to supply both reactants at 6.0 ml min^{-1} to avoid extensive consumption. 5.0 ml min^{-1} was the optimum flow rate for dichromate; the latter generated the weakest emission from all oxidants examined.

3.2. Effect of sulphite concentration

The effect of sulphite concentration on the intensity obtained is shown in Fig. 3. The optimum sulphite concentration was 1.00×10^{-3} M for permanganate, bromate and dichromate and 7.00×10^{-4} M for cerium(IV). Hence, the optimum sulphite concentration is practically independent of the nature of the oxidant.

3.3. Effect of oxidant and sulphuric acid concentration

The effect of concentration of each oxidant is shown in Fig. 4. The oxidation of sulphite is chemiluminogenic only in acidic solutions due to the evolution of sulphur dioxide. Sulphuric acid is

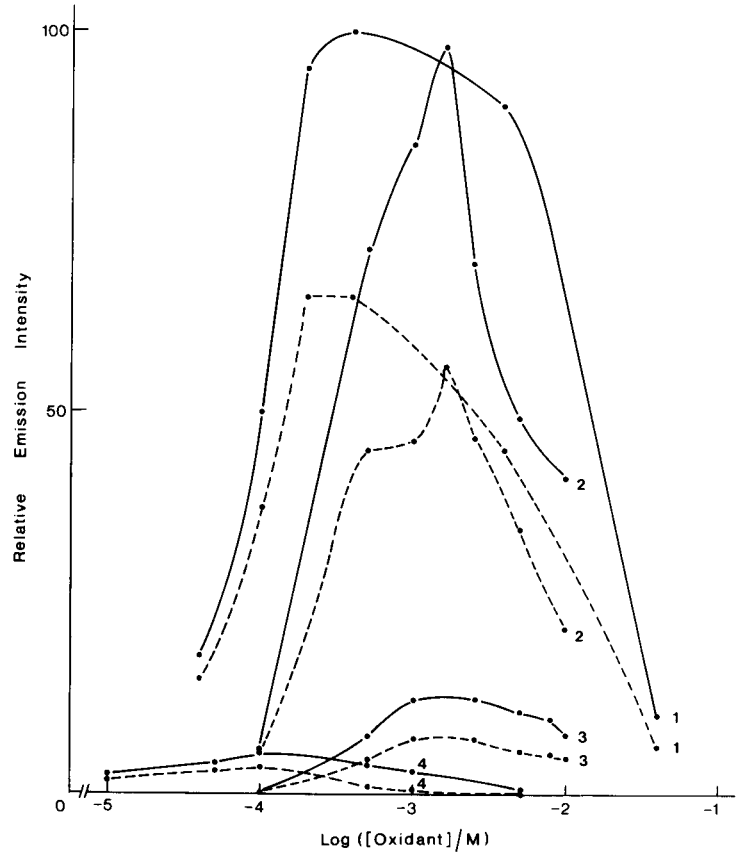

Fig. 4. Effect of concentration of (1) permanganate in 0.10 M sulphuric acid, and (2) cerium(IV), (3) bromate and (4) dichromate in 0.50 M sulphuric acid on the emission intensity from 1.00×10^{-3} M sulphite in the presence of 10.0 (dashed line) and 20.0 (solid line) $\mu g\ ml^{-1}$ cholic acid.

the most commonly used acid and the effect on the CL intensity is shown in Fig. 5.

The optimum conditions for flow rate and concentration of sulphite and sulphuric acid for each oxidant are summarized in Table 1. The emission intensity from the same concentration of cholic acid follows the order cerium(IV) > permanganate ≫ bromate > dichromate. Therefore, cerium(IV) was chosen for evaluating the analytical parameters of the bile acids studied.

Table 1
Experimental conditions and relative emission intensity (REI) from 20.0 μg ml^{-1} cholic acid for each redox system studied [a]

Oxidant	Concentration (M)			REI
	Oxidant	Acid	Sulphite	
Ce(IV)	1.50×10^{-3}	0.50	7.00×10^{-4}	100
$KMnO_4$	4.00×10^{-4}	0.10	1.00×10^{-3}	90
$NaBrO_3$	1.00×10^{-3}	0.50	1.00×10^{-3}	14
$K_2Cr_2O_7$	1.00×10^{-4}	0.10	1.00×10^{-3}	10

[a] Both were supplied at equal flow rates. Ce(IV), permanganate and bromate were supplied at 6.0 ml min^{-1} while dichromate was supplied at 5.0 ml min^{-1}.

3.4. Analytical parameters

The log(emission intensity, mV) vs. log(C, μg ml^{-1}) calibration equations are shown in Table 2. The relative standard deviations for determination of 2.00 and 8.00 μg ml^{-1} of cholic acid were 0.97 and 0.28%, respectively (n = 10), which were typical for all bile acids studied.

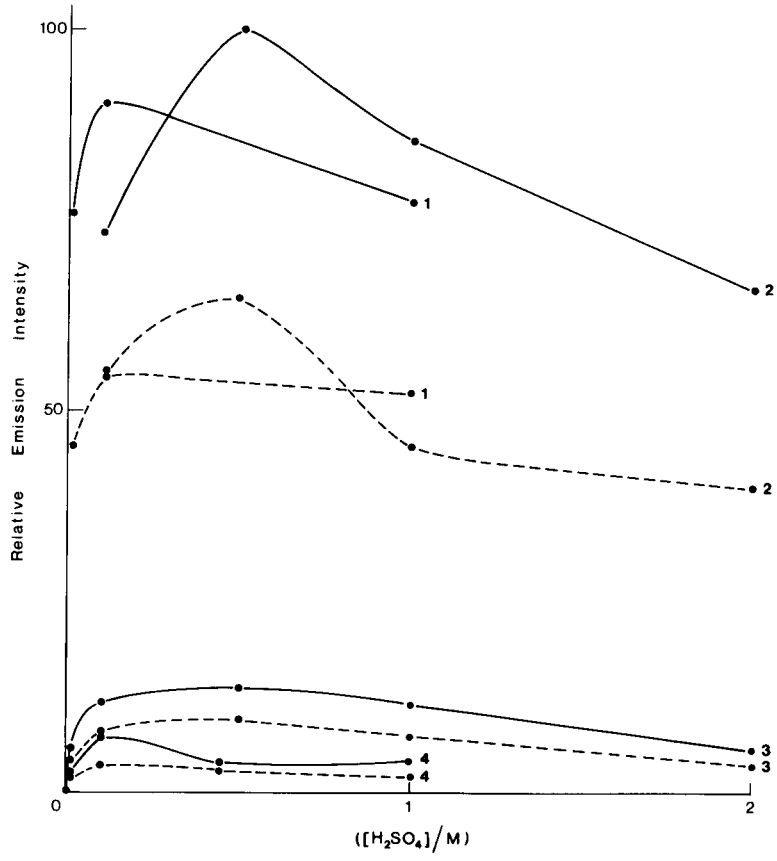

Fig. 5. Effect of concentration of sulphuric acid in (1) 4.00×10^{-4} M permanganate, (2) 1.00×10^{-3} M cerium(IV), (3) 1.00×10^{-3} M bromate and (4) 1.00×10^{-4} M dichromate on the emission intensity from (1, 3 and 4) 1.00×10^{-3} M, and (2) 7.00×10^{-4} M sulphite in the presence of 10.0 (dashed line) and 20.0 (solid line) μg ml^{-1} cholic acid.

Table 2
Analytical characteristics for bile acids by the proposed method

Compound	$\mu g\ ml^{-1}$		Regression line [c]		
	Linear range	LOD [a]	Slope	Intercept	$r\ (n)$ [b]
Cholic acid	2.00–20.0	1.02	0.821	0.568	0.9997 (7)
Ursodeoxycholic acid	2.00–50.0	1.06	0.663	0.674	0.9991 (7)
Chenodeoxycholic acid	3.00–30.0	1.01	0.675	0.581	0.99990 (6)
Deoxycholic acid	2.00–30.0	1.05	0.735	0.946	0.9995 (7)

[a] Limit of detection (analyte concentration giving a signal equal to the intercept plus three times its standard deviation). [b] Correlation coefficient (number of measurements). [c] log(emission intensity, mV) vs. log(C, μg bile acid ml^{-1}).

3.5. Nature of sensitization effect

Bile acids are not fluorogenic compounds and, therefore, cannot be excited by energy-transfer CL. Their ability to form micelles is well-known [28] with typical CMC values of 4.4×10^{-3} and 1.0×10^{-2} M for sodium deoxycholate and cholate, respectively [29]. The highest concentrations within the linear portion of the calibration graphs are in the range of ca. 5×10^{-5}–12×10^{-5} M for sodium cholate and ursodeoxycholate, respectively. These values are below the CMC values. The most reasonable explanation of the sensitization effect of bile acids seems to be the change of normal reduction potential of the oxidant which is accompanied by a wavelength shift of maximum absorbance of the final coloured reaction solution. Hence, the absorption of the CL intensity by the coloured reaction solution is decreased. The suggestion is strengthened by the conclusion that the most intense radiation is generated in the presence of cerium(IV) which forms a variety of complexes while permanganate, bromate and dichromate do not possess this property.

4. Conclusions

The measurement of bile acids by their sensitizing effect on the oxidation of sulphite by some common oxidants is not sensitive for application in biological samples. Nevertheless, it is a direct CL procedure for bile acids and does not require derivatization before the chemiluminogenic reaction. The sensitizing effect of bile acids is currently investigated by other analytical techniques in order to reveal the phenomenon and improve the sensitivity of the proposed method.

References

[1] R.W. Abbott, A. Townshend and R. Gill, Analyst, 111 (1986) 635.
[2] I.I. Koukli, A.C. Calokerinos and T.P. Hadjiioannou, Analyst, 114 (1989) 711.
[3] S.A. Halvatzis, M.M. Timotheou-Potamia and T.P. Hadjioannou, Anal. Chim. Acta, 272 (1993) 251.
[4] R.S. Givens and R.L. Schowen, in J.W. Birks (Ed.), Chemiluminescence and Photochemical Reaction Detection in Chromatography, VCH, New York, 1989.
[5] A. Nishitani, Y. Tsukamoto, S. Kanda and K. Imai, Anal. Chim. Acta, 251 (1991) 247.
[6] W. Baeyens, J. Bruggeman and B. Lin, Chromatographia, 27 (1989) 191.
[7] H. Kouwatli, J. Chalom, M. Tod, R. Farinotti and G. Mahuzier, Anal. Chim. Acta, 266 (1992) 243.
[8] V.K. Mahant, J.N. Miller and H. Thakrar, Anal. Chim. Acta, 145 (1983) 203.
[9] J.L. Burguera and A. Townshend, Talanta, 27 (1980) 309.
[10] M. Yamada and S. Suzuki, Anal. Chim. Acta, 193 (1987) 337.
[11] M. Ishii, M. Yamada and S. Suzuki, Anal. Lett., 19 (1986) 1591.
[12] M. Yamada, T. Nakada and S. Suzuki, Anal. Chim. Acta, 147 (1983) 401.
[13] J.S. Lancaster, P.J. Worsfold and A. Lynes, Analyst, 114 (1989) 1659.
[14] T. Kawasaki, M. Maeda and A. Tsuji, J. Chromatogr., 328 (1985) 121.
[15] S. Higashidate, K. Hibi, M. Seda, S. Kanda and K. Imai, J. Chromatogr., 515 (1990) 577.
[16] I.M. Psarellis, E.G. Sarantonis and A.C. Calokerinos, Anal. Chim. Acta, 272 (1993) 265.
[17] J. Stauff and W. Jaeschke, Atmos. Environ., 9 (1975) 1038.

[18] K. Takeuchi and T. Ibusuki, Anal. Chim. Acta, 174 (1985) 359.
[19] F. Meixner and W. Jaeschke, Fresenius' Z. Anal. Chem., 317 (1984) 343.
[20] R.W.B. Pearse and A.G. Gaydon, The Identification of Molecular Spectra, Chapman and Hall, London, 4th edn., 1976.
[21] I.I. Koukli and A.C. Calokerinos, Anal. Chim. Acta, 236 (1990) 463.
[22] I.I. Koukli and A.C. Calokerinos, Analyst, 115 (1990) 1553.
[23] A.B. Syropoulos, E.G. Sarantonis and A.C. Calokerinos, Anal. Chim. Acta, 239 (1990) 195.
[24] N.T. Deftereos and A.C. Calokerinos, Anal. Chim. Acta, 290 (1994) 190.
[25] S.A. Al-Tamrah, A. Townshend and A.R. Wheatley, Analyst, 112 (1987) 883.
[26] I.I. Koukli, E.G. Sarantonis and A.C. Calokerinos, Analyst, 113 (1988) 603.
[27] I.I. Koukli, E.G. Sarantonis and A.C. Calokerinos, Anal. Lett., 23 (1990) 1167.
[28] D.M. Small, in P.P. Nair and D. Kritchevsky (Eds.), The Bile Acids, Plenum Press, New York, 1971.
[29] B.M. Fung, W. Williams and R.L. Smith, J. Chem. Educ., 55 (1978) 198.

ELSEVIER

Analytica Chimica Acta 294 (1994) 35–42

ANALYTICA CHIMICA ACTA

Chemiluminescent flow sensor for the determination of Paraoxon and Aldicarb pesticides

Aldo Roda [a], Pavel Rauch [b], Elida Ferri [c], Stefano Girotti [c,*], Severino Ghini [c], Giacomo Carrea [d], Roberto Bovara [d]

[a] *Department of Pharmaceutical Sciences, University of Bologna, Bologna, Italy*
[b] *Department of Biochemistry and Microbiology, Institute of Chemical Technology, 166 28 Prague, Czech Republic*
[c] *Institute of Chemical Sciences, University of Bologna, Via S. Donato, 15-40127 Bologna, Italy*
[d] *Institute of Hormone Chemistry, CNR, Via M. Bianco, 9-20131 Milan, Italy*

(Received 15th November 1993; revised manuscript received 11th March 1994)

Abstract

A chemiluminescence-based flow method for the determination of some organophorus and carbamate pesticides based on inhibition of acetylcholinesterase was developed. Acetylcholinesterase in solution or immobilized on methacrylate beads (Eupergit C) was coupled to choline oxidase and peroxidase immobilized on Eupergit C. In this system choline formed by acetylcholinesterase was oxidized by choline oxidase and the H_2O_2 produced was determined via the luminol/peroxidase luminescent reaction. The detection limits (3 σ) for Paraoxon and Aldicarb were 0.75 μg l^{-1} and 4 μg l^{-1}, respectively, when soluble acetylcholinesterase was used under the following optimized experimental conditions: 56 μM luminol in working solution, sample volume 60 μl, flow-rate 0.3 ml min^{-1} and 60 min incubation time. The flow sensor device using all the three enzymes in the immobilized form had a higher detection limit of 125 μg l^{-1} for Paraoxon. The mid-range relative standard deviation ($n = 10$) using 1 mM standard substrate solution was 3.7%. The recovery from contaminated samples (soil, vegetables) varied from 81 to 108%. The results obtained by the developed methods were in good agreement with those obtained by a commonly used colorimetric test.

Key words: Chemiluminescence; Flow system; Carbamates; Organophosphorus compounds; Pesticides

1. Introduction

The increasing use of pesticides all over the world has generated among the scientific community a growing interest for their environmental monitoring. Organophosphorus compounds are powerful inhibitors of the enzymes involved in nerve function [1–3]. Such compounds can form stable complexes with acetylcholinesterase (AChE), thus preventing, by phosphorylation, its function [4–6]. One of the most used organophosphorus pesticides is Paraoxon, an insecticide with a wide range of biological effects and very toxic to mammals; the human oral lethal dose is 5 mg kg^{-1} [2,3,7].

* Corresponding author.

SSDI 0003-2670(94)00118-6

The need for simple, rapid and specific determination of organophosphorus pesticides with a low detection limit has led to the development of a variety of analytical methods for their identification and quantification [8,9]. For preliminary screening, in laboratories where large number of samples must be processed rapidly, a rapid method with adequate sensitivity is thus required [6].

The multianalyte assay of pesticides in food and agricultural commodities requires complex and expensive instrumentation like gas chromatography or high performance liquid chromatography [7–9], and cannot be done easily outside the laboratory. In addition, these methods need time because of sample preparation and preconcentration [10]. On the other hand, enzyme reactors or biosensors offer the great advantage of reducing time and costs by using immobilized biological compounds which are very selective for the analyte [11,12]. Some sensitive enzyme immunoassays for pesticides have been described and are now commercially available [13]. Nowadays, the use of biomolecules such as enzymes and antibodies in flow injection has increased rapidly [14] and the idea to adapt the enzyme inhibition tests to flow systems was put forward recently [6,14]. In vitro enzyme inhibition tests are of great interest because the toxicity of most pollutants, e.g. heavy metals and pesticides, can be extrapolated to in vivo enzyme inhibition. Despite good specificity biochemical tests involving enzyme inhibition could become more reliable than those involving, e.g. gas or liquid chromatography [14]. Only a few biosensors or enzyme tests using acetylcholinesterase and its irreversible inhibition by pesticides have been described until now [10,15–18]. The enzyme activity was measured by a colorimetric reaction in a cuvette [5], in microtiter plates [19], within a flow-injection analysis system [6,14], with AChE electrodes [20–22], also using butyrylcholinesterase [23] and an ISFET (ion-sensitive field effect transistor) [24] or with acetylcholinesterase optrodes [15,25].

The advent of efficient and non-denaturing procedures for the immobilization of enzymes on various carriers has presented opportunities for their practical application. Such water-insoluble enzyme derivatives can be packed into columns and the combination of a flow-injection system with an immobilized enzyme reactor column would seem to have many advantages. These flow systems were succesfully used recently [6,11,12, 14].

This paper describes a simple flow-injection determination of Paraoxon, as a representative organophosphorus pesticide, by three coupled enzyme reactions (where two or three enzymes are immobilized) with a chemiluminescent end-point detection according to the following scheme:

$$\text{Acetylcholine} \xrightarrow{\text{acetylcholinesterase}} \text{acetate} + \text{choline} \quad (1)$$

$$\text{choline} \xrightarrow{\text{choline oxidase}} \text{betaine} + H_2O_2 \quad (2)$$

$$\text{luminol} + 2H_2O_2 + OH^- \xrightarrow{\text{peroxidase}} \text{aminophthalate anion} + N_2 + 3H_2O + \text{light} \quad (3)$$

The chemiluminescent detection is known to be a very sensitive one [11,12] and thus can enable the low detection limit necessary for Paraoxon determination to be reached. Finally, because also carbamates inhibit, but reversibly, acetylcholinesterase [2] the attempt was done to determine Aldicarb as representative compound of this pesticide group.

2. Experimental

2.1. Materials

All chemicals were purchased from Merck (Darmstadt) and were of analytical-reagent grade. Acetylcholinesterase (EC 3.1.1.7, from electric eel, 820 U mg^{-1} or from bovine erythrocytes, 0.46 U mg^{-1}), acetylcholine, choline oxidase (ChOX) (EC 1.1.3.17, 12.7 U mg^{-1}), and Eupergit C (oxirane acrylic beads, approximately 150 μm macroporous particles) were obtained from Sigma (St. Louis, MO). Horseradish peroxidase (HRP) (EC 1.11.1.7, type VI-A, 940 U mg^{-1}) and luminol (5-amino-2,3-dihydro-1,4-phthalazinedione)

were from Boehringer (Mannheim). Paraoxon (diethyl-*p*-nitrophenylphosphate) and Aldicarb [2-methyl-2-(methylthio)propionaldehyde-*O*-methylcarbamoyloxime] were a gift from LabService Analytica (Bologna, Italy). Both pesticides were dissolved in a few drops of dimethylsulfoxide and fresh stock solutions in 0.2 M Tris–HCl [tris(hydroxymethyl)aminomethane–HCl] buffer, pH 8, were prepared before experiments. The same buffer was used to prepare standard solutions. Pyrogen-free purified water (Milli-Q System, Millipore, UK) was used throughout all experiments. The non-treated biological samples were obtained from the private farm Case Bianche (Bologna, Italy).

2.2. Enzyme immobilization

Five different samples of immobilized enzymes were prepared using the same procedure. To each 500 mg of dry Eupergit C were added 1.5 ml of 0.5 M potassium phosphate buffer, pH 8.0, containing respectively: (i) 30 U of choline oxidase, (ii) 1800 U of peroxidase, (iii) 1360 U of acetylcholinesterase (from electric eel), (iv) 30 U of choline oxidase, 1800 U of peroxidase and 7 U of acetylcholinesterase (from bovine erythrocytes), (v) 30 U of choline oxidase and 1800 U of peroxidase.

After standing at room temperature (25°C) for 30 h, the swollen gel was washed with 0.5 M potassium phosphate buffer, pH 8.0, containing 0.1 M triethanolamine and incubated in the same buffer for two hours. Finally, the gel was washed extensively with 0.1 M potassium phosphate buffer, pH 8.0, and stored in the same buffer. For one column, approximately 200 mg of wet weight of Eupergit C were used.

2.3. Working chemiluminescent solution

The working chemiluminescent solution was 0.2 M Tris–HCl buffer, pH 8.0, containing 56 μM luminol. The solution was prepared 20–30 min before analysis. The working chemiluminescent solution was not altered after 8–10 h in the dark at room temperature: the light emission of a standard solution of acetylcholine measured at the end of the working day displayed no significative differences ($\pm$3%) from the same measurement done at the beginning of the day.

2.4. Apparatus

Two manifolds for the chemiluminescent continuous-flow determination of acetylcholinesterase activity and/or determination of choline (Fig. 1) were developed on the basis of similar manifolds previously utilized [11,12].

The first flow system (Manifold A, Fig. 1), making use of a multi-channel peristaltic pump (Minipuls HP4, Gilson) and one small plexiglass column (2 mm I.D., 3 cm length), involved two streams: the first supplied (0.1 ml min^{-1}) the buffer or the sample, injected through a Rheodyne valve equipped with loops of different volumes in the range 20–100 μl, and the second stream (0.2 ml min^{-1}) was a continuous flow of working chemiluminescent solution. The total flow-rate, measured at the output of the apparatus, was 0.3 ml min^{-1}. The column, packed with choline oxidase and peroxidase immobilized on Eupergit C, was positioned inside the luminometer (LKB Model 1250, Sweden) in front of the photomultiplier window. The samples consisted of acetylcholinesterase and acetylcholine with or without pesticide. The second flow system (Manifold B, Fig. 1) uses two columns: the first column was packed with Eupergit C-immobilized acetylcholinesterase (from electric eel) placed outside the luminometer (B) and the second one was the

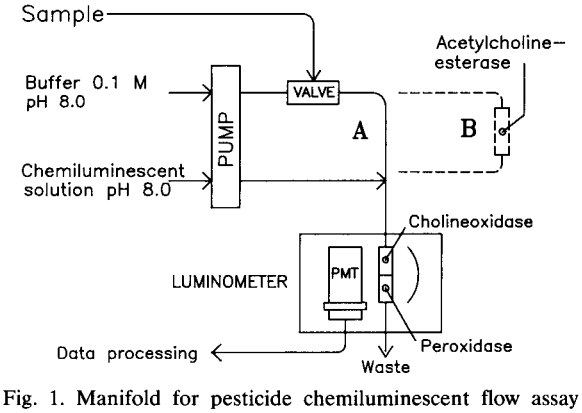

Fig. 1. Manifold for pesticide chemiluminescent flow assay with (A) free or (B) immobilized acetylcholinesterase.

same as in manifold A. Acetylcholine, with or without pesticide, served as the substrate. All other arrangements were identical to those of former system A.

2.5. Recovery tests

An amount of 2 g of sample was homogenized and mixed with 10 ml of 0.2 M Tris–HCl buffer, pH 8.0. To the homogenate (2 ml) was added a known amount of Paraoxon and the samples were kept at room temperature for 1 h to allow an homogeneous distribution of the pesticide. After this time the sample was filtered through filter paper and the residue was washed twice with 1 ml of the same buffer. The filtrate was refiltered by a membrane filter (pore size 0.2 μm, Millipore, UK). An aliquot (40 μl) of the filtrate was incubated for 1 h with 20 μl of a suitable amount of acetylcholinesterase (ca. 20 mU). After that, 20 μl of 5 mM acetylcholine were added and 60 μl of the reaction mixture were immediately used for luminescent measurement.

2.6. Inhibition measurements

The percentage inhibition ($I\%$) was calculated on the basis of the following equation:

$$I\% = \frac{H_0 - H_i}{H_0} 100$$

where H_0 is the peak height in the absence of inhibitor and H_i is the peak height in the presence of inhibitor.

2.7. Colorimetric assay

Spectrophotometric determination of Paraoxon was carried out by using a "Cholinesterase Inhibition Test", produced by Boehringer Mannheim, according to the manufacturer's instructions.

3. Results and discussion

3.1. Optimization of experimental conditions

All experiments were carried out with acetylcholinesterase from electric eel because the enzyme from bovine erythrocytes had too low an activity.

In manifold A, luminol concentration, flow-rate and sample volume were selected following preliminary tests to optimize the conditions for maximum light emission and reproducibility.

The light emission increased by increasing luminol concentration and approached its maximum at 56 μM above which the light intensity slightly decreased. Therefore, this luminol concentration was used for routine analysis of samples.

The effect of sample volume was tested over a wide range (20–100 μl). The highest peaks were obtained with 60-μl samples and therefore this volume was used through all analyses. The analytical signal was not significantly increased by larger volumes and the peaks were broader and lower.

The best total flow-rate was 0.3 ml min^{-1}. The lower responses obtained with other flow-rates can be attributed to the decrease in the contact time between the immobilized enzymes and the substrates (higher flow-rates), or to products accumulation (lower flow-rates), which is known to inhibit the enzymes [4]. The optimal pH and ionic strength of the working chemiluminescence buffer was found to be 0.2 M Tris–HCl, pH 8.0, according to literature data [5].

Finally, the optimal amount of choline oxidase and peroxidase, separately immobilized, was tested (Fig. 2). It was found that, under the conditions used for enzymes immobilization, the largest signal was obtained at a 16:1 (w/w) ratio of choline oxidase to peroxidase. Therefore a column prepared in this way was used for all experiments. Other ratios of immobilized enzymes gave significantly lower responses, as shown in Fig. 2.

3.2. Paraoxon and Aldicarb determination

Measurements were carried out using manifold A (Fig. 1) and pesticide standard solutions in the range 0–100 $\mu g\ l^{-1}$. It is well known that the inhibition of acetylcholinesterase by organophosphates and carbamates is time dependent [20]. At a fixed concentration of pesticide, the degree of inhibition increases with increase in the incuba-

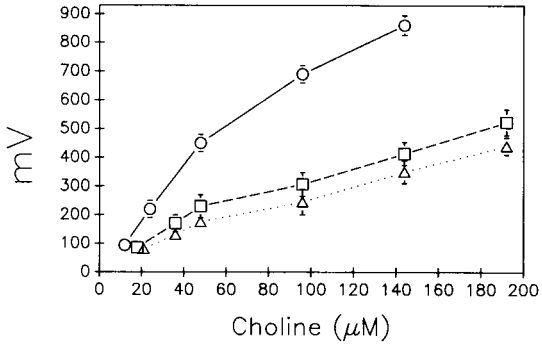

Fig. 2. Effect of different ratios of immobilized choline oxidase to peroxidase on peak height of luminescent signal (mV) at various concentrations of choline (μM). 8:1 (△), 16:1 (○) and 32:1 (□) choline oxidase:peroxidase ratios.

tion time (Fig. 3), reaching a maximum after 1 h. At longer incubation times the increase in inhibition becomes negligible. A 30-min incubation time allows, for both compounds, a detection limit of 100 $\mu g\ l^{-1}$ to be attained, enough for routine screening analysis; to obtain a more sensitive system, therefore, the determination of Paraoxon and Aldicarb in standard solutions was carried out after 60-min incubation of acetylcholinesterase with pesticide, giving a detection limit of 0.75 $\mu g\ l^{-1}$ for Paraoxon and 4 $\mu g\ l^{-1}$ for Aldicarb.

For the determination of low concentrations of pesticides it was better to use a higher concentration of substrate (5 mM acetylcholine). In contrast, to increase the calibration linearity or to determine higher concentrations of pesticides it was preferable to use a lower level of acetylcholine (0.5 mM) (Fig. 4). In this way it was possible to obtain good calibration linearity over the range 0–100 $\mu g\ l^{-1}$ for Aldicarb ($y = 0.42x + 0.61$; $r = 0.997$, $n = 7$) and over the range 0–75 $\mu g\ l^{-1}$ for Paraoxon ($y = 0.94x + 2.46$; $r = 0.995$, $n = 6$), where y is peak height intensity (arbitrary units) and x is the pesticide concentration ($\mu g\ l^{-1}$).

The analytical characteristics for determination of Paraoxon and Aldicarb are shown in Table 1. The use of soluble acetylcholinesterase allows, in our system, very low detection limits with low relative standard deviations to be obtained. The throughput of samples was 15 per hour.

3.3. Assay with immobilized acetylcholinesterase

Many researchers have tried to construct biosensors using immobilized acetylcholinesterase [6,14,20–25] with the disadvantage of the irreversible inhibition of this enzyme, and the advantage of eliminating laborious pretreatment. In manifold B with immobilized acetylcholinesterase (Fig. 1), acetylcholine is completely hydrolyzed since the same signals were obtained for acetylcholine and choline at the same molar concentrations, but the detection limit was fairly poor (40 $\mu g\ l^{-1}$), as reported in Table 1. There were several reasons for this: with the two-column ar-

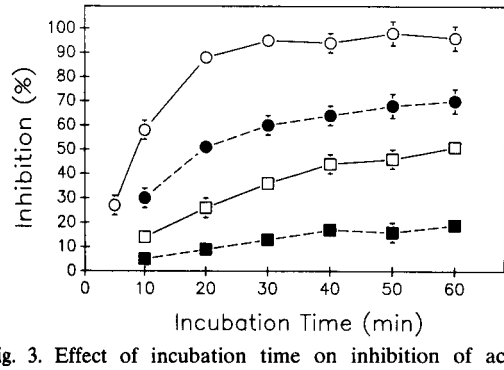

Fig. 3. Effect of incubation time on inhibition of acetylcholinesterase by pesticides. Paraoxon: 100 $\mu g\ l^{-1}$ (○) and 10 $\mu g\ l^{-1}$ (□); Aldicarb: 100 $\mu g\ l^{-1}$ (●) and 10 $\mu g\ l^{-1}$ (■).

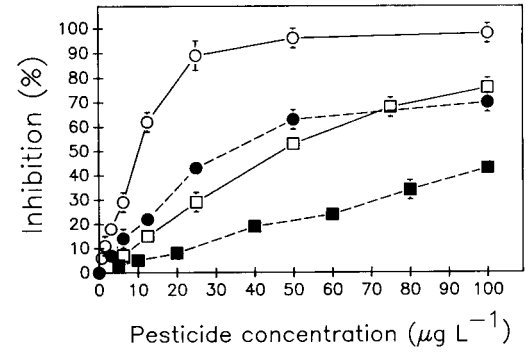

Fig. 4. Effect of pesticide concentration ($\mu g\ l^{-1}$) on inhibition of acetylcholinesterase after 60 min incubation at different acetylcholine concentrations. Paraoxon: at 5 mM acetylcholine (○) and at 0.5 mM acetylcholine (□); Aldicarb: at 5 mM acetylcholine (●) and at 0.5 mM acetylcholine (■).

Table 1
Analytical characteristics for Paraoxon and Aldicarb determination

Immobilized enzymes	Detection limit [a]			
	Paraoxon		Aldicarb	
	$\mu g\ l^{-1}$	R.S.D. (%) [c]	$\mu g\ l^{-1}$	RSD (%) [c]
Choline oxidase + peroxidase	0.75	3.8	4	6.6
Acetylcholinesterase + choline oxidase + peroxidase	125	28	n.d. [b]	n.d.

[a] 3σ values.
[b] n.d. = Not determined.
[c] Relative standard deviation for 10 measurements.

Table 2
Matrix effect of samples of different nature on the response of the choline oxidase–peroxidase reactor

Sample	Response [a]		A/C
	Acetylcholine (5 mM) + acetylcholinesterase (20 mU) (A)	Choline (5 mM) (C)	
Soil	94	90	1.04
Cabbage	54	56	0.96
Tomato	85	82	1.04
Melon	64	62	1.03
Salad	44	42	1.05
Salad (Brasil)	53	54	0.98
Water	102	102	1.00
Buffer	100	100	1.00

[a] Relative to buffer taken as 100.

rangement the concentration of Paraoxon in the acetylcholinesterase column is three times lower than in the injected sample; the short contact time of the pesticide with acetylcholinesterase (prolongation of incubation time by stopping the flow did not improve the situation); and the Michaelis–Menten constant of this enzyme after immobilization is markedly greater (2.6 mM) than that for the soluble enzyme (0.18 mM).

3.4. Samples assay

Manifold A was used to determine Paraoxon added at known concentrations to samples that had not been treated previously with pesticides. The extracts of the untreated samples, with the exception of water and soil, surprisingly decreased significantly the light emission when using acetylcholine plus acetylcholinesterase (first row, Table 2). This effect could be caused either by unknown contamination by pesticides on the samples, theoretically free from each type of pesticide, or simply by the matrix itself. To solve this problem a molar concentration of choline equal to the acetylcholine concentration (5 mM) was added to the extracts. The results were closely similar to those obtained for acetylcholine plus acetylcholinesterase, as proved by acetylcholine : choline response ratios which for all samples were very close to 100% (Table 2). It is therefore likely that extracts influence the response by quenching the light emission by the immobilized choline oxidase–peroxidase reactor and not by inhibiting acetylcholinesterase activity. To overcome this drawback, it seemed to be necessary to compare the inhibition caused by samples containing pesticides with the results obtained with non-contaminated samples in the same matrix. This hypothesis was proved by addition of two different concentrations of Paraoxon to plant tissue homogenates (Table 3). The results clearly show the feasibility of the developed method. The recovery

Table 3
Recovery of Paraoxon from samples of different nature

Sample	Recovery (%) ± S.D. [a]	
	10 $\mu g\ l^{-1}$	100 $\mu g\ l^{-1}$
Soil	90.3 ± 3.8	106 ± 4
Cabbage	89.8 ± 4.6	108 ± 5
Tomato	93.5 ± 2.8	101 ± 3
Melon	87.1 ± 1.9	104 ± 5
Salad	81.6 ± 3.9	99 ± 6
Salad (Brasil)	80.8 ± 6.1	91 ± 8
Water	106.0 ± 2.0	102 ± 2
Buffer (treated as samples)	99.5 ± 1.1	101 ± 1
Buffer (control)	100.0 ± 1.2	100 ± 2

[a] Standard deviation for 6 measurements.

at the 100 μg l^{-1} level was satisfactory. The lower recovery at 10 μg l^{-1} level may be caused by partial absorption and/or cleavage of Paraoxon in the analyzed homogenates.

3.5. Correlation of luminescent and colorimetric determination of Paraoxon

The results obtained from samples contaminated at different levels by Paraoxon were also checked by a standard colorimetric method. The calculated linear regression and correlation coefficient were: $y = (1.03 \pm 0.04)x - (1.45 \pm 0.09)$, $r = 0.997$, $n = 7$, $P < 0.001$, where y are the resets of the colorimetric method and x those of the luminescence assay. This indicates a very good agreement between the results of the luminescence and colorimetric methods over a wide range of Paraoxon concentrations.

4. Conclusions

The results showed that Paraoxon determination with soluble acetylcholinesterase was about 2 orders of magnitude more sensitive than that with immobilized enzyme. However, the use of soluble acetylcholinesterase is not a drawback from the operative point of view. Thus, in the preparation of 20–40 samples, one can incubate the sample with enzyme for 60 min, and immediately afterwards start the analyses, which makes it possible to obtain the first results after 1 h with a throughput of 2–4 min per sample. This method can also easily be carried out outside the laboratory if the non-immobilized reagents are batched previously and treated to avoid degradation, for example by lyophilisation.

The residual activity of the immobilized choline oxidase–peroxidase system after 1 week of use and analysis of about 60 samples per day was about 50% of the original. The lifetime of the proposed sensor, defined as the time during which accurate results can be obtained within the full calibration range, was about 2 weeks.

The developed method is, in comparison with other biosensing systems described recently [6,14,20–25], similarly simple and fast, but with a better sensitivity and good reproducibility.

Acknowledgement

This research was supported by grants from MURST (Ministero della Università e della Ricerca Scientifica e Tecnologica) and by Community's Action for Cooperation in Science and Technology with Central and Eastern European Countries, No. 0693.

References

[1] J.R. Corbett (Ed.), The Biochemical Mode of Action of Pesticide, Academic Press, New York, 1974.
[2] J.R. Coats (Ed.), Insecticide Mode of Action, Academic Press, New York, 1982.
[3] P.A. Dahm, in R.D. O'Brien and I. Yamamoto (Eds.), Biochemical Toxicology of Insecticides, Academic Press, New York, 1970.
[4] H.U. Bergmeyer, M. Grassi and H.-E. Walter, in H.U. Bergmeyer (Ed.), Method of Enzymatic Analysis, Vol. II, Verlag Chemie, Weinheim, 1983, p. 128.
[5] M. Whittaker, in H.U. Bergmeyer (Ed.), Method of Enzymatic Analysis, Vol. IV, Verlag Chemie, Weinheim, 1984, p. 52.
[6] M.E. Leon-Gonzalez and A. Townshend, Anal. Chim. Acta, 236 (1990) 267.
[7] G. Russo and S. Calmotti, Chim. Ind., 71 (1989) 52.
[8] A.K. Singh, R.J. Zeleznikar and L.R. Drewes, J. Chromatogr., 324 (1985) 163.
[9] M.L. Shih and R.I. Ellin, Anal. Lett., 19 (1986) 2197.
[10] P. Herzsprung, L. Weil, K.E. Quentin and I. Zombola, Wasser, 74 (1990) 399.
[11] A. Roda, S. Girotti, S. Ghini and G. Carrea, J. Biolumin. Chemilumin., 4 (1989) 423.
[12] S. Girotti, E. Ferri, S. Ghini, P. Rauch, G. Carrea, R. Bovara, A. Roda, M.A. Giosuè, P. Masotti and G. Gangemi, Analyst, 118 (1993) 849.
[13] J.S. Collins, Anal. Proc., 30 (1993) 74.
[14] R. Kindervater, W. Künnecke and R.D. Schmid, Anal. Chim. Acta, 234 (1990) 113.
[15] W. Höbel and J. Polster, Fresenius J. Anal. Chem., 343 (1992) 101.
[16] G.G. Guilbault, M.H. Sadar, S.S. Kuan and D. Casey, Anal. Chim. Acta, 52 (1970) 75.
[17] G. Schmaland and M. Schulert, Acta Hydrochim. Hydrobiol., 14 (1986) 19.
[18] H. Breuer, J. Chromatogr., 243 (1982) 183.

[19] P.S. Hammond and J.S. Forster, Anal. Biochem., 180 (1989) 380.
[20] M. Bernabei, C. Cremisini, M. Mascini and G. Palleschi, Anal. Lett., 24 (1991) 1317.
[21] M. Bernabei, S. Chiavarini, C. Cremisini and G. Palleschi, Biosensors Bioelectronics, 8 (1993) 265.
[22] P. Skládal, Anal. Chim. Acta, 252 (1991) 11.
[23] L. Campanella, M. Achilli, M.P. Sammartino and M. Tomassetti, Bioelectrochem. Bioenerg., 26 (1991) 237.
[24] C. Dumschat, U. Müller, K. Stein and G. Schwedt, Anal. Chim. Acta, 252 (1991) 7.
[25] K.R. Rogers, C.J. Cao, J.J. Valdes, A.T. Eldefrawi and M.E. Eldefrawi, Fundam. Appl. Toxicol., 16 (1991) 810.

ELSEVIER

Analytica Chimica Acta 294 (1994) 43–47

ANALYTICA CHIMICA ACTA

Continuous flow assay of ammonia in plasma using immobilized enzymes

R. Quiles [a], J.M. Fernández-Romero [b], E. Fernández [a], M.D. Luque de Castro [b,*]

[a] *Department of Biochemistry, Hospital Virgen de la Salud, E-45005 Toledo, Spain*
[b] *Department of Analytical Chemistry, Faculty of Sciences, University of Córdoba, E-14004 Córdoba, Spain*

(Received 1st February 1994)

Abstract

A simple, convenient and rapid enzymatic method for the determination of ammonia in plasma based on the immobilization of glutamate dehydrogenase and on a continuous flow system is proposed. The fixed-time measuring principle allows shortening of the assay time without loss of sensitivity, so a sampling frequency of 40 h^{-1} can be achieved in a linear range of 5–500 μM with a coefficient of variation of less than 2%. The method correlates well with the results of the Kodak Ektachem analyzer and can also successfully be compared with other automated batch methods which it surpasses in rapidity, simplicity and lower cost of the assay.

Key words: Enzymatic methods; Flow-injection analysis; Ammonia; Immobilized enzymes; Plasma

1. Introduction

Data on the ammonia content of plasma are of great value in the management of hepatic coma when intoxication is suspected, in the iatrogenic hyperammonemia of the newborn with possible defects involving enzymes of the urea cycle, in Eck's fistula, and in Reye's coma syndrome. It is a test frequently requested in a variety of situations, particularly on paediatric subjects. Among the analytical techniques available for the determination of ammonia in plasma, enzymatic assays are the methods of choice because they are simple, rapid, and specific. Plasma ammonia determinations with use of glutamate dehydrogenase [GLDH, L-glutamate: $NAD(P)^+$ oxidoreductase (deaminating), EC 1.4.1.3.] were introduced by Mondzac et al. in 1965 [1]. The earlier ammonia separation techniques of distillation [2,3] and ion-exchange chromatography [4–6] were eliminated in favour of the substrate-specific glutamate dehydrogenase, which acts as follows:

$$\text{2-Oxoglutarate} + NH_4^+ + \text{NADH} \xrightarrow{\text{GLDH}} NAD^+ + \text{Glutamate} + H_2O$$

When 2-oxoglutarate, GLDH and reduced nicotinamide adenine dinucleotide (NADH) are present in excess, the equilibrium of the reaction lies far to the right. The reaction can then be

* Corresponding author.

SSDI 0003-2670(94)00120-B

followed by measuring the total consumption of NADH [7–9] or by measuring the reaction rate [10–13]. Kinetic methods [14,15] were proposed at the end of the seventies to reduce assay time as the reaction takes more than 40 min for completion [15]. No recent contributions to or improvements of those enzymatic methods, either by batch or continuous approaches, have been reported.

The flow-injection (FI) technique has been used here to propose a continuous fixed-time method for plasma ammonia determination based on the immobilization of the catalyst on a suitable support (controlled-pore glass), and its subsequent package in a microcolumn, making its usage more reliable and inexpensive. Despite the number of methods for ammonia/ammonium determination described in the literature on FI [16] none of them is based on enzyme catalysis.

2. Experimental

Instruments and apparatus

A Perkin-Elmer 204 spectrofluorimeter equipped with a Hellma 178.12QS flow-cell (inner volume 25 μl) and connected to a Perkin-Elmer E56 recorder and a Perkin-Elmer UDR3 voltammeter was used. A Gilson Minipuls-2 four-channel peristaltic pump with rate selector, a Rheodyne 5041 low-pressure injection valve, a PTFE tubing of 0.5 mm I.D., a Julabo 5 water-bath thermostat and a Beckman ϕ72 pH meter were also used. A Kodak Ektachem 700 XR automated analyzer (ammonia assay based on dialysis, reaction with Bromophenol Blue and reflectometric measurements at 600 nm) was used for the correlation study.

A 150 mM triethanolamine (Merck 8379) solution (pH 8.0, adjusted with 5 M HCl) was used as carrier. Reagent 1 (R_1) was a solution of 25 mM 2-oxoglutarate (Sigma K-1750), 1 mM adenosine 5'-diphosphate (Sigma A-4386) and 0.2 mM NADH (Sigma N-8129) in the triethanolamine buffer. $(NH_4)_2SO_4$ (Merck 1217) was used for preparing the standards. The reagents used for immobilization of the enzyme were (3-aminopropyl)triethoxysilane (Aldrich, No. 11,339-5), glutaraldehyde (Merck, No. 820603) and controlled-pore glass 240 (120–200 mesh) (Electronucleonics, Fairfield, NJ).

Distilled water from a Millipore Milli-RQ system was used throughout the experiments.

Samples

Heparinized plasma was collected in Venojet tubes (Terumo Europe N.V. 3001, Leuven, Belgium). Prior to their injection into the FI manifold the samples were diluted (1:5, v/v) with the buffer/carrier solution.

Standards

A 0.5 mM aqueous solution of $(NH_4)_2SO_4$ was prepared from another more concentrated solution (50 mM) and both were kept at 4°C. Ammonia standards of 25, 50, 100 and 200 μM were prepared daily from the former and used for calibrating the FI system.

Immobilization and storage of GLDH

The catalyst was immobilized by using the Masoom and Townshend procedure [17]. The enzyme–support conjugate was packed into glass tubings of 1.0 mm I.D. and different lengths (IMERs), whose ends were packed with filter material to avoid loss of enzyme support, and placed in the continuous flow system. When not in use, the IMERs were stored at 4°C in a 10 mM (pH 6.0) triethanolamine buffer with 50% glyc-

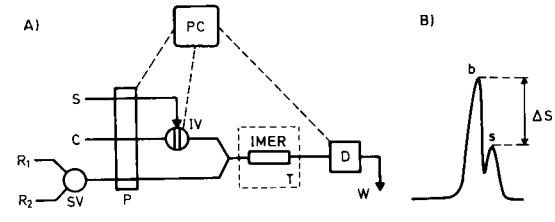

Fig. 1. (A) Flow-injection manifold for the enzymatic determination of ammonia. S = sample; C = carrier; SV = switching valve; R_1 = reagent mixture; R_2 = reagent mixture without 2-oxoglutarate; P = peristaltic pump; IV = injection valve; IMER = reactor of immobilized glutamate dehydrogenase; D = fluorimetric detector; W = waste. (B) Blank (b) and sample (s) peaks and analytical signal (AS).

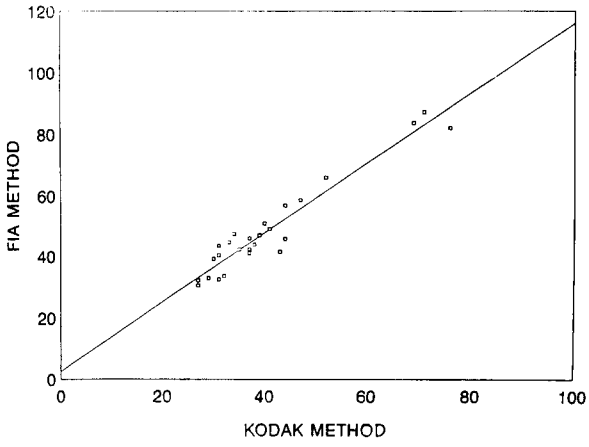

Fig. 2. Correlation graph of proposed method versus Kodak Ektachem method.

erol, where their activity remained stable for at least eight months.

Flow-injection manifold and procedure

Fig. 1A is a scheme of the continuous-flow configuration used in which the sample, after a 1:5 dilution, is aspirated and fills the loop of the injection valve (IV), which inserts the 300-μl plug into the buffer carrier. After merging with the substrate–coenzyme mixture the plug reaches the IMER where conversion of the coenzyme into the oxidized form takes place before reaching the detector where the decrease in fluorescence due to NADH consumption is monitored. The switching valve (SV) allows to select either the R_1 or R_2 channels for sample or blank measurements, respectively. The difference between blank and sample negative peaks provides the value of the contribution of ammonia (Fig. 1B) and is used as the analytical signal. The FI system and the reagent reservoirs are kept at 37°C during the assay.

3. Results and discussion

Optimization of variables

The variables which affect the overall system can be classified into chemical, FI and physical ones. Table 1 shows this classification; the ranges within the variables were studied and the optimal values found.

Chemical variables. Triethanolamine buffer was chosen as the best after checking that phosphate buffer caused partial inhibition of the enzyme. The maximal value of the analytical signal was obtained at pH 8.0, and decreased for lower and higher values of the buffer pH. A 0.2 mM NADH solution was selected as higher values produced partial enzyme inhibition, while lov er ones shortened the range in which the analytical signal was proportional to the analyte concentration.

A saturated solution of substrate (20 mM) provided the maximal rate of the enzymatic reaction.

ADP acted as an activator of GLDH up to a 1 mM concentration. At higher values the activator effect remained constant. In addition to this effect, ADP in the reagent stream minimized the interference of endogenous ADP in the samples and stabilized the biocatalyst [16].

A 5-cm length of the IMER ensured total consumption of the analyte for ammonia concentrations in the samples below 1 mM.

Physical variable. The increase in temperature had a positive effect on the enzymatic reaction up to 40°C; above this temperature the analytical signal decreased due to the denaturation of the immobilized biocatalyst.

Table 1
Optimization of variables affecting the overall system

Type	Variable	Range studied	Optimal value
Chemical	Triethanolamine (mM)	–	150
	pH	6 – 8.5	8
	NADH (mM)	0.05– 0.4	0.2
	2-Oxoglutarate (mM)	5 – 40	25
	ADP (mM)	0 – 2	1
	IMER length (cm)	1 – 7	5
Physical	Temperature (°C)	20 – 45	37
FI	Flow-rate (ml min^{-1})	0.5 – 1.2	0.8
	Injected volume (μl)	50 –500	300

Flow-injection variables. The increment of the injection volume from 50 to 300 μl provided a growing signal, but above 300 μl the increase was slight and the peak very wide, which was detrimental to the sampling frequency. Although the analytical signal decreased on increasing the flow-rate, a compromise value of 0.8 ml min^{-1} was taken which allowed to perform 40 assays per hour.

Halting of the flow when the sample–substrate plug was in the IMER was assayed in order to improve the sensitivity of the method. No significant increase in the analytical signal was observed, which indicated completion of the enzymatic reaction in the working dynamic regime.

The above-commented studies were performed using aqueous ammonia samples. When plasma samples were injected, their native fluorescence made it necessary to inject two aliquots of the sample into the manifold: (1) merging of R_2 [reagent solution without one of the substrates (2-oxoglutarate)] with the main channel. The signal obtained corresponded to the native fluorescence of the sample in the highly fluorescent carrier. (2) switching SV and merging R_1 with the main stream. In this case the signal obtained is a contribution of both the native fluorescence and the consumption of NADH due to the enzymatic reaction (see Fig. 1B).

Features of the method

Seven standard solutions in the range 5–500 μM were prepared to run the calibration graph. The linear equation obtained was as follows:

$$Y = (7.9 \pm 0.9) + (1.019 \pm 0.007)X$$

where Y is the relative fluorescence, expressed in mV, and X is the ammonia concentration in μM. The S_{xy} and r^2 values were 1.63 and 0.999990, respectively.

The system was calibrated every day before starting work.

Precision and recovery of the method

The precision of the method was checked by injecting in triplicate controls at three concentration levels (I, 50; II, 100; and III, 250 μM for the within-run study and I, 60; II, 115; and III, 175 μM for the between-run study). The coefficient of variation was smaller than 2% (see Table 2) for both studies.

Table 2
Precision of the proposed method

	Concentration level	n	Average	C.V.%
Within run	I	11	52.11	1.6
	II	11	92.09	1.3
	III	11	253.27	0.8
Between run	I	10	60.15	1.8
	II	10	116.15	1.7
	III	10	174.30	1.7

I, II, III: 50, 150 and 250 μM for the within-run study and 60, 115 and 175 μM for the between-run study.

The analytical recovery was determined by adding to the plasma-pool aliquots two amounts of aqueous ammonia standards (50 and 200 μM). The recoveries were in the range 94–110% in all instances.

Effects of potentially interfering substances

The effects of potential interferents, including anticoagulants and endogenous components of blood were investigated [18]. All specimens were prepared by adding the test material to normal plasma. The determinations involved two measurements (blank and sample). Both heparinized plasma (2 g l^{-1}) and samples collected in EDTA (20 μM) were used to check the influence of these anticoagulants as an unstable initial absorbance was observed by Dorwart and Saner [19]. No differences were observed between both types of samples. No interference was caused by the presence of creatinine (2.0 μM), bilirubin (0.4 μM), oxalate (10 mM), citrate (10 mM) and albumin (1.3 mM).

Comparison of methods

Regression parameters for comparison of 26 heparinized plasma samples by the proposed continuous-flow method, Y (samples injected in triplicate) and the Kodak Ektachem 700 XR ana-

lyzer, X, were as follows: slope: 1.1; intercept: 2.3; correlation coefficient: 0.960. The higher values found by the conventional method can be justified since the standards prepared to be used in developing the proposed method would have a slightly higher concentration than those of the Kodak analyzer. This is supported by two facts: (a) when our standards were used in the Kodak analyzer the signals were higher than those provided by the Kodak standards of the same concentration; (b) the commercial Kodak standards for ammonia provided higher values than those obtained by this analyzer both when used in the proposed manifold and in the manual enzymatic method (Boehringer Mannheim, Monotest Ammonia, Ref. 125857). The analysis time is similar for the Kodak and the proposed methods, but the cost of the analysis is dramatically reduced in the FI method.

Compared with the commercial manual enzymatic method the one proposed here shows advantages such as the dramatic reduction of both the analysis time (from 30 to 5 min) and the sample volume (from 1 ml to 50 μl). In addition, the possibility of contamination from the environment is excluded in the FI method.

With regard to time the proposed method surpasses that one proposed by Li and Shull based on the use of a centrifugal analyzer [14] in which though the analysis time for a run was 70 s, it required manual sample delivery and a 10-min preincubation time. The FI method also surpasses the previous enzymatic methods reducing costs both by substituting NADPH by NADH and by immobilizing the biocatalyst in a very stable way.

In cases where the use of a fluorimetric detector can be a shortcoming, a conventional spectrophotometer could be used.

Acknowledgements

We thank Dirección General de Investigación Científica y Técnica for financial support.

References

[1] A. Mondzac, E.G. Ehrlich and J.E. Seegmiller, J. Lab. Clin. Med., 66 (1965) 526.
[2] E.J. Conway and A. Byrne, Biochem. J., 27 (1933) 419.
[3] D. Seligson and K. Hirahara, J. Lab. Clin. Med., 49 (1957) 962.
[4] S.G. Dienst, J. Lab. Clin. Med., 58 (1961) 149.
[5] G.E. Miller and J.D. Rice Jr., Am. J. Clin. Pathol., 39 (1963) 97.
[6] J.H. Hutchinson and D.H. Labby, J. Lab. Clin. Med., 60 (1962) 170.
[7] K.L. Fawaz and K. Von Dahl, Leban. Med. J., 16 (1963) 169.
[8] K.L. Reichelt, E. Kvamme and B. Tveit, Scand. J. Clin. Lab. Invest., 16 (1964) 433.
[9] I. Oreskes, C. Hirsh and S. Kupfer, Clin. Chim. Acta, 26 (1969) 185.
[10] A. Ishihara, K. Kurahasi and H. Uehara, Clin. Chim. Acta, 41 (1972) 255.
[11] H.A.M. Jacobs and F.M.G. Olthuis, Clin. Chim. Acta, 43 (1973) 81.
[12] H.C. Van Anken and M.E. Schiphorst, Clin. Chim. Acta, 56 (1974) 151.
[13] F. Von da Fonseca-Wollheim, J. Clin. Chem. Clin. Biochem., 11 (1973) 421.
[14] P.K. Li and B.C. Shull, Clin. Chem., 25 (1979) 611.
[15] A.W. Bruce, C.M. Leiendecker and E.F. Freier, Clin. Chem., 24 (1978) 782.
[16] B. Karlberg and G.E. Pacey, Flow Injection Analysis. A Practical Guide, Elsevier, Amsterdam, 1989, p. 244.
[17] M. Masoom and A. Townshend, Anal. Chim. Acta, 166 (1984) 111.
[18] B.A. Humphries, M. Melnychuk, E.J. Donegan and E.D. Snee, Clin. Chem., 25 (1979) 26.
[19] W.V. Dorwart and M. Saner, Clin. Chem., 38 (1992) 16.

ELSEVIER

Analytica Chimica Acta 294 (1994) 49–56

ANALYTICA CHIMICA ACTA

Flow-injection analysis with bulk extraction based optical sensor membranes

Peter C. Hauser *, J. Christopher Litten

The University of Auckland, Department of Chemistry, Private Bag 92019, Auckland, New Zealand

(Received 31st January 1994)

Abstract

The use of recently described optical sensing membranes as solid phase photometric detectors in flow-injection analysis is described. These membranes are based on ionophores and lipophilic pH indicators contained in poly(vinyl chloride). The flow-injection mode of operation not only automates measurements with these optode membranes but also allows on-line mixing of the samples with pH buffer. The method therefore represents a good solution to the pH cross-sensitivity of the membranes. Absorbance measurements were carried out with a light emitting diode/photodiode transducer which was connected directly to an integrated circuit logarithmic amplifier. This inexpensive detector system allows highly precise absorbance measurements. It is further demonstrated that simultaneous measurements can easily be carried out with a slightly modified assembly.

Key words: Flow injection; Sensors; Bulk extraction; Optical sensor membranes

1. Introduction

A design principle for optical sensing membranes recently developed by Simon and coworkers [1–13] relies on the extraction of the analyte into a thin poly(vinyl chloride) (PVC) membrane. Such membranes have been described by that group for the determination of K^+ [1], NH_4^+ [2], Na^+ [3], Ca^{2+} [4], Zn^{2+} [5], Pb^{2+} [6], NO_3^- [7,8], Cl^- [9], HSO_3^- [10], ethanol [11], H_2O [12] and NH_3 [13,14]. Lipophilic specific reagents, often ionophores known from ion-selective electrodes, are dissolved in the membrane. The two functions of analyte recognition and optical response may or may not be contained in the same molecule, and the response behaviour is governed by the solvent extraction and electroneutrality principles [15]. Commonly a lipophilic pH indicator is incorporated in the membrane, and it is the protonation respectively deprotonation of this indicator, coupled to the extraction of analyte from the sample through the electroneutrality principle, which is monitored. The cross-sensitivity for pH generally requires pH buffering of all samples and standards. To date the measurements have been carried out by casting the membranes onto glass disks mounted in a special cell which was placed in a conventional spectrophotometer. Solutions were premixed with pH buffer prior to the measurements [1–14]. Flow-injection analysis (FIA) provides an elegant

* Corresponding author.

SSDI 0003-2670(94)00121-2

on-line means to carry out this otherwise tedious pretreatment. The sample volume required is also significantly reduced in the FIA method. Furthermore, for some of this type of membranes relatively slow response times have been obtained. The precise timing and reproducibility of the FIA mode should allow the acquisition of transient signals without the need to wait for steady state. The use of transducers based on light-emitting diodes (LEDs) and photodiodes represents a significant simplification of the detection cell while allowing a precision of absorbance measurements equal to or better than conventional photometers. The use of LEDs for transmittance measurements is well established and LED/photodiode couples have been used for flow cells in photometric FIA detection [16]. It has also been shown that direct absorbance measurements with LEDs may be obtained by employing a logarithmic converter [17,18]. Some loss of sensitivity compared to measurements with a spectrophotometer may be found depending on the extent of the spectral match, but this is not a problem because of the high precision obtained with the optoelectronic devices. A slight curvature due to the not strictly monochromatic nature of the LED light sources may be encountered for calibration graphs otherwise following Beer-Lambert's law [18].

The use of chemical sensors in FIA leads to a simplification of the system and may provide higher selectivity compared to the common spectrophotometric mode of operation. The often expensive reagent streams can be omitted. Electrochemical sensors such as ion-selective electrodes have therefore often been employed in flow-injection analysis. The use of optical sensors on the other hand has rarely been reported. This is not surprising considering that these devices are not as well established as electrochemical sensors. Reports on simple absorbance type reversible optical chemical sensors in FIA have largely been limited to the use of commercial indicator pads for pH measurements [19,20]. The term optosensing has been employed in this context [21]. A related method in FIA is solid phase detection with ion-exchange beads [22,23]. In this mode the analyte–dye complexes are adsorbed and detected on ion-exchange beads located in a flow-through cuvette which leads to preconcentration and lower detection limits. However, in most cases the reagent cannot be permanently immobilized by this means.

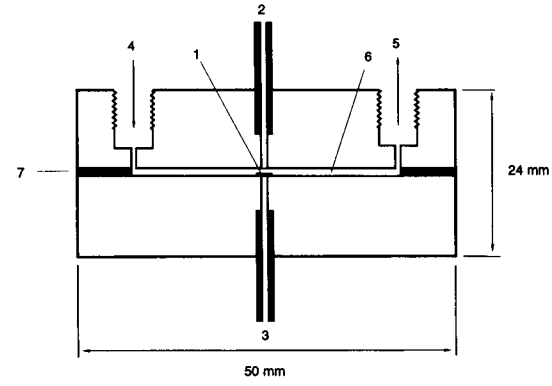

Fig. 1. Cross-sectional view of the transducer-cell: (1) membrane, (2) optical fibre from LED, (3) optical fibre to detector, (4) liquid inlet, (5) liquid outlet, (6) flow channel defined by a slit in the spacer between the two cell halves, (7) spacer.

2. Experimental

2.1. Flow-through cell

A drawing of the flow-cell is given in Fig. 1. It consists of two black perspex halves which are separated by a PTFE sheet of 1 mm thickness. A flow channel is defined by a slit 1.5 mm in width cut into this spacer. Fluid in- and outlet is achieved via standard $28 \times 1/4''$ fittings. Plastic core optical cables of 1 mm active diameter (Radiospares, Auckland) are used to pass the detecting light beam through the cell. These are glued into the cell with fibre optic grade epoxy (Epo-Tek 353ND, Epoxy Technology, Billerica, MA) and the epoxy is polished flush with the surface of the cell body after hardening. A Watson Marlow 503U peristaltic pump (Watson Victor, Auckland) was used to propel solutions and Rheodyne Type 50 valves (Rheodyne, Cotati, CA) to carry out the injections.

2.2. Electronics

The circuitry is given in Fig. 2. The system is essentially a double-beam photometer employing

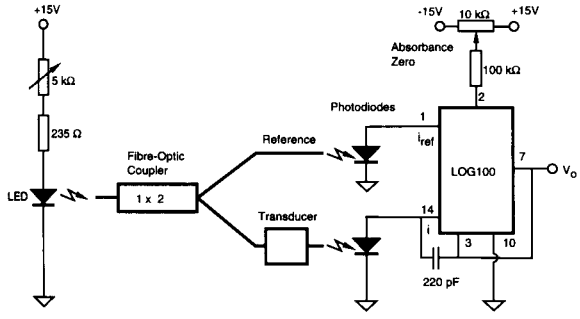

Fig. 2. Electronic circuitry for the detector.

a single source and separate detectors. The output intensity of LEDs is generally stable to better than 1% over several hours [24], however for the high precision measurements required for this work, it was preferable to correct for this small drift. The light from a LED was therefore coupled into a 1 mm optical fibre which guides it to a 1×2 fibre optic coupler (PF-TC 1×2 1000, Luxmatic, Baar, Switzerland). One of the two outputs was connected to the cell and the other directly to the reference photodiode. A logarithmic ratio amplifier contained in a single integrated circuit package (LOG100JP, Burr-Brown, Tucson, AZ) was employed to give a direct absorbance output from the current of the two photodiodes [$V_o = \log(i_{ref}/i)$] [17,18]. The noise level obtained with this circuitry is typically about 5×10^{-5} V, corresponding to 5×10^{-5} absorbance units (AU) as evidenced by operating a chart recorder at 10 mV full scale sensitivity. The optoelectronic components were obtained from Siemens (Siemens, Wellington). The LED emitters (green, peak wavelength 560 nm, SFH 751 and red, 660 nm, SFH 750V) and photodiode detectors (SFH 250V) are designed to couple with the 1 mm diameter plastic fibre. Peak heights were acquired with a strip chart recorder.

2.3. Optical sensor membranes

All membranes were made up according to the original recipes (Ca^{2+} [4], NH_4^+ [2], Zn^{2+} [5], NO_3^- [7] and K^+ [1]), but the poly(vinyl chloride) was replaced with vinyl chloride (91%)–vinyl acetate (3%)–vinyl alcohol (6%) copolymer (OH-PVC) because of its improved adhesion. The ionophores [ETH 1001 (Ca^{2+}), Nonactin (NH_4^+), tridodecylmethylammonium chloride (TDMACl, NO_3^-), Valinomycin (K^+)], lipophilized pH indicators {9-(diethylamino)-5-octadecanoylimino-5*H*-benzo[*a*]phenoxazine (ETH 5294, Ca^{2+}, NH_4^+ and K^+) and 3-hydroxy-4-(4-nitrophenylazo)-phenyl octadecanoate (ETH 2412, NO_3^-)}, additives {potassium tetrakis(4-chlorophenylborate (KpClTPB) and sodium tetrakis[3,5-bis(trifluoromethyl)phenyl]borate [$NaTm(CF_3)_2PB$]}, plasticizers [2-nitrophenyl octyl ether (o-NPOE) and bis(2-ethylhexyl)sebacate (DOS)] and the polymer were obtained from Fluka (Buchs). 1-octadecyloxy-4-(2-pyridylazo)resorcinol (Zn^{2+}) was synthesized according to the procedure given in Ref. [5]. The membrane mixtures were made up by adding approximately 1 ml of freshly distilled tetrahydrofuran per 100 mg of mixture. After overnight dissolution, one droplet of the solution was applied to the top of the optical fibre with a micropipette. The thickness of the membranes produced in this manner can be reproduced to about $\pm 30\%$ as evidenced by absorbance readings. From a comparison of these values with the ones reported in the original papers (typically 4 μm) [1,2,4,5,7] the thicknesses obtained here must be somewhat less.

2.4. Solutions

pH buffer solutions were made up from 0.01 M acetic acid (pH 5.0 and 6.0) or NaH_2PO_4 (pH 7.0) which were adjusted to the desired pH value with a highly concentrated solution of NaOH. Standard solutions were made up from KNO_3, NH_4Cl, $CaCl_2$ and $ZnCl_2$ salts. All reagents were of analytical reagent grade.

3. Results and discussion

3.1. Ca^{2+}

The membrane employs a calcium ion selective ionophore (ETH 1001) and lipophilic derivative of the pH indicator Nile Blue [4], whose proto-

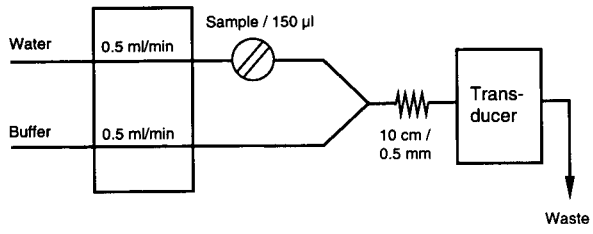

Fig. 3. FIA manifold.

nated form shows a pronounced doublet absorption band with maxima at 615 and 660 nm. The red LED with the emission at 660 nm was therefore chosen to monitor the deprotonation of the indicator on extraction of the analyte ion into the membrane. The peaks obtained were thus negative, i.e., they represent a decrease in absorbance. The FIA manifold is shown in Fig. 3. Deionized water was used as the carrier stream into which, following the sample injection point, the pH buffer was merged in a 1:1 ratio. The short coil assures good mixing of the two streams before entering the detector cell.

The calibration curve obtained extends over four orders of magnitude and is given in Fig. 4. The curve compares well with the original steady state one reported in the literature [4] and the top of the peaks were indeed found to be close to equilibrium as evidenced by the fact that these were not significantly higher when larger volumes were injected. Peak heights could typically be reproduced to better than $\pm 3 \times 10^{-4}$ AU. This corresponds to a relative precision in the concentration between about 5 and 10%. The injection rate is determined by the time required for return to baseline, which was found to depend on the concentration injected and to vary between less than one minute and several minutes for the highest concentration injected.

3.2. NH_4^+

The FIA manifold was identical. The membrane contained the Nile Blue derivative, therefore the red LED was again employed for the measurements. The calibration curves obtained for this system are given in Fig. 5. The use of a

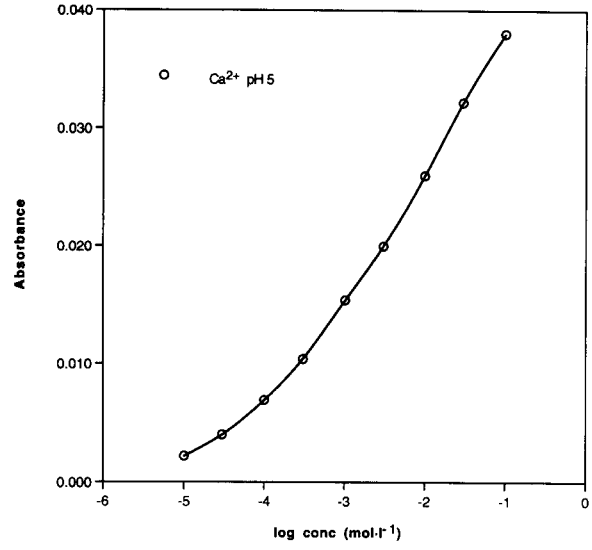

Fig. 4. Calibration curve for Ca^{2+}. Membrane composition: 7.8 wt% ETH 1001, 2.2 wt% ETH 5294, 4.7 wt% $NaTm(CF_3)_2PB$, 56.7 wt% DOS and 28.6 wt% OH-PVC [4]. Red LED.

buffer solution of pH 5.0 yielded a dynamic range of about three orders of magnitude. The shape of the calibration curve is strongly dictated by the

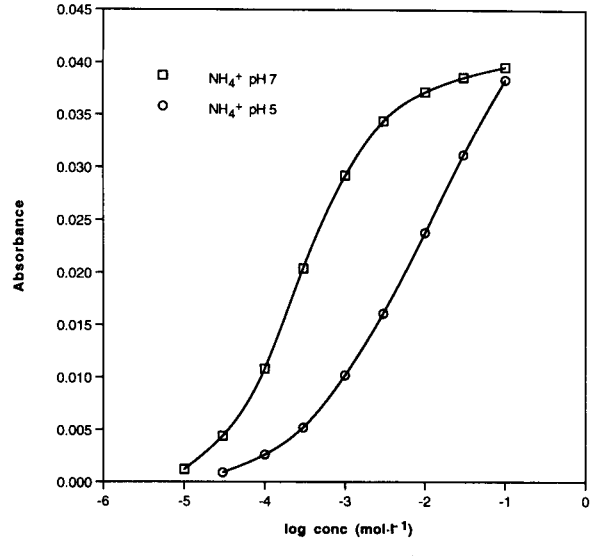

Fig. 5. Calibration curves obtained for NH_4^+ at two pH values. Membrane composition: 2.4 wt% Nonactin, 1.6 wt% ETH 5294, 1.6 wt% KpClPB, 62.9 wt% DOS and 31.5 wt% OH-PVC [2]. Red LED.

pH of the buffer, as is expected for this type of membrane and illustrated by the calibration curve for pH 7 in the figure. It is therefore of advantage to choose a buffer pH that yields the highest sensitivity in the range of the sample concentrations. With the FIA system this pH buffering of the standards and samples is carried out on-line and may therefore be adapted rapidly as needed. Changeover of streams only requires a few minutes to complete. The performance of this system in terms of precision and kinetic response were comparable to the Ca^{2+} system reported above.

3.3. Zn^{2+}

The membrane contains a lipophilic derivative of 4-(2-pyridylazo)resorcinol (PAR). This compound shows an absorbance band between about 450 and 590 nm with a maximum at 523 nm when complexed with Zn^{2+} [5]. A fairly good overlap of this absorption band with the emission of a green LED with a maximum at 560 nm is obtained. It was reported that the response of the membrane to a three-fold increase or decrease in concentration is in the order of 5 minutes [5]. The time required to measure a single sample is longer when larger concentration changes are involved. The slow asymptotical approach to equilibrium makes it also very difficult for the operator to decide when to make the final reading. This membrane is therefore not well suited for conventional measurements of steady state response and a good candidate for examining the use of membranes of this type in FIA.

First experiments were carried out using an acetate buffered solution at pH 5 as a carrier in the manifold used for the experiments reported above. It was found however that the return to baseline, i.e., complete decomplexation after injection of a sample, was slow in this mode. It was necessary to use a carrier with a pH of 2 or lower to facilitate decomplexation and to achieve reasonable sampling rates. However, such pH values are too low for measurements of metal ion concentrations with the membrane and the samples have to be buffered at a higher pH value. The FIA manifold designed to achieve on-line mixing of samples with a buffer of an appropriate pH

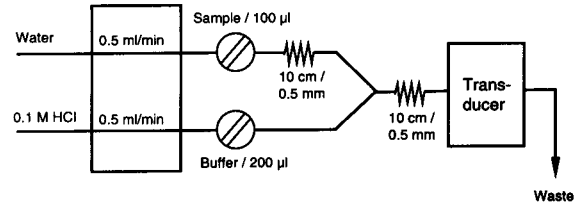

Fig. 6. FIA manifold for the determination of Zn^{2+}.

value while maintaining a low carrier pH value is shown in Fig. 6. A sample plug and a buffer plug are injected simultaneously into two subsequently merging streams. A single multi-port injection valve may be employed rather than the two separate valves used here. The sample plug is delayed slightly in a short coil in order to allow the pH gradient to reach the membrane before the sample. This feature is not essential but makes more efficient use of the injected sample volume. As was expected, injection of the pH buffer alone did not cause any peak since a change in pH alone cannot lead to complexation and hence colour change of the PAR derivative.

Typical values obtained on injection of Zn(II) solutions of different concentrations are shown in Fig. 7. The return to baseline after injection of Zn(II) solutions took about 1 to 2 min for this membrane depending on the analyte concentration. The time required for a single determination is therefore significantly reduced compared to equilibrium measurements [5]. The detection limit of approximately 1×10^{-5} mol l^{-1} (or 0.8 ppm) (peak height = 3 × R.S.D., $n = 5$) is only slightly higher than that found for Zn(II) with PAR in conventional spectrophotometry (approximately 0.1 ppm) [18].

3.4. NO_3^- and K^+

A modified cell which was fitted with two sets of optical fibres was used for the simultaneous determination of nitrate and potassium ions at a common pH of 5.0. The detector circuitry was duplicated for this purpose and a dual channel chart recorder used for the acquisition of the peak heights. The green LED was used again to monitor the nitrate selective membrane which

contains a lipophilic derivative of Azo Violet [7]. This dye shows a wide absorption band between about 420 and 650 nm with a peak at 550 nm in the deprotonated form [7]. The potassium selective membrane contains the Nile Blue derivative [1] so that the red LED was used for these measurements. The original FIA manifold of Fig. 3 was used. As can be seen from the calibration graphs of Fig. 8, a response over about 4 orders of magnitude was obtained for both systems. The reproducibility of the peak heights was comparable with the previous results.

As an example of a potential application of the system, the concurrent determination of potassium and nitrate in several commercial liquid fertilizer mixtures was carried out. The results obtained are compared with the corresponding atomic absorption spectroscopy (AAS) (potassium) and ion chromatography (IC) (nitrate) results. The original fertilizer solution had been diluted by a factor of 1000. Potassium: (1) 2.3 ± 0.2 mol l^{-1} (AAS, 2.2 ± 0.1 mol l^{-1}), (2) 1.8 ± 0.2 (1.7 ± 0.1), (3) 1.6 ± 0.2 (1.6 ± 0.1), (4) 1.7 ± 0.2 (1.8 ± 0.1), 1.4 ± 0.2 (1.2 ± 0.1). Nitrate: (1) 0.56 ± 0.05 mol l^{-1} (IC, 0.71 ± 0.02 mol l^{-1}), (2) 1.12 ± 0.05 (1.08 ± 0.02), (3) 1.06 ± 0.05 (1.03 ± 0.02). As can be seen from the data, a good agreement was generally obtained. The correlation coefficient is 0.9488 for the potassium data and 0.9996 for the nitrate data.

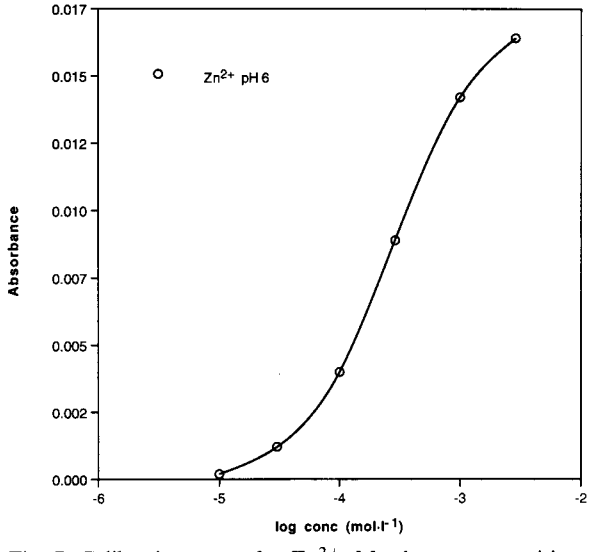

Fig. 7. Calibration curve for Zn^{2+}. Membrane composition: 1.3 wt% 1-octadecyloxy-4-(2-pyridylazo)resorcinol, 65.5 wt% DOS and 33.2 wt% OH-PVC [5]. Green LED.

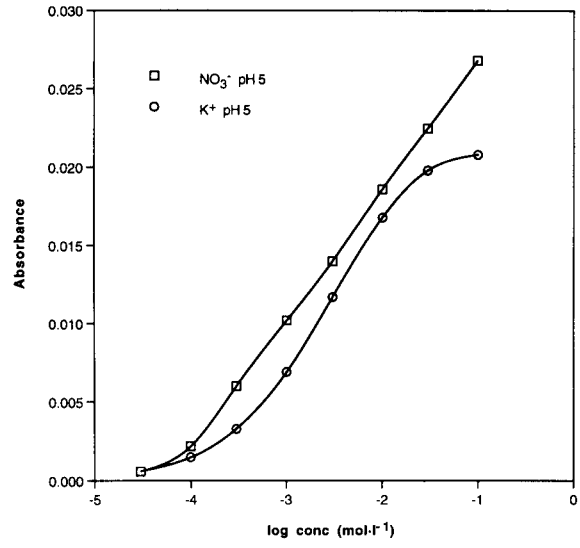

Fig. 8. Calibration curves for NO_3^- and K^+ obtained concurrently with a modified cell containing two fibre optic cable pairs. Membrane compositions; NO_3^-: 2.3 wt% ETH 2412, 5.3 wt% TDMACl, 61.6 wt% o-NPOE and 30.8 wt% OH-PVC [7]; K^+: 1.4 wt% valinomycin, 0.5 wt% ETH 5294, 0.5 wt% KpClTPB, 66.9 wt% DOS and 31.7 wt% OH-PVC [1]. Red (K^+) and green (NO_3^-) LEDs.

4. Conclusions

The good performance of the LED-based photometric transducer and the ease of sample handling in FIA yielded a more practical method of measurements with the optode membranes as compared to the original work [1,2,4,5,7]. Relatively large volume cells located in conventional spectrophotometers were generally filled in a batch-wise mode. The availability of LEDs with colours ranging from the blue (470 nm) to the infrared will allow the matching of any visible indicator that may be employed in such membranes. It has further been shown that simultaneous determinations can easily be carried out. It

should in most cases be possible to find a compromise buffer pH or to modify the membrane response by using a lipophilized pH indicator with a different pK_a.

The four ionophore based systems (Ca^{2+}, NH_4^+, NO_3^- and K^+) constitute an alternative to flow-injection potentiometry with ion-selective membranes containing the same ionophores and therefore having very similar selectivities and detection limits. The advantages of optical sensors can be clearly seen in a comparison of the two systems. First, the flow cell for the optical membranes is simpler in construction and less prone to failure because a reference optode is not required. Secondly, ion-selective electrodes are liable to electromagnetic noise pick-up. In flow-injection systems, streaming potentials (derived from surface charges) are present [25]. These produce fluctuations in the measured potentials due to pulsations from the peristaltic pumps and therefore have to be minimized by addition of an ionic strength buffer with a concentration of at least 0.1 mol l^{-1} [26]. Particularly in multi-ISE systems it is difficult to find an appropriate buffer that does not lead to an interference in terms of selectivity and to a compromise in detection limits. Such an ionic strength adjustment buffer is not needed with the optical membranes and pulsations from the pump were not found to have an effect on the measured signal. In electromagnetically noisy environments, e.g., as caused by NMR spectrometers in chemistry departments, effective shielding is very difficult to achieve and cumbersome. On the other hand, optical sensors are generally more complex than electrochemical sensors because an additional signal transduction from the optical into an electrical domain is required. However, the use of the optoelectronic components in combination with optical fibres approximates the simplicity of potentiometric sensors while providing a performance in terms of signal-to-noise ratio as good as or better than that of much more complex optical instrumentation. A slight drift of baseline and some loss of sensitivity was observed with the systems employing the lipophilized Nile Blue. This was presumed to be due to leaching of the pH indicator and should be overcome by using one of the more lipophilic derivatives of this compound reported by Bakker et al. [27].

The system based on the PAR derivative is an alternative to using PAR itself in the reagent stream in FIA [28]. The main difference in using the membrane in FIA is the logarithmic response obtained. This leads to a dynamic range of at least 2.5 orders of magnitude compared to the one decade usually accepted for conventional photometric measurements. This may be considered an advantage since the requirements on dilution of the samples to match the dynamic range of the method are not as stringent as in the conventional approach. A certain loss in precision is a disadvantage. The other benefit in using the membrane is the fact that the expensive PAR reagent is not consumed.

Acknowledgement

The authors thank Dean Clark from Siemens Wellington for providing samples of optoelectronic components.

References

[1] K. Wang, K. Seiler, W.E. Morf, U.E. Spichiger, W. Simon, E. Lindner and E. Pungor, Anal. Sci., 6 (1990) 715.
[2] K. Seiler, W.E. Morf, B. Rusterholz and W. Simon, Anal. Sci., 5 (1989) 557.
[3] K. Seiler, K. Wang, E. Bakker, W.E. Morf, B. Rusterholz, U.E. Spichiger and W. Simon, Clin. Chem., 36 (1991) 1350.
[4] W.E. Morf, K. Seiler, B. Rusterholz and W. Simon, Anal. Chem., 62 (1990) 738.
[5] K. Wang, K. Seiler, B. Rusterholz and W. Simon, Analyst, 117 (1992) 57.
[6] M. Lerchi, E. Bakker, B. Rusterholz and W. Simon, Anal. Chem., 64 (1992) 1534.
[7] P.C. Hauser, P.M.J. Périsset, S.S.S. Tan and W. Simon, Anal. Chem., 62 (1990) 1919.
[8] S.S.S. Tan, P.C. Hauser, N.A. Chaniotakis, G. Suter and W. Simon, Chimia, 43 (1989) 257.
[9] S.S.S. Tan, P.C. Hauser, K. Wang, K. Fluri, K. Seiler, B. Rusterholz, G. Suter, M. Krüttli, U.E. Spichiger and W. Simon, Anal. Chim. Acta, 255 (1991) 35.
[10] M. Kuratli, M. Badertscher, B. Rusterholz and W. Simon, Anal. Chem., 65 (1993) 3473.

[11] K. Seiler, K. Wang, M. Kuratli and W. Simon, Anal. Chim. Acta, 244 (1991) 151.
[12] K. Wang, K. Seiler, J.-P. Haug, B. Lehmann, S. West, K. Hartman and W. Simon, Anal. Chem., 63 (1991) 970.
[13] S. Ozawa, P.C. Hauser, K. Seiler, S.S.S. Tan, W.E. Morf and W. Simon, Anal. Chem., 63 (1991) 640.
[14] S.J. West, S. Ozawa, K. Seiler, S.S.S. Tan and W. Simon, Anal. Chem., 64 (1992) 533.
[15] W.E. Morf, K. Seiler, B. Lehmann, C. Behringer, K. Hartman and W. Simon, Pure Appl. Chem., 61 (1989) 1613.
[16] M. Trojanowicz, P.J. Worsfold and J.R. Clinch, Trends Anal. Chem., 7 (1988) 301.
[17] P.K. Dasgupta, H.S. Bellamy, H. Liu, J.L. Lopez, E.L. Loree, K. Morris, K. Petersen and K.A. Mir, Talanta, 40 (1993) 53.
[18] P.C. Hauser and D.W.L. Chiang, Talanta, 40 (1993) 1193.
[19] B.A. Woods, J. Růžička, G.D. Christian, N.J. Rose and R.J. Charlson, Analyst, 113 (1988) 301.
[20] B.A. Woods, J. Růžička, G.D. Christian and R.J. Charlson, Anal. Chem., 58 (1986) 2496.
[21] J. Růžička and E.H. Hansen, Anal. Chim. Acta, 173 (1985) 3.
[22] M. Valcárcel and M.D. Luque de Castro, Analyst, 115 (1990) 699.
[23] M.D. Luque de Castro and M. Valcárcel, Trends Anal. Chem., 10 (1991) 114.
[24] P.C. Hauser, D. Chiang and N. Cates, unpublished results.
[25] P. Van den Winkel, J. Mertens and D.L. Massart, Anal. Chem., 46 (1974) 1765.
[26] P.C. Hauser, S.S. Tan, T.J. Cardwell, R.W. Cattrall and I.C. Hamilton, Analyst, 113 (1988) 1551.
[27] E. Bakker, M. Lerchi, T. Rosatzin, B. Rusterholz and W. Simon, Anal. Chim. Acta, 278 (1993) 211.
[28] D. Betteridge, E.L. Dagless, B. Fields and N.F. Graves, Analyst, 103 (1978) 897.

ELSEVIER

Analytica Chimica Acta 294 (1994) 57–68

ANALYTICA CHIMICA ACTA

Purification of analytical reagents by constant-current electrodeposition of heavy metals at ultra-trace levels from highly concentrated salt solutions

K. Hoppstock [a,1], R.P.H. Garten [a], P. Tschöpel [a,*], G. Tölg [a,b]

[a] *Max-Planck-Institut für Metallforschung, Stuttgart, Laboratorium für Reinststoffanalytik (LRA), Bunsen-Kirchhoff-Strasse 13, D-44139 Dortmund, Germany,*

[b] *Institut für Spektrochemie und Angewandte Spektroskopie, Bunsen-Kirchhoff-Strasse 12, D-44139 Dortmund, Germany*

(Received 9th November 1993; revised manuscript received 2nd March 1994)

Abstract

The constant-current electrodeposition of trace elements (Cd, Co, Cu, Fe, Mn, Ni, Pb and Zn) onto a graphite tube cathode from highly concentrated NH_4F solutions was studied. Element concentrations in the ng ml^{-1} range were decreased to values of $\leqslant 3$ pg ml^{-1} (^{60}Co) within 60–120 min of electrolysis except for manganese. A recrystallized solid ultra-high purity product with an impurity level in the low pg g^{-1} range was obtained by partly evaporating the solvent of these high-purity NH_4F solutions in a specially designed evaporation device, in order to minimize contamination and decomposition of the reagent. The element concentrations at the ng ml^{-1} and pg ml^{-1} level were determined using a "direct" electrothermal atomic absorption spectrometric procedure for NH_4F solutions up to 20%. To improve the detection limits and to verify the accuracy a multi-step ion-exchange procedure was used to separate and preconcentrate the trace elements from the matrix (up to 40% NH_4F solutions).

Key words: Ion exchange; Constant-current electrodeposition; Trace elements; Heavy metals; Highly concentrated salt solutions

1. Introduction

Because of the rapidly increasing efficiency of trace analysis since the early 1970s, the purity of purchased analytical reagents, which are necessary for sample preparation in ultra-trace analysis, very often did not satisfy the increasingly stringent demands [1,2]. Therefore, the reagents used had to be purified further in the laboratories and many papers dealing with this subject can be found [3–10]. Some methods employed for purification of analytical reagents and their efficiency are compiled in Table 1.

In recent years the importance of the rapid and reliable (trace) analytical characterization of environmental samples, high purity materials, and advanced ceramics has steadily increased [11,12].

* Corresponding author.

[1] Present address: Forschungszentrum Jülich GmbH, Zentralabteilung für chemische Analysen, Postfach 1913, D-52405 Jülich.

0003-2670/94/$07.00
SSDI 0003-2670(94)00115-3

Table 1
Examples of methods for the purification of analytical reagents and the resulting trace metal concentration, as reported in the literature

Substance	Method	Conc. before the process (ng g^{-1})								Conc. after the process (ng g^{-1})								Ref.
		Cd	Co	Cu	Fe	Ni	Mn	Pb	Zn	Cd	Co	Cu	Fe	Ni	Mn	Pb	Zn	
HNO_3	Subboiling distillation	< 0.2	0.47	0.78	7.19	13.2	0.14	0.2	1.3	< 0.2	< 0.02	0.08	0.6	0.02	< 0.04	0.04	0.14	28
P_2O_5	Sublimation (two step)							1000–10000								< 0.1		29 30
H_2O_2	LT sublimation		1000	1000	1000	1000	1000				0.4	< 2	< 2		0.9			3
NH_2NH_2	LT sublimation		40	3	41	13	2				ND	0.3	2		ND			3
$POCl_3$	LT sublimation		< 1	11	433	1300	4		12		< 1	18	30	< 1	2		< 1	31
Mo	Zone refining		10000		100000	5000					< 100		< 100	< 100				32
Al	Zone refining	3500	⩽ 10	1900	3000	2500	250		17000–20000	⩽ 2	⩽ 10	20	< 1000	⩽ 50	120		⩽ 50	33
Na_2CO_3 1.0 M	Electrolysis Hg pool 40 h		< 2		1		7		30		< 2		1		< 2		< 2	6
NaAc 1.0 M	Electrolysis Hg pool 40 h		< 2		30		1		11		< 2		< 2		1		4	6
$NaBH_4$ 0.4% in 0.1 M NaOH	Ion exchange Precipitation onto $BaSO_4$					0.6 0.6								⩽ 0.005 ⩽ 0.01				34
EDTA	Recrystallization	ND	ND	ND	205	67	12		NDi	ND	63	ND	76	ND	63		33	35
NH_4F	Recrystallization			5	430	30	15	36	28			1.5	140	9	3.9	14.3	7.6	36
				0.8	10	1.5	1.6	1.6	3			0.2	2.6	0.4	0.2	0.4	0.4	
$K_2S_2O_8$ [a]	Pure production			20–60	1400	70–150			90			< 3	1200			< 3	< 6	37

LT sublimation = low-temperature sublimation, ND = ⩽ DL. [a] Purity before = commercially quality. DL = Detection limit.

Although there are several extremely sensitive methods available, (e.g., ETAAS, ICP-MS) the metal traces of interest normally have to be isolated (using e.g., ion exchange, electrodeposition, etc.) to avoid matrix-interferences [13,14], requiring the use of dissolved samples. Especially, compact refractory materials, such as SiC- or ZrO_2-based ceramics, have to be decomposed by fusion procedures requiring a high excess of solid flux reagents. To avoid high contaminations due to the large amount of solid salts employed, salts of the highest possible purity are obligatory. Another powerful strategy for decomposing refractory substances is the use of elemental fluorine in a specially designed apparatus. This technique requires high-purity NH_4F solutions to dissolve the residue of non-volatile fluorides [15].

This paper describes the use of constant current electrodeposition of metal traces from concentrated NH_4F solutions for the purification of this electrolyte as well as the process of recrystallization to get a solid NH_4F of ultra-high purity. Two methods are described to determine the concentrations of trace elements in concentrated NH_4F solutions: A "direct" electrothermal atomic absorption spectrometric (ETAAS) determination and an ETAAS determination after trace/matrix separation and preconcentration of the trace elements using an ion-exchange procedure.

Recent studies, which will be published later, have proved the possibility of trace metal electrodeposition from concentrated salt solutions other than NH_4F for purification purposes.

2. Experimental

2.1. Reagents

All reagents were obtained from Merck (Darmstadt). HCl p.a. and HNO_3 p.a. were further purified by subboiling distillation in a quartz glass still. High purity water was obtained from a quartz glass bidistillation device placed inside a cleanroom (Class 1000) and stored in Polyethylene (PE) bottles. Cell-TETPA (triethylentetraminepentaacetic acid), a chelating ion exchanger based on microcrystalline cellulose, was provided by P. Burba (ISAS Dortmund).

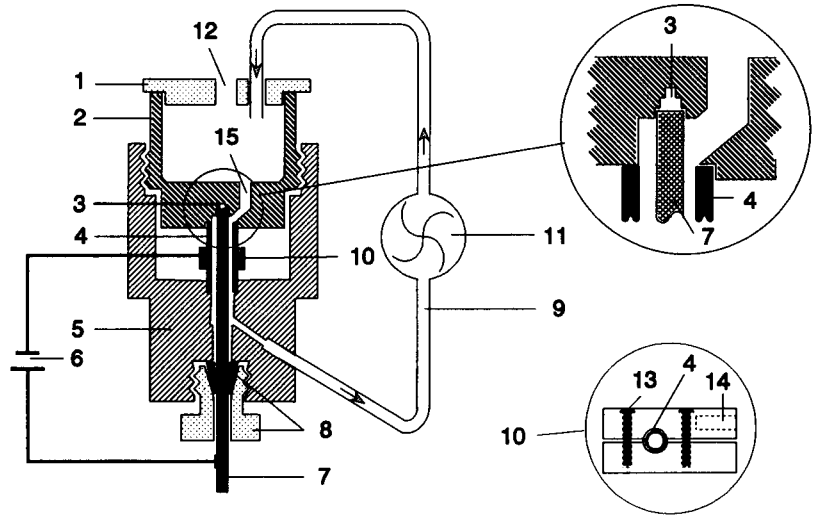

Fig. 1. Electrolytic cell made of PTFE (not to scale): 1 = cover, 2 = storage tank approx. 60 ml, 3 = bore holes for centering the anode, 4 = graphite tube cathode, 5 = basis, 6 = constant current power supply, 7 = glassy carbon anode, 8 = PTFE sealing and stopper, 9 = PTFE tubings, 10 = graphite contact, 11 = PTFE pump, 12 = vent and sampling hole, 13 = PP screw, 14 = bore hole for electric contact (diam. 5 mm), 15 = electrolyte entrance.

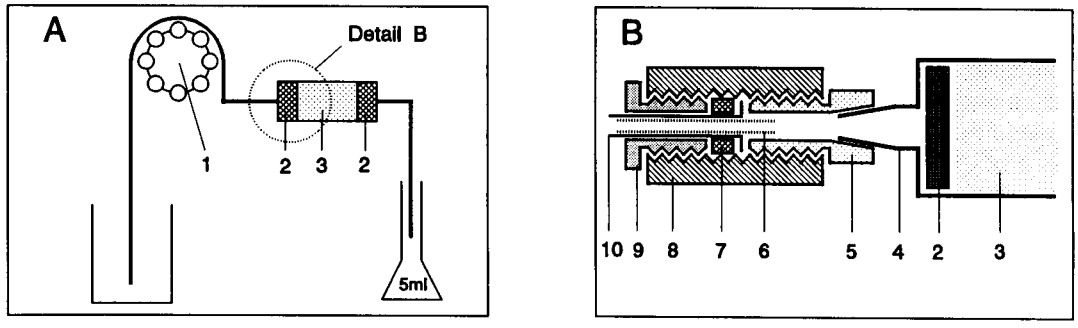

Fig. 2. (A) Schematic representation of the ion-exchange device for trace/matrix separation and preconcentration of trace elements: 1 = peristaltic pump, 2 = frit, 3 = cellulose ion exchanger (100 mg). (B) Detail enlargement: 4 = 1 ml PE disposal syringe, 5 = fitting, 6 = PTFE capillary, 7 = washer (PTFE) (laboratory-built), 8 = coupling device, 9 = fitting, 10 = peristaltic pump tubing (silicone).

2.2. Apparatus

Electrolysis was performed using the flow-through electrolysis cell made of PTFE shown in Fig. 1 and a constant-current device (laboratory-built) capable of supplying currents up to approx. 1.8 A. The electrolyte was circulated by a PTFE saturn pump (Fluorocarbon, Anaheim, CA) enabling flow-rates of 50 to 550 ml min^{-1}.

ETAAS determinations of trace elements were performed using a PE Z 5000 (Bodenseewerk Perkin Elmer, Überlingen) or a SpectrAA 300 (Varian, Darmstadt) graphite furnace atomic absorption spectrometer. Both were equipped with Zeeman background correction. A 3″ × 3″ well-type NaI(Tl) detector (Harshaw, Wermelskirchen) shielded with 7 cm of lead and connected to a multichannel ND 60 analyzer (Nuclear Data, Schaumburg, IL) was used for radioactivity measurements.

A flow-through system for trace/matrix separation on the basis of ion exchange was used as shown in Fig. 2 using a peristaltic pump (Gilson Minipuls 2) with silicone tubing of 1.3 mm i.d., a disposable syringe, plastics frits with a pore size of 250 μm (Berghof, Eningen), and several fittings from the Latek low-pressure chromatography system (Latek, Heidelberg).

The closed evaporation device (see Fig. 3) was assembled using a 250 mm i.d. polycarbonate desiccator with a 250 ml polyethylene flask as condenser. Two IR lamps of 150 W (Phillips IR 150 R) were used for heating.

PTFE beakers of different sizes, polypropylene (PP) and perfluoroalkoxy (PFA) were used for handling fluoride-containing solutions. For the preparation of standard solutions, vapour-cleaned quartz glass flasks were used.

When using large currents, the anodes had to withstand the attack of aggressive and extremely oxidizing agents. Three different materials were tested, a palladium rod and glassy carbon rods of Sigradur®K and Sigradur®G (Sigri, Meitingen). The use of Pd anodes resulted in high Pd concen-

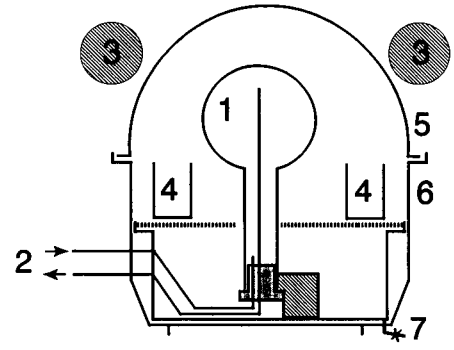

Fig. 3. Closed evaporation device: 1 = condenser (250 ml polypropylene flask), 2 = coolant in and out, 3 = infrared lamps, 4 = sample beakers, 5 = desiccator cover (polycarbonate), 6 = desiccator base (polypropylene), 7 = drain with stop-cock.

Table 2
Detection limit (DL) for the "direct" ETAAS determination procedure for trace elements in NH_4F solutions (100 g l^{-1}) using an injected sample volume of 20 μl

Element	Cd	Co	Cu	Fe	Mn	Ni	Pb	Zn
DL (ng ml^{-1})	0.04	0.2	0.25	0.1	0.05	0.2	0.15	0.05

trations in the electrolyte solution even though it is deposited in μg amounts onto the cathode. Therefore this material was unsuitable. Sigradur®K was entirely inappropriate, whereas Sigradur®G was very suitable even for high electrolysis currents. Because of the fixed cathode dimensions, the distance between the electrodes was varied using glassy carbon anodes with diameters of 3, 4 and 5 mm, corresponding to distances of 1.5, 1.0 and 0.5 mm. No effect on the deposition was observed.

3. Results and discussion

3.1. Determination of trace elements in concentrated solutions of NH_4F

NH_4F decomposes at temperatures above approx. 200°C, so it was possible to determine trace quantities of Cd, Co, Cu, Fe, Ni, Pb and Zn in solutions of $\leqslant 200$ g l^{-1} without further sample preparation using ETAAS and appropriate temperature programs. The detection limits (3σ) achieved for this "direct" ETAAS determination procedure are listed in Table 2, and Table 3 summarizes the experimental parameters.

To verify the "direct" ETAAS procedure and to improve the limits of detection, an efficient multi-step procedure was developed. Based on ion exchange, this method allowed the trace metals to be preconcentrated and separated from the matrix. The sample solution was pumped through the ion-exchange resin with a flow-rate of 1 ml min^{-1} followed by 2 ml of bidistilled water in order to rinse the system. The trace elements were then eluted with a volume of $\geqslant 3$ ml of 0.7 M HNO_3 directly into a vapour cleaned quartz glass flask (typically 5 ml) and subsequently determined using ETAAS.

The linear response range was tested using increasing volumes of the 40% NH_4F solution (MOS Selectripur®, Merck) as the sample and determining the elemental concentrations in the eluent (5 ml). Fig. 4 demonstrates that there was a linear correlation between the element concentrations in the eluate up to a sample volume of 50 ml, except for Zn where it was linear only up to a volume of 20 ml. The recoveries are listed in Table 4, and vary between 91 and 108%.

Rinsing the assembly with approx. 500 ml of 0.7 M HNO_3 conditioned it sufficiently so that contaminations were limited by the rinsing and elution solutions only. Memory effects were not observed. Table 5 summarizes the blank concentrations and the detection limits (3σ) observed. For Cu, Mn, Ni, Pb and Zn, the results of both methods matched very good as can be seen in

Table 3a
Experimental conditions for the "direct" ETAAS determination procedure for trace elements in NH_4F solutions

Step	General temperature program						
	Dry	Ash I	Ash II	Ash III	Ash IV	Atomize	Clean
Temperature (°C)	125	180	250	ES	ES	ESAT	ESC
Ramptime (s)	20	1	15	10		ESAR	1
Hold (s)	10		5	5	0.5 [a]	ESAH [a,b]	2

[a] Gas stop. [b] Read. ES = Element specific ashing temperature, ESAT = element specific atomization temperature, ESAR = element specific atomization step ramp time, ESAH = element specific atomization step hold time, ESC = element specific cleaning step temperature.

Table 3b
Element specific values for ashing, atomization and cleaning step (e.g., temperature, ramp time, hold time)

Element	Element specific values							
	Cd	Co	Cu	Fe	Mn	NI	Pb [a]	Zn
ES (°C)	250	900	800	1100	700	1000	700	350
ESAT (°C)	1800	2300	2200	2100	2400	2500	2400	1900
ESAR (s)	1	1	0.8	1	0.9	0.8	MP	1
ESAH (s)	2	2	2	2	1.5	2	5	2
ESC (°C)	2100	2500	2500	2500	2700	2700	2700	2400
λ (nm)	228.8	242.5	324.7	248.3	279.5	232.0	282.3	213.9
HCL current (mA)	4	8	8	8	8	8	8	8

Tubes in all cases except Pb: Varian pyro-coated partitioned. [a] Using PE Z 5000 with pyrocoated graphite tube with L'vov platform, MP = maximum heating rate. HCL = Hollow cathode lamp.

Fig. 5. Because Fe was not exchanged, it was not possible to determine Fe using this ion-exchange procedure.

3.2. Purification of NH_4F

Theoretical treatment of the electrodeposition process

The rate of heterogeneous reactions is normally influenced by the rate of mass transport and of the chemical reactions itself. Chemical reactions, such as the electrodeposition of metal ions, typically are very fast so that, as a rule, the mass transport to the cathode is the rate controlling process. Owing to frictional forces, there is no flow at an interface [16], consequently, mass transport directly at the electrode surface is only a result of diffusion processes (except for electrostatic attraction, which can be neglected due to high concentrations of supporting electrolyte). Assuming that every cation is discharged at the electrode in the first collision (deposition probability, $w = 1$), the concentration changes of cations in the electrolyte solution are described by Eq. 1 [17]:

$$\frac{dc_t}{dt} = -\frac{DAc_t}{V\delta_N} \quad (1)$$

where c_t is the concentration of cations in the electrolyte at time t, D the diffusion coefficient of the cations, V the volume of the electrolyte, δ_N thickness of the Nernst diffusion layer and A is the surface area of the cathode.

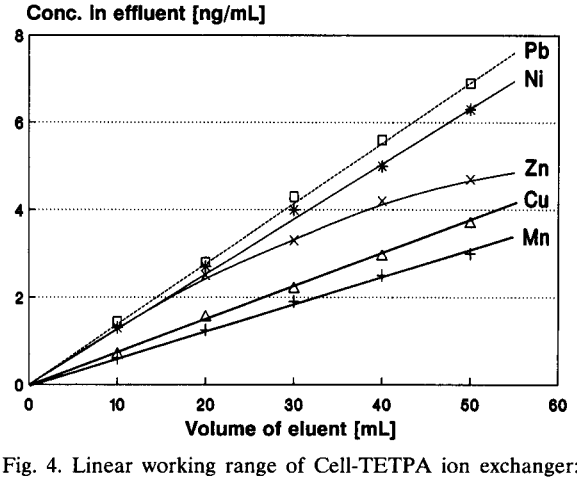

Fig. 4. Linear working range of Cell-TETPA ion exchanger: column filled with 100 mg exchanger; sample, 10–50 ml 40% NH_4F solution (MOS Selectipur®); eluent, 5 ml 0.7 M HNO_3. △, Cu; +, Mn; *, Ni; □, Pb; ×, Zn.

Table 4
Recovery rates for the multi-step procedure based on ion exchange [ion exchanger, Cell-TETPA on microcrystalline cellulose; sample, 10 ml 40% NH_4F solution (MOS Selectipur®)]

	Element in 10 ml unspiked 40% NH_4F solution (MOS Selectipur®)		Added (ng)	Found ($n = 3$) (ng)	Recovery (%)
	(ng)	R.S.D. (%)			
Cu	2.6	3.7 ($n = 6$)	20	21.4–24.4	95–108
Mn	6.8	2.2 ($n = 6$)	10	16.4–17.1	98–102
Ni	4.0	3.1 ($n = 6$)	10	12.7–15.0	91–107
Pb	5.8	1.5 ($n = 6$)	10	14.9–16.1	94–102
Zn	10.0	3.5 ($n = 4$)	10	20.0–21.0	100–105

Table 5
Blanks and detection limits (DL) for the multi-step procedure based on ion exchange (sample, 40% NH_4F solution; volume, 50 ml)

	Cu	Mn	Ni	Pb	Zn
Blank concentration in the eluate ($ng\ ml^{-1}$)	$\leqslant 0.25$	$\leqslant 0.06$	$\leqslant 0.4$	$\leqslant 0.15$	$\leqslant 0.05$
DL ($ng\ ml^{-1}$)	0.025	0.01	0.05	0.05	0.02 [a]

[a] Sample volume 20 ml.

Assuming the ions to be spherical, the diffusion coefficient D is expressed by Eq. 2 according to Stoke's law:

$$D = \frac{kT}{6\pi\eta r} \tag{2}$$

where k is the Boltzmann constant; T the temperature; η the dynamic viscosity and r is the ionic radius.

The result of substituting Eq. 2 into Eq. 1 is (after integration and some transformations [16]):

$$c_t = c_0 \cdot \exp - \left(\frac{wkTAt}{6\pi r\eta\delta_N V} \right) \tag{3}$$

that can be abbreviated by defining a deposition constant λ:

$$c_t = c_0 \cdot e^{-\lambda t} \tag{4}$$

where c_0 is the initial concentration in the electrolyte, c_t the concentration of cations at time t, λ the deposition constant $[\lambda = (wkTA)/(6\pi\delta_N\eta V)]$.

The effect of physical properties such as temperature (T) or dynamic viscosity (η) on the rate of transportation and the rate of deposition is evident. A more illustrative representation for the rate of deposition is the half-life of electrodeposition $t_{1/2}$ (i.e., the time that is necessary to decrease the initial concentration to half) (Eq. 5):

$$t_{1/2} = \ln 2/\lambda \tag{5}$$

Thus the concentration decreases exponentially with the time of electrolysis if the metal traces are electrodeposited according to this simple model. This dependence of concentration upon time was verified even in the range of a few ng $\cdot l^{-1}$ as will be shown below.

According to Eq. 3 the rate of deposition should increase by increasing the temperature, by enlarging the electrode surface, or by decreasing the thickness of the diffusion layer δ_N. Using a fixed temperature and a surface area fixed by the dimensions of the ETAAS graphite tube used as the cathode as well as a fixed electrolyte composition, the only variable parameter remains the thickness of the Nernst diffusion layer. In 1903 Nernst [18] and Brunner [19] reported on the influence of the stirring rate on the thickness of the diffusion layer. A detailed study on the problems of mass transport at the interface of an electrode was presented by Ibl [20]: even a poor electrolytic gas production on the electrode provides a more efficient mass transport than powerful stirring.

3.3. Galvanostatic electrodeposition onto a graphite tube cathode

Determining the concentration decrease in the electrolyte solution versus electrolysis time allows the calculation of the deposition constant, λ, and the half-life of electrodeposition, $t_{1/2}$, respectively, using logarithmic curve fitting [21]. In Table

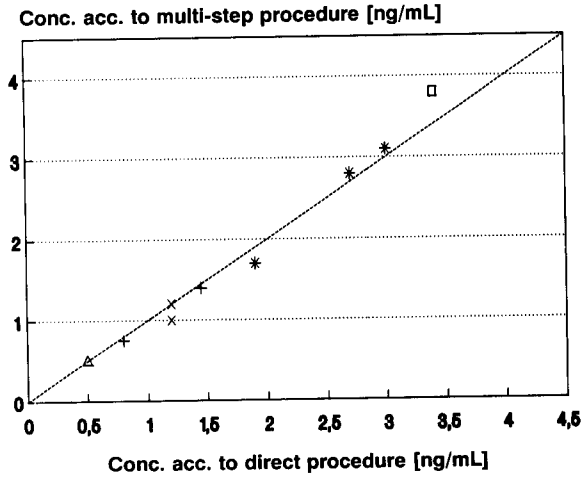

Fig. 5. Results of the "direct" ETAAS determination procedure and the multi-step procedure based on ion exchange. The different values for Mn, Ni and Zn result from the analysis of different samples (NH_4F MOS-Selectipur®, different lots of solid NH_4F, p.a.). For key to symbols see Fig. 4.

Table 6
Concentration decrease during electrolytic deposition: experiment 1

Electrolysis time (min)	0	5	10	22	35
Co concentration (ng ml^{-1})	64.5	47.3	32.8	13.7	5.5
R.S.D. (%) ($n = 3$)	1.5	1.8	1.8	1.5	2.2

Listed are the mean values of 3 separate electrolysis runs. Conditions: 10% NH_4F solution, doped with 64.5 ng ml^{-1} Co; $I = 1.5$ A; glassy carbon anode 4 mm diam.; Co concentrations determined by ETAAS. The resulting λ value is 0.07086 with a correlation factor of 0.99982 (for exponential regression).

6 the results are listed for experiment 1, covering a concentration range of 65 to 5.5 ng Co ml^{-1}. The calculated value for λ is 0.07086 min^{-1} (correlation coefficient, $r = 0.99982$).

Using this λ value, it is possible to estimate the decrease of Co concentration over several orders of magnitude down to the pg ml^{-1} range with good correlation to the tracer experiments (^{60}Co) as indicated in Table 7. This model can also be used to describe the concentration fall of other elements such as Ni, Pb, Fe and Zn. The half-lives of electrodeposition, $t_{1/2}$, for these elements are 11.0, 9.3, 12.2 and 23.6 min, respectively.

To study the influence of experimental parameters and to optimize them, the dependence of electrolysis time on the analyte concentration in the electrolyte was monitored. Figs. 6 and 7 show the influence of experimental parameters such as electrolysis current and flow rate on the deposition rate and the residual Co concentration after

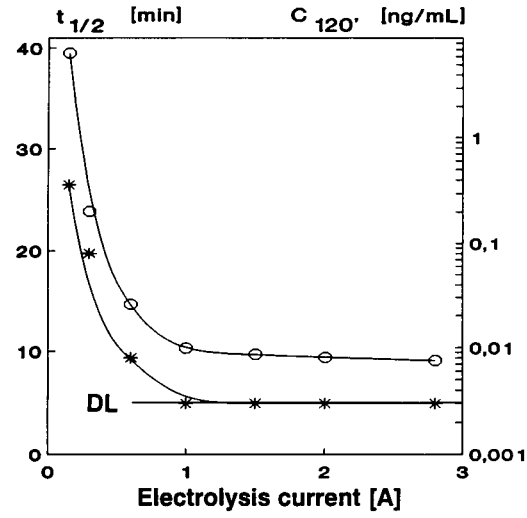

Fig. 6. Half-life time of electrodeposition ($t_{1/2}$) vs. electrolysis current. ○ = half-life of electrodeposition ($t_{1/2}$); * = residual Co concentration ($c_{120'}$) after 120 min of electrolysis. Initial concentration 2 ng ml^{-1} Co; radiochemically using ^{60}Co.

120 min of electrolysis. The NH_4F concentration plays an important role too. The deposited amount decreases when the total electrolyte concentration exceeds 10 g ml^{-1}. Table 8 summarizes the optimum conditions for the electrolysis. Despite the vigorous gas formation (some ml min^{-1}), the pH of the solution remained constant.

Figs. 8 and 9 demonstrate that the optimized process is efficient for the purification of NH_4F solutions. The concentrations of many electroac-

Table 7
Cobalt concentrations during electrodeposition: comparison of experiment and calculation

Electrolysis time (min)	Experiment 2, initial concentration $c_0 = 1.8$ ng ml^{-1}		Experiment 3, initial concentration $c_0 = 20.0$ ng ml^{-1}	
	Experiment (ng ml^{-1})	Calculation * (ng ml^{-1})	Experiment (ng ml^{-1})	Calculation * (ng ml^{-1})
30	0.2	0.215		
32			2.18	2.08
60	0.021	0.026	0.28	0.28
90	0.003	0.003	0.03	0.034
λ (min^{-1})	0.07148		0.071285	
r	0.9990		0.9998	
$t_{1/2}$ (min)	9.70		9.72	

[a] Calculated using the λ value (0.07086) derived from experiment 1 (see Table 6) and the corresponding initial concentrations.

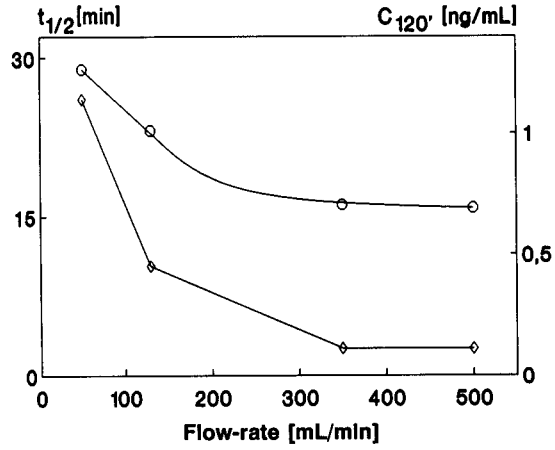

Fig. 7. Half-life of electrodeposition ($t_{1/2}$) vs. flow-rate; including the residual Co concentration ($c_{120'}$) after 120 min of electrolysis with 1.0 A. Initial concentration 18 ng ml^{-1} Co. $\diamond = c_{120'}$; $\circ = t_{1/2}$.

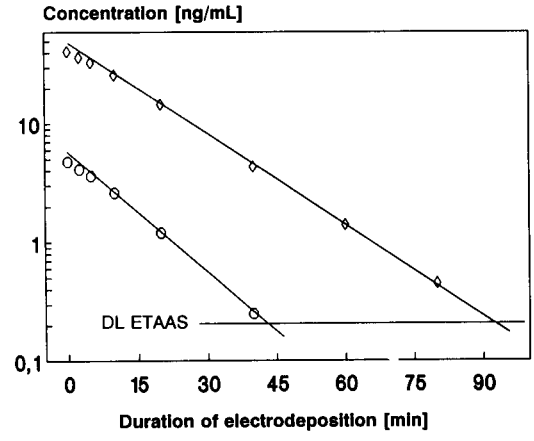

Fig. 8. Electrodeposition of Fe and Pb from 10% NH_4F solutions with 1.5 A ($\circ$ = Pb, $\diamond$ = Fe).

tive metals such as Cd, Co, Cu, Fe, Ni, Pb and Zn are decreased from the upper ng ml^{-1} range down to a few pg ml^{-1} within a reasonable electrolysis time of 60 to 120 min. Manganese is not electrodeposited, so that its concentration remains constant. Table 9 summarizes the initial and the corresponding concentrations after 120 min of electrolysis.

Some initial experiments indicate that the described system is also suitable for the purification of electrolyte solutions other than NH_4F as demonstrated in Fig. 10, which shows the concentration vs. time development for some trace metals in 8% aqueous NH_4NO_3 solution.

Table 8
Optimized parameters of electrolysis

Optimized parameters of electrolysis	
Cathode:	pyro-coated graphithe tube, diam. = 6 mm, length = 27 mm; geometric surface area = 950 mm^2 (Perkin-Elmer Type 910 504)
Anode:	glassy carbon rod (Sigradur® G), diam. = 4 mm, distance cathode to anode = 1 mm
Current:	1.5 A
Voltage:	about 7 V using a 10% NH_4F aqueous solution
Flow-rate:	$\geqslant$ 300 ml min^{-1} (with voltage applied)
Electrolyte concentration:	100 g l^{-1}

3.4. Recrystallization procedure

Most purification methods require an aqueous solution of the salt so that H_2O has to be removed subsequently. This time consuming process is rather susceptible to contamination. For

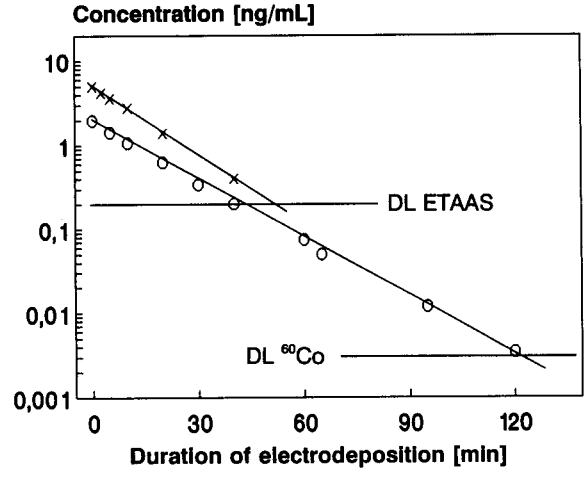

Fig. 9. Electrodeposition of Co and Ni from 10% NH_4F solutions (I = 1.5 A): $\circ$ = Co (radiochem. ^{60}Co); $\times$ = Ni.

Table 9
Effect of 120 min of electrolysis (1.5 A) on several elemental concentrations in NH_4F solutions (100 g ml^{-1})

Element	Initial concentration (ng ml^{-1})	Final concentration (ng m^{-1})
Cd	0.5 [a]	⩽ 0.05
Co	3.5 [a]	⩽ 0.2 [c]
Co	5.8 [a,b]	⩽ 0.003 [b]
Cu	13.0	⩽ 0.08
Fe	40.0	⩽ 0.2 [c]
Mn	1.5	1.5
Ni	5.0 [a]	⩽ 0.08
Pb	5.0	⩽ 0.05
Zn	25.0	⩽ 0.08

[a] Spiked. [b] Radiochemically (^{60}Co). [c] "Direct" ETAAS determination.

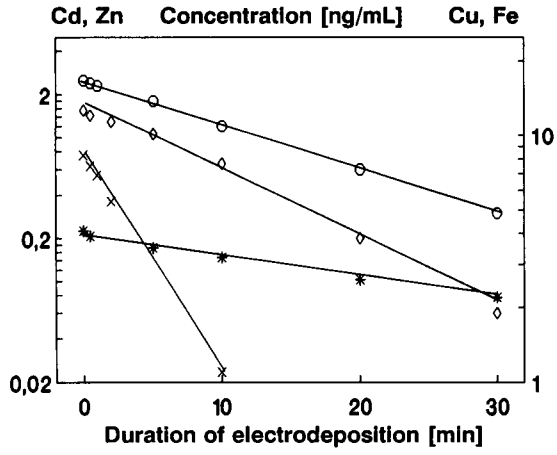

Fig. 10. Concentration–time development of the electrodeposition of Cd, Cu, Fe and Zn from an 8% NH_4NO_3 solutions. Conditions: $I = 0.3$ A; Pd anode. ◇ = Cd; × = Cu; * = Fe; ○ = Zn.

the removal of the solvent several different constructions have been described [e.g., 22–25] which are all closed to the outside to a large extent and are flushed with purified air or other gases. All these assemblies are useless for the removal of water from NH_4F solutions in order to obtain high-purity solid NH_4F because of the evolution of NH_3. In order to suppress the decomposition of NH_4F and the formation of NH_4HF_2, a completely closed device has been built to maintain a NH_3-containing atmosphere (see Fig. 3). Using the principle of subboiling distillation [26], the simultaneous removal of solvent from several samples is possible without cross-contaminations. The evaporation efficiency obtained varied between 0.8 and 1.6 ml h^{-1} for 40% NH_4F solutions.

A vapour-cleaned [27] vacuum funnel made of PTFE provided with a perforated plate has been used to separate the precipitated crystals from the residual solution (typically a few ml). Boreholes with a diameter of 1.2 mm were small enough to retain the fibrous NH_4F crystals so that no additional filter paper was necessary. The resulting wet product has been dried in a vacuum desiccator over silica gel for several hours.

Table 10
Effect of recrystallisation

	NH_4F MOS Selectipur®			NH_4F p.a.		
	Initial concentration (ng g^{-1})	Concentration recrystallization (ng g^{-1})	Purification (%)	Initial concentration (ng g^{-1})	Concentration after recrystallization (ng g^{-1})	Purification (%)
Cu	0.8	0.22 ± 0.04 ($n = 6$)	72	5	1.5 ± 0.2 ($n = 3$)	70
Fe	10	2.6 ± 0.2 ($n = 6$)	74	400	140 ± 10 ($n = 3$)	65
Mn	1.6	0.20 ± 0.1 ($n = 6$)	87	15	3.9 ± 0.7 ($n = 4$)	74
Ni	1.5	0.39 ± 0.07 ($n = 7$)	74	30	9 ± 1.2 ($n = 4$)	70
Pb	1.6	0.40 ± 0.1 ($n = 7$)	75	36	14.3 ± 1.8 ($n = 4$)	60
Zn	3	0.40 ± 0.2 ($n = 7$)	85	28	7.6 ± 1.6 ($n = 4$)	73

Purification(%) = $\{1 - (c_a/c_e)\} \cdot 100$; concentrations refer to the solid material. p.a.: (Lot 022 B 244064); MOS Selectipur®: (Lot 03 92 011 B 223 656). Recrystallization yield 50–60%.

Table 11
Efficiency of the entire procedure

Trace element	Reactant initial concentrations solid NH_4F p.a. ($ng\ g^{-1}$)	Product solid NH_4F ultra high purity ($ng\ g^{-1}$)	Purification (%)
Cu	5	≤ 0.2	96
Fe	400	≤ 2 [a]	99.5
Mn	15	3.9–4.5	70–75
Ni	30	≤ 0.3	99
Pb	36	≤ 0.15	99.6
Zn	28	≤ 0.1	99.6

[a] "Direct" ETAAS determination.

It was also found that the recrystallization of commercially available high-purity NH_4F decreases the concentrations of trace elements, as indicated in Table 10. Consequently, the recrystallization also increases the purity of the resulting solid product, provided that an adequately clean surrounding and carefully cleaned labware is maintained.

Table 11 illustrates the purification efficiency of the whole procedure (dissolving the reactant, 120 min electrolysis with 1.5 A, evaporation of the solvent and recrystallization of NH_4F, separating the crystals obtained from the residual solution and drying them in a vacuum desiccator, weighing them, and redissolving them) starting with solid NH_4F (p.a.) and ending with an ultra-high purity solid recrystallisate with a contamination level in the lower pg g^{-1} range.

4. Conclusions

It is possible to lower concentrations of electrochemically active elements in highly concentrated NH_4F solutions to values in the lower pg ml^{-1} range. The time consuming process of recrystallisation is shown to present another possible means for the purification of analytical reagents for ultra-trace analysis. The high recovery rates of the described multi-step procedure, even in the lower ng ml^{-1} range, imply the possible use of ion exchange as a fast and efficient method for the removal of ionic contaminations from (concentrated) salt solutions.

Acknowledgements

The authors would like to thank P. Burba (ISAS, Dortmund) for providing the cellulose based ion exchanger.

References

[1] G. Tölg and P. Tschöpel, Anal. Sci., 3 (1987) 199.
[2] G. Tölg and P. Tschöpel, in Z.B. Alfassi (Ed.), Determination of Trace Elements, VCH Verlag, Weinheim, in press.
[3] J.W. Mitchell, Talanta, 29 (1982) 993.
[4] M.Z. Haas and St. Bruckenstein, Anal. Chem., 46 (1974) 1962.
[5] L. Meites, Anal. Chem., 27 (1955) 416.
[6] J.W. Mitchell and C. McCrory, Separation and Purification Methods, 9 (1980) 165.
[7] X. Wang and R.M. Barnes, J. Anal. At. Spectrom., 4 (1989) 509.
[8] J.S. Preston and R.J. Whewell, J. Inorg. Nucl. Chem., 39 (1977) 1675.
[9] J.W. Mitchell, Anal. Chem., 45 (1973) 492A.
[10] J.W. Mitchell, Anal. Chem., 50 (1978) 194.
[11] K. Hoppstock, F. Alt, K. Cammann and G. Weber, Fresenius' J. Anal. Chem., 335 (1989) 813.
[12] J.A.C. Broekaert, T. Graule, H. Jenett, G. Tölg and P. Tschöpel, Fresenius' J. Anal. Chem., 332 (1989) 825.
[13] J.P. Matousek, Prog. Anal. Atom. Spectrosc., 4 (1981) 247.
[14] F.O. Jensen, J. Dolezal and F.J. Langmyhr, Anal. Chim. Acta, 72 (1974) 245.
[15] U. Richts, R.P.H. Garten, E. Jacob and G. Tölg, Fresenius' J. Anal. Chem., (1994) in press.
[16] H. Schlichting, Grenzschicht-Theorie, Braun, Karlsruhe, 5th edn., 1965.
[17] J. Fahland and G. Herrmann, Z. Anorg. Allg. Chem., 316 (1962) 141.
[18] W. Nernst, Z. Phys. Chem., (1904) 52.
[19] E. Brunner, Z. Phys. Chem., (1904) 56.
[20] N. Ibl, Chemie-Ing.-Techn., 33 (1961) 69.
[21] R. Schäfer and R. Schönhagen, in H. Schmidt (Ed.), Computer-Praxis Physik, Ferd. Dümmlers Verlag, Bonn, 1990.
[22] J.W. Mitchell, J. Radioanal. Chem., 69 (1982) 47.
[23] G. Tölg, Grundlagen der Spurenanalyse, Analytiker-Taschenbuch, Vol. 2, Springer Verlag, Berlin, 1981, pp. 724–744.
[24] G. Tölg, Analyst, 94 (1969) 705.
[25] G. Tölg and I. Lorenz, Fortschritte der Chemischen Forschung, 11 (1969) 507.
[26] E.C. Kuehner, R. Alvarez, P.J. Paulsen and T.J. Murphy, Anal. Chem., 44 (1972) 2050.

[27] P. Tschöpel, Pure Appl. Chem., 54 (1982) 913.
[28] A. Prange, K. Kramer and U. Reuss, Spectrochim. Acta, 46B (1991) 1385.
[29] M. Zief and J.W. Mitchell, Contamination Control in Trace Element Analysis, Chemical Analysis, Vol. 47, Wiley, New York, 1976, p. 135.
[30] M. Zief and R. Speights, Ultrapurity Methods and Techniques, Marcel Dekker, New York, 1972, p. 107.
[31] J.W. Mitchell, J. Cryst. Growth, 75 (1986) 42.
[32] H. Schildknecht, Zonenschmelzen, Verlag Chemie, Weinheim, 1964, p. 164.
[33] Ph. Albert, Pure Appl. Chem., 1 (1960) 111.
[34] W. Drews, Dissertation, Dortmund, 1990, p. 100.
[35] J.W. Mitchell, C. Herring and E. Bylina, Appl. Spectrosc., 38 (1984) 653.
[36] K. Hoppstock, R.P.H. Garten, P. Tschöpel and G. Tölg, Fresenius' J. Anal. Chem., 343 (1992) 778.
[37] R.Th. Keel and Th. Tisue, Int. J. Environ. Anal. Chem., 34 (1988) 89.

ELSEVIER

Analytica Chimica Acta 294 (1994) 69–74

ANALYTICA CHIMICA ACTA

Retention behaviour of metal chelates in ion-pair reversed-phase liquid chromatography as a function of mobile phase composition with methanol–water and acetonitrile–water mobile phases

Chizuko Ohtsuka *,[a], Kimiyo Matsuzawa [a], Hiroko Wada [b], Genkichi Nakagawa [1,b]

[a] *Mizuho College, Shunko-cho, Mizuho-ku, Nagoya, Japan*
[b] *Department of Applied Chemistry, Nagoya Institute of Technology, Showa-ku, Nagoya, Japan*

(Received 16th September 1993; revised manuscript received 28th February 1994)

Abstract

The retention behaviour of Cu(II), Co(III), Ni(II) and Fe(II) chelates with 2-(5-bromo-2-pyridylazo)-5-[*N*-propyl-*N*-(3-sulphopropyl)amino]phenol (5-Br-PAPS) and 2-(5-nitro-2-pyridylazo)-5-[*N*-propyl-*N*-(3-sulphopropyl)amino]-phenol (nitro-PAPS) in ion-pair reversed-phase liquid chromatography was examined with mobile phases of methanol–water and acetonitrile–water binary systems containing 0.05 M sodium ion and 0.02 M Tris buffer (pH 7). The correlation of log k' with the solubility parameter was different between the methanol–water and acetonitrile–water systems. The resolution among chelates and reagents was complete with the acetonitrile–water system and far better than with the methanol–water system.

Key words: Liquid chromatography; Ion chromatography; Metal chelates; Mobile phase composition

1. Introduction

Retention in reversed-phase liquid chromatography (RPLC) involves transfer of solute from the mobile phase into or on to the stationary phase. A widely adopted model has been the solvophobic theory [1,2] for simple molecules, such as hydrocarbons, for which the dominant interaction is due to induced dipoles [3–7]. The solvophobic theory predicts that the retention should depend only on the surface tension of the mobile phase solvent and not on the surface tension of the stationary phase. Many papers have been presented that indicate that solute retention and selectivity in RPLC depend on both the mobile and stationary phase variables [8]. In general, the solute adsorbs at the ends of the grafted chains or/and penetrates into the grafted chain phase. So far, the adsorption and partition mechanisms of solute retention have been considered experimentally as a function of the chemically bonded chain (the chain length [9–11], the intrinsic chain stiffness [12,13], the surface coverage [14] and carbon number etc. [15]), the silica substrate (pore size and residual silanol, etc. [16,17]) and the

* Corresponding author.
[1] Present address: Faculty of Science and Engineering, Meiji University, Ikuta, Kawasaki, Japan.

SSDI 0003-2670(94)00113-Z

organic modifier in the mobile phase (the composition and the content extracted in the grafted chain phase).

The organic solvent or modifier has been shown to play a particularly important role in RPLC. The organic solvent distributes between the mobile phase and stationary phase and establishes the structure of the stationary phase. The most commonly used mobile phases in RPLC are binary mixtures of water with an organic solvent modifier such as methanol and acetonitrile. Recently, the amount of extracted modifier [3–5,18–20] and the species in binary solution have been also studied spectroscopically [21–26]. Significant differences in methanol–water and acetonitrile–water systems have been found as a function of the volume fraction of water [27]. The difference has been examined mainly for comparison of the isotherms on the stationary phase, and rarely for comparison of the retention behaviours of multiple components. Water-soluble pyridylazosulphoaminophenol derivatives, which react with many metal ions to form the anionic chelates, have been employed for the determination of trace of metals by RPLC owing to the high sensitivity and solubility in water. Several ion pairs of anionic metal chelates with pyridylazosulphoaminophenol derivatives and sodium ions have been completely separated on a grafted stationary phase (C_{18}) [28–30].

In this study, the effect of modifier composition on the retention behaviour of the ion pairs formed from Cu(II), Co(III), Ni(II) and Fe(II) chelates with 2-(5-bromo-2-pyridylazo)-5-[*N*-propyl-*N*-(3-sulphopropyl)amino]phenol (5-Br-PAPS) and 2-(5-nitro-2-pyridylazo)-5-[*N*-propyl-*N*-(3-sulphopropyl)amino]phenol (nitro-PAPS) with sodium ion added was examined by using a binary mobile phase consisting of methanol–water or acetonitrile–water.

2. Experimental

2.1. Apparatus

The liquid chromatograph consisted of a Shimadzu (Kyoto) LC-6A pump (0.3 ml min^{-1}), a Shimadzu SPD-M6A spectrophotometric detector and a Rheodyne Model 7125 injector with a PTFE sample loop (20 μl). A Kaseisorb LC ODS-300-5 (particle size 5 μm) column (250 × 4.6 mm i.d.) (Tokyo Kasei, Tokyo) was employed at 30°C and maintained by means of a Taiyo (Tokyo) Thermo Minder Ace-80 circulating water bath.

2.2. Reagents and procedures

5-Br-PAPS and nitro-PAPS, which were purchased from Dojindo (Kumamoto), were dissolved in water to give 1×10^{-3} M solutions.

Sample solutions were prepared by mixing 1×10^{-5} M metal ion solution and more than a threefold molar excess of the chelating reagent, and the pH was adjusted with the buffer used for the mobile phase.

The concentration of organic solvent in the buffered mobile phase was varied from 57 to 75% methanol and from 30 to 45% acetonitrile. Both mobile phases contained 0.05 M sodium chloride. Tris–HCl (pH 7) and acetic acid–sodium acetate (pH 6) buffers were used to control the pH of the mobile phase. The capacity factor (k') was calculated using the column void volume of sodium nitrate [31].

3. Results and discussion

3.1. Effect of mobile phase composition on retention and selectivity

As a measure of the efficiency of a separation, the most commonly used parameter is the resolution (R_s) (Eq. 1) for peaks of equal size.

$$R_s = \frac{1}{4}\left(\frac{\alpha - 1}{\alpha}\right)\left(\frac{k'}{1+k'}\right)(L/H)^{1/2} \quad (1)$$

where α, k', L and H are the separation factor, capacity factor, column length and plate height, respectively. It should be considered as expressing the following concept: Resolution = selectivity × retention × efficiency. The first two factors are essentially thermodynamic, whereas the L/H term is mainly associated with the kinetic features of chromatography. The first and second terms

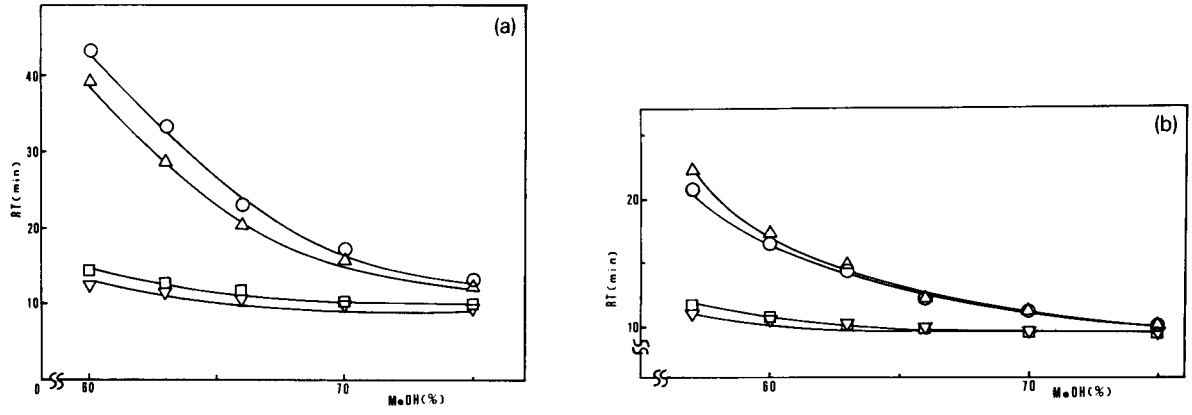

Fig. 1. Effect of methanol concentration on retention times. (a) 5-Br-PAPS chelates; (b) nitro-PAPS chelates. ▽ = Cu(II); □ = Co(II); △ = Ni(II); ○ = Fe(II).

are sensitive to changes in the values of the separation factor and capacity factor, respectively. In this study we considered the capacity factor and separation factor. Chromatographic selectivity is an important experimental parameter in studies of the solute retention process.

The solvent strength in a binary solvent mobile phase is usually varied by changing the proportions of strong and weak solvents. In reversed-phase separations, methanol and acetonitrile, which are preferably used as organic solvents, are strong, whereas water is weak. Hence the binary solvent systems methanol–water and acetonitrile–water were used to examine the retention and chromatographic selectivity of Cu(II), Co(III), Ni(II) and Fe(II) chelates with 5-Br-PAPS and nitro-PAPS. The effects of these chelates on the retention in methanol–water are shown in Fig. 1a and b, respectively. As the solvent strength decreased with decrease in methanol concentration in the methanol–water mobile phase, both 5-Br-PAPS and nitro-PAPS chelates were strongly retained. The concentration of methanol in the mobile phase controlled the retention but not the separation.

The effects of 5-Br-PAPS and nitro-PAPS chelates on the retention in acetonitrile–water are shown in Fig. 2a and b, respectively. As the

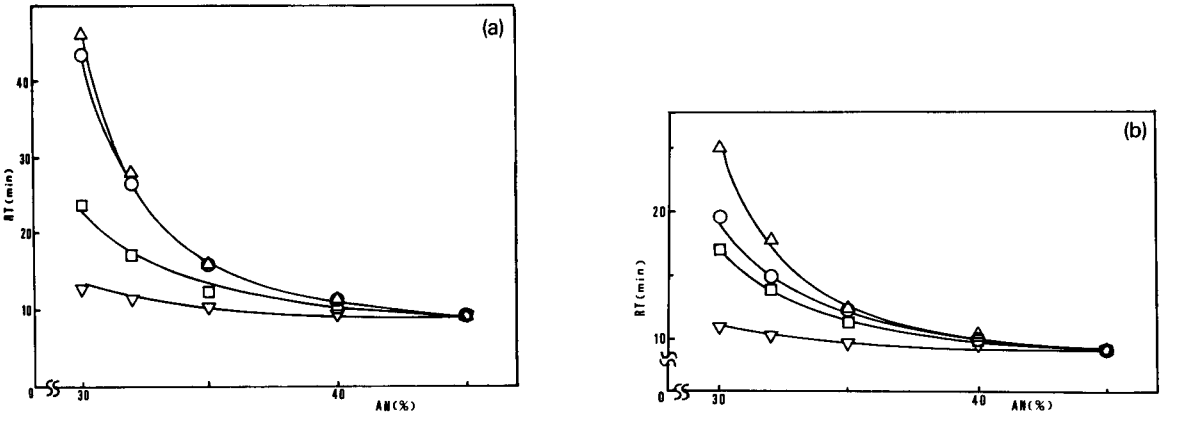

Fig. 2. Effect of acetonitrile concentration on retention times. (a) 5-Br-PAPS chelates; (b) nitro-PAPS chelates. Symbols as in Fig. 1.

solvent strength decreased with decrease in acetonitrile concentration in the acetonitrile–water mobile phase, both the 5-Br-PAPS and nitro-PAPS chelates were strongly retained. In the acetonitrile–water system, the concentration of acetonitrile in the mobile phase controlled not only the retention but also the separation of the chelates. For every band pair of nitro-PAPS chelates, baseline resolution ($\alpha > 1.5$) was easily attained.

3.2. Solubility parameter of organic solvent–water binary system

The retention of a solute is often expressed by the solubility parameter of the eluent or stationary phase [32–34]. Hence the difference in retention behaviour between the above binary systems should be discussed with respect to the correlation of log k' with the solubility parameter of the mobile phase. The solubility parameters of organic solvent–water binary systems were calculated by the method for regular solution mixtures, that is, as the arithmetic average of these values for pure solvent, weighted according to the volume fraction of each solvent. The equation used was

$$\delta_T = \phi_a \delta_a + \phi_b \delta_b \qquad (2)$$

where ϕ_a and ϕ_b are the volume fractions of solvent A and B, respectively, δ_a and δ_b refer to the solubility parameters of pure solvent A and B and δ_T is the solubility parameter of the binary system. Solubility parameters in the range examined were calculated using Eq. 2 using the solubility parameters of methanol, acetonitrile and water of 15.85, 13.15 and 25.52 $cal^{1/2}$ $cm^{-3/2}$ at 20°C, respectively [32].

It should be pointed out that the solvent behaviour of mixture of methanol and water would be difficult to explain as a binary mixture [35,36]. Such mixtures have often been explained by division into three parts according to the volume fraction of methanol, viz., two binary mixture parts (water–associated methanol and methanol–associated methanol) and a ternary mixture part (water–methanol–associated methanol). The retention in this study was examined in very limited concentration range corresponding to the ternary mixture part. Generally, the strength of the interaction of a solute with free methanol is likely to be much greater than that between the solute and the associated methanol [35]. Hence the volume fraction for the concentration ranges examined in this study was converted into the volume fraction on the assumption of a simple binary mixture consisting of free methanol and free water keeping the volume fraction ratio of free water to free methanol, as it is in the ternary mixture. For the binary system of acetonitrile–water, associated acetonitrile hardly exists in the concentration range examined, so the volume fraction was kept intact.

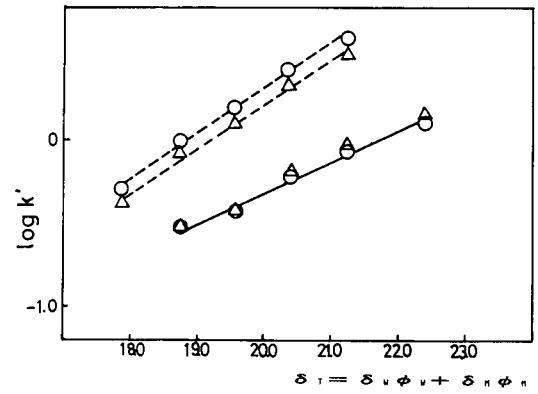

Fig. 3. Relationships between log k' values [Ni(II) and Fe(II) chelates] and solubility parameter (δ_T) for the methanol–water system. Solid line, 5-Br-PAPS; dashed line, nitro-PAPS.

It was found that with the methanol–water system the correlations of log k' with the solubility parameter for both 5-Br-PAPS and nitro-PAPS chelates, shown in Fig. 3, were linear, whereas with the acetonitrile–water system they were curved for both chelates, as shown in Fig. 4.

The difference in the correlations between the methanol–water and acetonitrile–water systems might correspond to the differences in the contents on the surface of the stationary phase. The isotherms for the distribution of methanol, acetonitrile and tetrahydrofuran between a bulk mobile phase and a bonded stationary phase had been presented by McCormik and Karger [18] with a gas chromatographic approach. Of the three modifiers studied in their work, methanol

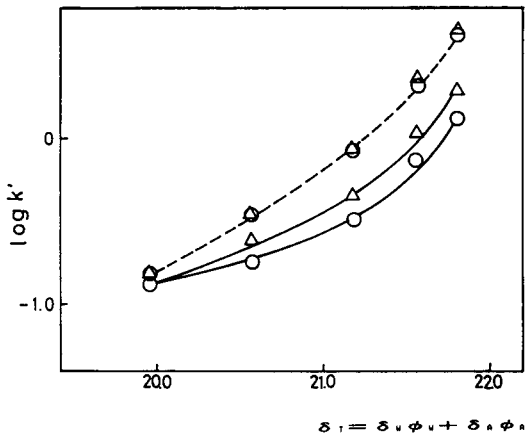

Fig. 4. Relationships between log k' values [Ni(II) and Fe(II) chelates] and solubility parameter (δ_T) for the acetonitrile–water system. Solid line, 5-Br-PAPS; dashed line, nitro-PAPS.

was least extracted into the stationary phase, tetrahydrofuran was extracted to the greatest extent and acetonitrile exhibited intermediate behaviour. In the methanol–water system, the stationary phase tends to be unaffected by changes in modifier composition. Hence, the retention strength depends mainly on the mobile phase, i.e., the volume fraction of free methanol in the mobile phase.

An important problem for the elucidation of the retention mechanism in RPLC is the evaluation of the relative contributions of the mobile phase and stationary phase, for instance, with the acetonitrile–water system. The effect of changes in the acetonitrile concentration on species in the mobile phase is considered. The acetonitrile–water system is used in many branches of chemistry, and the properties of such mixtures are therefore of considerable interest. A great deal of work [18,19,21–23,26] has already been done on the thermodynamic and spectroscopic properties of these mixtures. At low acetonitrile concentrations the water structure appears to be dominant in the mobile phase. As acetonitrile is added to pure water, it first enters cavities in the water structure [27,37]. The solute therefore comes less into contact with acetonitrile and more into contact with water. The solute was retained strongly owing to the hydrophobic interactions. With decrease in water content, acetonitrile can no longer be accommodated solely within these cavities. At higher acetonitrile concentrations, the non-polar solute can be sought and be preferentially solvated in an acetonitrile structure attributed to self-associated acetonitrile, principally the dimer [26]. Hence the solute becomes hardly retained. Consequently, the solute was retained suitably at intermediate acetonitrile concentrations.

Next, the effect of changes in the acetonitrile concentration on the amount of the modifier extracted onto the stationary phase is considered. As mentioned above, McCormick and Karger [18] reported the adsoption isotherms of acetonitrile on a hydrophobic stationary phase (C_{18}). These results were supported by studies of the retention of several alkylbenzenes by Alvarez-Zepeda et al. [27] with a thermodynamic approach. In general, solute retention is the result of both enthalpic and entropic effects. As ΔH becomes more negative, the solute is retained longer; as ΔS becomes more negative, the solute is retained less. The range examined in this study corresponds to the range examined by Alvarez-Zepeda et al., where the enthalpy, ΔH, becomes progressively more negative and the entropy, ΔS, is comparatively independent of composition. Retention is therefore dominated by ΔH. The progressive change in ΔH corresponds to the surface change of the stationary phase with extraction of acetonitrile. According to Pauling, owing to the large dipole moment, the CN bond can posses as much as 21% ionic character. Therefore, the stationary phase becomes more polar with increasing acetonitrile content. In the acetonitrile–water system, changes in the organic modifier component tends to induce changes in the properties not only of the mobile phase but also of the stationary phase. This makes the retention behaviour complex but effective in the present chromatographic studies.

4. Conclusion

Different organic modifiers were found to affect the retention and separation of ion pairs of metal chelates in RPLC. With the methanol–

water system, the retention mainly depended on the concentration of the free methanol in the mobile phase, whereas with the acetonitrile–water system the retention depended not only on the species in the mobile phase but also on the amount of extracted modifier, and thus led to a good separation. In the range of acetonitrile concentrations from 35 to 45% (v/v), the amount extracted modifier was shown to be suitable for the separation of ion pairs of the metal chelates examined.

References

[1] C. Horváth, W. Melander and I. Molnár, J. Chromatogr., 125 (1976) 129.
[2] D.E. Martire and E. Boehm, J. Phys. Chem., 87 (1983) 1045.
[3] E. Grushka, H. Colin and G. Guiochon, J. Chromatogr., 248 (1982) 325.
[4] D. Reymond, G.N. Chung, J.M. Mayer and B. Testa, J. Chromatogr., 391 (1987) 97.
[5] J.J. Michels and J.G. Dorsey, J. Chromatogr., 457 (1988) 85.
[6] W.J. Cheong and P.W. Carr, J. Chromatogr., 499 (1990) 373.
[7] S. Herron and A. Tchapla, J. Chromatogr., 556 (1991) 219.
[8] J.G. Dorsey and K.A. Dill, Chem. Rev., 89 (1989) 331.
[9] P.E. Antle, A.P. Goldberg and L.R. Snyder, J. Chromatogr., 321 (1985) 1.
[10] W. Cheng, M. McCown, J. Chromatogr., 318 (1985) 173.
[11] A.M. Krstulovic, H. Colin and A. Tchapla and G. Guiochon, Chromatographia, 17 (1983) 228.
[12] L.C. Sander and S.A. Wise, Anal. Chem., 56 (1984) 504.
[13] C.H. Lochmüller, M.L. Hunnicutt and J.F. Mullaney, J. Phys. Chem., 89 (1985) 5770.
[14] B. Buszewski, L. Nondek, A. Jurasek and D. Berek, Chromatographia, 23 (1987) 442.
[15] A. Tchapla, H. Colin and G. Guiochon, Anal. Chem., 56 (1984) 621.
[16] J. Köhler and J.J. Kirkland, J. Chromatogr., 352 (1986) 275.
[17] J. Köhler and J.J. Kirkland, J. Chromatogr., 385 (1987) 125.
[18] R..M. McCormik and B.L. Karger, Anal. Chem., 52 (1980) 2249.
[19] E.H. Slaats, W. Markovski, J. Fekete and H. Poppe, J. Chromatogr., 207 (1981) 299.
[20] K.B. Sentell and J.G. Dorsey, J. Chromatogr., 4610 (1989) 193.
[21] A. Loewenschuss and N. Yellin, Spectrochim. Acta, Part A, 31 (1975) 207.
[22] K. Kamogawa and T. Kitagawa, J. Phys. Chem., 90 (1986) 1077.
[23] J.W. Carr and J.M. Harris, Anal. Phys. Chem., 58 (1986) 626.
[24] M.J. Wirth, J. Phys. Chem., 91 (1987) 3926.
[25] M.J. Wirth and D.A. Hahn, J. Phys. Chem., 91 (1987) 3099.
[26] K.L. Rowlen and J.M. Harris, Anal. Chem., 63 (1991) 964.
[27] A. Alvarez-Zepeda, B.N. Barman and D.E. Martire, Anal. Chem., 64 (1992) 1978.
[28] C. Ohtsuka, H. Wada, T. Ishizuki and G. Nakagawa, Anal. Chim. Acta, 223 (1989) 339.
[29] C. Ohtsuka, K. Matsuzawa, H. Wada and G. Nakagawa, Anal. Chim. Acta, 252 (1991) 181.
[30] C. Ohtsuka, K. Matsuzawa, H. Wada and G. Nakagawa, Anal. Chim. Acta, 256 (1992) 91.
[31] M.J. Wells and C.R. Clark, Anal. Chem., 53 (1981) 1341.
[32] R. Tijssen, H.A.H. Billiet and P.J. Schoenmakers, J. Chromatogr., 122 (1976) 185.
[33] T.L. Hafkenscheid and E. Tomlinson, J. Chromatogr., 264 (1983) 47.
[34] K.M. Okamura, K. Hibi and H. Nakamura, Anal. Sci., 6 (1990) 857.
[35] E.D. Katz, K. Ogan and R.P.W. Scott, J. Chromatogr., 352 (1986) 67.
[36] E.D. Katz, C.H. Lochmüller and R.P.W. Scott, Anal. Chem., 61 (1989) 349.
[37] Y. Marcus and Y. Migron, J. Phys. Chem., 95 (1991) 400.

ELSEVIER

Analytica Chimica Acta 294 (1994) 75–84

ANALYTICA CHIMICA ACTA

Solvent study on the 9-substituted quinolizinocoumarins used as precolumn fluorescent and chemiluminescent reagents in liquid chromatography [1]

Falaye Traoré [a,b,*], Patrice Prognon [a], Georges Mahuzier [a]

[a] *Laboratoire de Chimie Analytique II, Faculté de Pharmacie, 5 rue J.B. Clément 92290 Châtenay-Malabry, France*
[b] *Faculté de Médecine et de Pharmacie de l'Université de Conakry, B.P. 1147 Conakry, Guinea*

(Received 30th July 1993; revised manuscript received 9th February 1994)

Abstract

9-substitued fluorescent quinolizinocoumarin derivatives (luminarins) were extensively studied spectroscopically, because of the wide variation in the emissions observed during liquid chromatographic detection in different mobile phases. Photophysical parameters measured at room temperature (λ_{ex}, λ_{em}, λ_{max}, $\nu'_a - \nu'_f$, Stokes' shift, relative quantum yield of fluorescence (ϕ_f), singlet level energy, molar absorptivity, etc.) were measured for eleven quinolizinocoumarin derivatives in twelve solvents. The observed spectroscopic variations associated with the change in solvents were analysed in terms of modification in the microenvironment of the luminarin derivatives. For this, a multiple linear regression analysis was performed in the linear solvation energy relationships model. The same regression model was used to describe and demonstrate the correlation between the structure of 9-sided chains and the observed spectral modifications. Finally, the practical consequences of such a study allowed the influence of the microenvironment on the fluorescence detection of luminarin derivatives after normal and reversed phase liquid chromatography to be demonstrated.

Key words: Fluorimetry; Chemiluminescence; Liquid chromatography; Luminarin; Quinolizinocoumarins

1. Introduction

Luminarins are quinolizinocoumarin compounds synthesized as fluorescent and chemiluminescent reagents especially for liquid chromatography [1–8]. Among the eleven luminarins commercially available eight have been of interest as precolumn fluorescent and chemiluminescent reagents, i.e., luminarins 3, 11 and 12 for aldehydes and ketones [6–8], luminarin 4 for carboxylic acids [3], luminarins 1 and 2 for amines [2,4,5], and recently luminarins 8 and 9 were developed for amines (data not published). The structural variations of the side chain at position 9 governs the reactivity of the probes: the important emis-

* Corresponding author.

[1] Presented at the *fifth International Symposium on Quantitative Luminescence Spectrometry in Biomedical Sciences, Ghent, Belgium, May 25–27, 1993*. The majority of papers presented at this symposium was published in *Anal. Chim. Acta*, Vol. 290/1-2, 1994.

SSDI 0003-2670(94)00119-7

sion properties are due to the highly conjugated quinolizinocoumarin nucleus (Fig. 1).

As with all fluorophores, luminarins have a relative fluorescence quantum yield (ϕ_f) highly influenced by the microenvironment. The selection of mobile phase is of great importance when luminarin compounds are used as derivatization reagents. Since these reagents have been successfully used both with normal and reversed phase eluents, a practical and analytical consequence was the important variation in the limit of detection (LOD) of the labelled compounds as a function of the chemical composition of the eluent. Since in all the studied applications [3,5–8] the emission of fluorescence is strictly due to the quinolizinocoumarin moiety in the absence of conjugation with labelled compounds (i.e., prostaglandin E_2, histamine, proline, tyramine, malonaldehyde, acrolein, pyrrolidine, hydroxymethylfurfural, etc.). The observed variation in LOD must be related to the influence of various mobile phases (chloroform, hexane, methyl and ethyl acetate, diisopropyl ether for normal chromatography [2,6,7], acetonitrile, water [2–7] for reversed phase chromatography) on the ϕ_f and molar absorptivity (ϵ) of the fluorophore component of the probe. In consequence, we tried to obtain a deeper knowledge of the absorption and emission properties of these quinolizinocoumarin reagents at room temperature, in order to establish a correlation between absorption and emission data, the microenvironment and especially with respect to the dipolarity/polarizability, donor and acceptor character of the solvent. In addition, the possible relation between the structure and the solvent–solute interaction and the importance of the linking side chain at position 9 will be discussed.

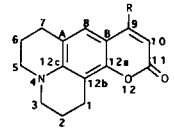

1	R : CH_3	(C.102)
2	R : $CH_2O(CH_2\text{-}CH_2O)_2\text{-}CH_3$	(C.102 HS)
3	R : $CH_2\text{-}OH$	(Lu. OH)
4	R : $CH_2\text{-}COOH$	(Lu.A134)
5	R : $CH_2\text{-}CO\text{-}NH\text{-}NH_2$	(Lu. 3)
6	R : $CH_2\text{-}CO\text{-}NH\text{-}(CH_2)_4\text{-}NH_2$	(Lu.4)
7	R : $CH_2\text{-}CO\text{-}NH\text{-}(CH_2)_5\text{-}COOH$	(Lu.8)
8	R : $(CH_2)_4\text{-}CO\text{-}NH\text{-}NH_2$	(Lu. 11)
9	R : $CH_2O(CH_2\text{-}CH_2O)_2\text{-}CH_2\text{-}CO\text{-}NH\text{-}NH_2$	(Lu.12)
10	R : $CH_2\text{-}CO\text{-}NH\text{-}(CH_2)_2\text{-}CH_2OH$	(Lu.NPROH)
11	R : $CH_2\text{-}CO\text{-}NH\text{-}N{=}CH\text{-}CH{=}CH_2$	(Lu.NNACR)

Fig. 1. Structures of the luminarins studied.

2. Experimental

2.1. Chemicals

9-substituted quinolizinocoumarins (luminarins) were synthesized or purchased from Eurobio (Les Ulis). The structures of the eleven compounds are depicted in Fig. 1.

All the solvents used in this study were of spectroscopic grade, and were carefully checked for the absence of fluorescent impurities; the water used was purified and distilled twice.

2.2. Methods

Absorbance spectra were recorded on a Model 2100 UV–visible spectrophotometer (Shimadzu) at 25°C using a 10 mm optical path quartz cuvette. All emission measurements were done at 25°C on an LS 50 luminometer (Perkin-Elmer) using a 10 mm optical path quartz cuvette. The emission and excitation slits were set at 2.5 nm. The relative fluorescence quantum yield was considered as the ratio of the total fluorescence intensity to the absorbance (I_F/A) at the maximum of excitation of the corresponding luminarin solutions (in arbitrary units) according to Parker and Rees [9]. The Stokes' shift ($\nu'_a - \nu'_f$) was calculated as $\nu'_a - \nu'_f(\text{cm}^{-1}) = 10^7(1/\lambda_{ex} - 1/\lambda_{em})$ where λ_{ex} and λ_{em} are the corrected maximum wavelengths for excitation and emission and are expressed in nanometers. The first singlet-state energy level (E_{s1}) was noted as the corresponding measured wavelength of the 0–0 transition λ_{0-0}. No statistical difference was found ($P < 0.05$) be-

tween measured λ_{0-0} and calculated λ_{0-0} values according to the following equation: $1/\lambda_{0-0} = 1/2(1/\lambda_{em} + 1/\lambda_{ex})$ [10].

For the linear solvation energy relationships (LSER) model, transformation to wavenumbers (ν') was systematically performed.

Multiple linear regression analysis (MLRA) was performed with STATWORKS™ software. In each run, the correlation coefficient (r) and the probability (P) related to the regression were systematically calculated. A P value < 0.05 was considered significant.

Attempts to correlate the photophysical data with the microenvironment as well as the structure of the 9-side chain of the eleven studied luminarins were achieved with the LSER of Kamlet and co-workers [11–14].

Thus, twelve solvents were chosen in order to study different chemical interactions with the luminarin derivatives. Moreover, the choice of the solvent was influenced by their possible use as eluent in normal or reversed phase LC. The selected solvent–solute interactions were: π^*, α and β according to the LSER model [14] for which corresponding values for the selected solvents are shown in Table 1 (π^* is the dipolarity/polarizability parameter which measures the ability of the solvent to stabilize a charge or a dipole by dielectric effect; α is the parameter describing the ability of the solvent to donate a proton (acidity); and β is the parameter which represents proton accepting ability, i.e., the basicity of the solvent). In order to simplify the whole LSER model, no other solvent–solute parameters were taken into account. Therefore, the multiple linear regression analysis between the measured spectroscopic parameters $Y(\nu'_{em}, \nu'_{0-0} \ldots)$ and the three main regressors describing the solvent–solute interactions leads to the general equation:

$$Y = a\pi^* + b\alpha + c\beta + e$$

where e is a constant and a, b and c are the coefficients respectively related to π^*, α, β and calculated by multiple linear regression analysis.

3. Results and discussion

3.1. Room temperature photophysical data

In order to correlate the spectroscopic data with the microenvironment and structure, six sets

Table 1
Solvatochromic parameters (π^*, α, β) according to Kamlet et al. [14]

Solvent (and abbr.)	Solvent type [a]	π^* [b]	α [c]	β [d]
Cyclohexane (CycH.)	NHB	0.00	0.00	0.00
Diisopropyl ether (DiisopE.)	HBA	0.27	0.00	0.49
Chloroform (Chlorf.)	NHB-HBD	0.58	0.44	0.00
Ethyl acetate (Eth.Ac.)	HBA	0.55	0.00	0.45
Tetrahydrofuran (THF)	HBA	0.58	0.00	0.55
Methylene chloride (Dichlorm.)	NHB	0.82	0.30	0.00
Dimethylsulfoxide (DMSO)	HBA	1.00	0.00	0.76
Dimethylformamide (DMF)	HBA	0.88	0.00	0.69
Ethanol (ETOH)	HBA-D	0.54	0.83	0.77
Acetonitrile (ACCN)	HBA-HBD	0.75	0.19	0.31
Methanol (MEOH)	HBA-D	0.60	0.93	0.62
Water	HBA-D	1.09	1.17	0.18

[a] NHB (non-hydrogen bonding solvent); HBA (hydrogen bond acceptor); HBD (hydrogen bond donor); HBA-D (amphiprotic hydrogen bond acceptor–donor); NHB-HBD (usually act as non-hydrogen bonding solvents, but have shown weak HBD properties with strong HBA indicator solutes).

[b] The π^* scale is an index of solvent dipolarity/polarizability, which measures the ability of the solvent to stabilize a charge or a dipole by virtue of its dielectric effect.

[c] The α scale of solvent HBD acidities describes the ability of the solvent to donate a proton in a solvent-to-solute hydrogen bond.

[d] The β scale of solvent HBA basicities provides a measure of the solvent's ability to accept a proton (donate a electron pair) in a solute-to-solvent hydrogen bond.

Table 2
Wavelengths of absorbance maxima (λ_{max}, in nm), for the luminarins studied in various solvents

Solvents	C.102	C.102HS	Lu.OH	Lu.A134	Lu.3	Lu.4	Lu.8	Lu.11	Lu.12	Lu.NPROH	Lu.NNACR
CycH.	363	373	364	364	374	363	355	365	–	371	389
DiisopE.	366	375	367	373	377	376	379	368	376	377	373
Chlorf.	372	392	390	395	403	401	404	392	394	403	399
Eth.Ac.	365	379	374	380	382	384	384	377	380	384	382
THF	368	380	376	382	383	385	384	378	381	383	383
Dichlm.	374	391	388	392	399	397	400	389	391	400	396
DMSO	374	393	389	388	396	394	395	391	392	395	397
DMF	372	389	385	384	392	392	391	388	389	391	392
ETOH	376	392	388	386	398	395	394	395	395	396	–
ACCN	370	387	384	382	391	391	391	385	387	392	393
MEOH	375	394	392	391	399	399	397	393	394	398	399
Water	386	404	398	393	408	408	408	399	404	408	408

of data were measured or calculated for the eleven luminarins in the twelve chosen solvents, i.e., λ_{max} (Table 2), ϵ (Table 3), λ_{ex} and λ_{em} (Table 4), $\nu'_a - \nu'_f$ (Table 5), I_F/A (Table 6) and λ_{0-0} (Table 7).

Such a large collection of data is difficult to interpret; nevertheless, some general trends can be defined. As can be seen, the emission band (Table 4) is almost constantly affected by the global polarity of the solvent with a shift depending on the compound. The generally observed bathochromic shift appears consistent with the $\pi \rightarrow \pi^*$ nature of the lowest transition of the luminarins. Moreover, the change in polarity has no effect on the shape of the excitation and the emission band.

On the other hand the $\pi \rightarrow \pi^*$ nature of the S_1 state is well supported by the increase in the Stokes' shift (Table 5), λ_{em} (Table 4) and λ_{0-0} (Table 7) with solvent polarity. Moreover, this strongly suggests that dipole–dipole interaction and hydrogen bonding can contribute to lower the S_1 state energy level and consequently increase the Stokes' shift. This latter point is in agreement with the decreased fluorescence emission (I_F/A) associated with the increase in polarity. In addition, such behaviour has already been reported with other coumarin derivatives [15].

Table 3
Molar absorptivity (ϵ, $\times 10^4$ l mol^{-1} cm^{-1}) for the luminarins studied in various solvents

Solvents	C.102	C.102HS	Lu.OH	Lu.A134	Lu.3	Lu.4	Lu.8	Lu.11	Lu.12	Lu.NPROH	Lu.NNACR
CycH.	2.78	2.03	–	–	1.52	–	–	–	–	–	2.83
DiisopE.	2.69	2.30	2.15	1.59	2.15	–	–	3.05	3.26	0.85	2.74
Chlorf.	1.91	2.59	2.57	2.42	2.83	1.85	2.57	3.09	3.15	2.38	2.97
Eth.Ac.	2.13	2.20	2.10	2.08	2.58	1.51	2.05	3.19	2.70	1.90	2.69
THF	2.36	2.81	2.71	2.76	2.71	2.00	2.68	3.07	2.80	2.52	2.61
Dichlm.	2.48	2.96	2.98	2.86	3.06	2.23	2.82	3.49	3.33	2.85	3.40
DMSO	1.91	2.27	2.25	2.24	2.46	1.78	2.18	2.81	2.82	1.99	2.66
DMF	1.94	2.29	2.21	2.23	2.47	1.77	2.12	2.82	2.56	1.99	2.56
ETOH	2.01	2.25	2.27	2.28	2.45	1.73	2.15	3.06	2.50	2.07	–
ACCN	1.93	2.39	2.26	2.19	2.56	1.64	2.12	2.72	2.62	2.06	2.67
MEOH	1.98	2.38	2.26	2.44	2.69	1.92	2.28	3.03	2.77	2.21	2.77
Water	–	1.63	1.14	0.74	1.96	1.17	1.21	2.07	2.04	1.52	1.98

Table 4
Excitation and emission wavelengths ($\lambda_{ex}/\lambda_{em}$, in nm) of the luminarins studied in various solvents

Solvents	C.102	C.102HS	Lu.OH	Lu.A134	Lu.3	Lu.4	Lu.8	Lu.11	Lu.12	Lu.NPROH	Lu.NNACR
CycH.	363/409	380/424	378/421	380/412	375/420	377/419	386/423	365/412	−/−	383/423	381/421
DiisopE.	366/418	381/428	365/424	373/419	377/424	384/425	383/423	368/416	381/441	385/424	379/423
Chlorf.	383/435	395/453	391/455	392/443	394/450	400/452	399/454	392/442	390/458	401/451	398/453
Eth.Ac.	376/427	385/448	380/447	386/443	387/444	387/444	388/448	384/429	384/451	391/447	389/444
THF	380/428	384/448	383/447	388/441	388/443	392/446	389/444	382/428	382/451	389/446	389/444
Dichlm.	388/442	393/460	393/462	391/440	399/456	399/452	397/462	389/443	393/459	400/455	395/454
DMSO	389/452	393/473	392/472	392/454	394/464	394/464	393/461	391/455	392/474	394/464	394/465
DMF	384/447	393/472	388/463	388/449	393/459	392/454	394/455	388/450	392/474	393/461	394/461
ETOH	389/463	393/483	391/475	392/461	397/475	395/474	395/476	394/468	393/490	393/472	−/−
ACCN	384/445	383/473	385/469	389/448	394/464	394/462	392/468	387/448	390/473	393/465	394/466
MEOH	390/465	396/489	392/486	393/470	399/481	395/479	394/481	393/471	394/498	397/476	397/480
Water	386/475	397/511	396/506	397/484	403/502	400/505	403/503	399/489	404/512	398/503	397/499

3.2. LSER model and 9-substitued quinolizinocoumarins

The above considerations, although of general interest, do not lead to a precise insight into the solvent–solute interactions as required. In this respected, numerous attempts to correlate spectroscopic data and the polarity of a solvent with respect to the structure of the solute have been described in the literature [11–14,16–19]. Although none of them perfectly describes the complexity of the solvent–solute interactions, we chose the LSER model because of numerous reports indicating its relative versatility in different areas of chemistry. On the other hand, valid results, related to the Dimroth and Reichardt's [$E_T(30)$], the dipole factor (Δf) and Hildebrand solubility (δ_H) parameters, were clearly established with some coumarinic fluorescent probes derivatized from the 7-amino coumarin [20–22]. These coumarin derivatives (as luminarins) appear to be of interest with respect to the LSER approach. Therefore, the described multi-linear regression analysis was performed for all above-mentioned spectroscopic parameters. The correlations, therefore, were analysed according to the classical statistical methodology of the analysis of variance. For spectroscopic significance of the LSER model, the dependent parameter (Y) must be directly correlated to solvatation energy, thus

Table 5
Stokes shifts ($\nu'_a - \nu'_f$, in cm^{-1}) for the luminarins studied in various solvents

Solvents	C.102	C.102HS	Lu.OH	Lu.A134	Lu.3	Lu.4	Lu.8	Lu.11	Lu.12	Lu.NPROH	Lu.NNACR
CycH.	3098	2731	2702	2044	2857	2659	2266	3125	–	2469	2494
DiisopE.	3399	2882	3812	2943	2940	2512	2469	3135	3571	2389	2745
Chlorf.	3121	3241	3597	2937	3158	2876	3036	2886	3807	2765	3051
Eth.Ac.	3177	3653	3944	3333	3317	3317	3452	2732	3869	3204	3184
THF	2951	3720	3738	3097	3200	3089	3184	2814	4005	3285	3184
Dichlm.	3149	3706	3800	2848	3133	2939	3544	3134	3659	3022	3290
DMSO	3583	4304	4324	3484	3829	3829	3753	3597	4413	3829	3875
DMF	3670	4259	4175	3501	3659	3484	3403	3551	4413	3753	3689
ETOH	4109	4741	4523	3818	4136	4219	4308	4013	5037	4259	–
ACCN	3570	4968	4652	3386	3829	3736	4143	3518	4499	3940	3921
MEOH	4136	4803	4934	4169	4273	4440	4591	4214	5300	4181	4356
Water	4854	5619	5490	4528	4894	5198	4933	4613	5221	5245	5149

Table 6
Relative fluorescence quantum yields (I_F/A, in arb. units) for the luminarins studied in various solvents, calculated in arbitrary units according to [9]

Solvents	C.102	C.102HS	Lu.OH	Lu.A134	Lu.3	Lu.4	Lu.8	Lu.11	Lu.12	Lu.NPROH	Lu.NNACR
CycH.	3.87	2.96	–	–	0.65	–	–	–	–	–	0.70
DiisopE.	3.04	2.46	2.36	0.25	0.71	–	–	1.50	0.97	3.13	3.07
Chlorf.	2.24	2.70	2.42	0.73	0.78	2.26	1.21	1.15	1.64	2.83	2.54
Eth.Ac.	2.06	2.27	2.33	1.73	3.29	2.22	2.19	3.52	2.30	2.92	2.96
THF	2.58	2.58	2.58	2.58	2.97	3.08	2.73	3.25	2.11	3.00	3.16
Dichlm.	3.81	3.64	3.08	1.26	2.62	2.44	0.28	3.50	1.69	3.43	3.38
DMSO	2.60	2.33	2.47	3.23	3.73	2.77	2.96	4.18	4.24	2.91	3.51
DMF	2.11	2.02	2.09	2.78	2.52	2.47	2.51	3.31	2.04	2.56	2.68
ETOH	2.18	1.67	1.72	2.49	2.25	1.94	2.14	2.90	1.56	2.14	–
ACCN	2.25	1.89	1,93	2.66	2.41	2.29	0.56	3.12	1.80	2.38	2.24
MEOH	2.04	1.45	1.53	2.29	2.53	1.82	1.98	2.62	1.38	2.00	2.13
Water	–	0.72	0.80	1.59	1.26	1.03	1.32	1.93	0.79	1.23	1.18

wavenumbers (ν') and frequencies (ν) must be selected [23]. The obtained correlations were not identical for all the tested photophysical parameters and follow the order: $\nu'_{0-0} > \nu'_{em} > \nu'_a - \nu'_f > \nu'_{ex}$ with ν'_{0-0}, ν'_{em}, ν'_{ex} (in cm^{-1}) corresponding to λ_{0-0}, λ_{em} and λ_{ex}, respectively.

As an example, Tables 8, 9, 10 and 11 report the LSER multi-linear regression analysis for ν'_{em} (average $r = 0.978$), ν'_{ex} (average $r = 0.830$), ν'_{0-0} (average $r = 0.987$) and $\nu'_a - \nu'_f$ (average $r = 0.925$). The emission wavenumbers (ν'_{em}) and 0–0 transition wavenumbers (ν'_{0-0}) appear as the most correctly correlated dependent parameters with respect to the variation of polarity of the twelve tested solvents and for the eleven luminarins. This suggests that the excited luminarins (S_1 state) are extremely sensitive to modification of the microenvironment, especially when dipole–dipole and/or hydrogen bonding occurs. Moreover, as shown in Tables 8–11, the coefficients a, b and c follow a common trend: the contribution of a and b appears to be generally more important that of c. This suggests that the spectroscopically observed variations of luminarins as a function of the polarity of the solvent is mainly governed by the dipole–dipole interaction and the ability of the solvent to donate protons (acidic character).

It should be pointed out that this is in agree-

Table 7
0–0 transition wavelengths (λ_{0-0}, in nm) for the luminarins studied in various solvents

Solvents	C.102	C.102HS	Lu.OH	Lu.A134	Lu.3	Lu.4	Lu.8	Lu.11	Lu.12	Lu.NPROH	Lu.NNACR
CycH.	386	397	397	388	395	394	397	388	–	399	400
DiisopE.	394	405	400	394	402	402	403	395	408	405	400
Chlorf.	412	427	426	417	428	429	431	415	428	430	424
Eth.Ac.	402	417	412	412	413	415	417	406	417	416	415
THF	403	416	411	412	414	414	415	405	417	415	415
Dichlm.	414	428	427	414	429	428	430	417	429	429	422
DMSO	419	435	428	422	429	429	429	423	435	429	427
DMF	414	429	424	418	425	425	424	420	431	425	425
ETOH	423	439	435	426	439	436	435	430	442	436	–
ACCN	415	431	426	417	427	427	428	418	431	427	427
MEOH	425	444	440	430	441	441	440	433	445	441	434
Water	429	465	462	446	462	460	461	448	466	462	442

Table 8
Equations incorporating solvatochromic parameters (π^*, α and β) and ν'_{em} values for the luminarins studied in various solvents

Compounds	$Y(\nu'_{em}, \text{in cm}^{-1}) = a\pi^* + b\alpha + c\beta + e$	r^a/P^b
C.102	$Y = -1714.16\pi^* - 1498.02\alpha - 902.17\beta + 24596.22$	0.984/< 0.001
C.102HS	$Y = -2213.10\pi^* - 1591.78\alpha - 792.18\beta + 23876.20$	0.975/< 0.001
Lu.OH	$Y = -2335.45\pi^* - 1513.02\alpha - 482.17\beta + 23937.98$	0.979/< 0.001
Lu.A134	$Y = -1736.76\pi^* - 1401.36\alpha - 818.23\beta + 24299.50$	0.974/< 0.001
Lu.3	$Y = -2029.57\pi^* - 1613.43\alpha - 576.65\beta + 23987.42$	0.982/< 0.001
Lu.4	$Y = -1967.14\pi^* - 1688.18\alpha - 559.04\beta + 23982.39$	0.985/< 0.001
Lu.8	$Y = -1963.01\pi^* - 1636.11\alpha - 217.14\beta + 23742.67$	0.971/< 0.001
Lu.11	$Y = -1863.86\pi^* - 1791.50\alpha - 734.79\beta + 24540.59$	0.983/< 0.001
Lu.12	$Y = -1841.93\pi^* - 1742.45\alpha - 1161.59\beta + 23675.60$	0.980/< 0.001
Lu.NPROH	$Y = -2072.43\pi^* - 1424.48\alpha - 429.72\beta + 23869.88$	0.976/< 0.001
Lu.NNACR	$Y = -2078.18\pi^* - 1468.74\alpha - 509.10\beta + 23943.53$	0.973/< 0.001

[a] Correlation coefficient.
[b] The value of P indicates the probability that correlation would occur by chance in sampling fluctuation. The smaller the value of P, the greater the probability that the correlation was due to the influence of the independent variable(s) on the dependent variable. A P value of less than 0.05 was considered significant in this study.

ment with structural considerations concerning quinolizinocoumarin compounds in which the presence of amino and carbonyl groups are susceptible to dipole–dipole formation and capable of accepting protons, because of the available electron pairs.

Therefore, luminarin derivatives should act as sensors of the variation of the dipolar character as well as the acidity character of the microenvironment. As a direct consequence, luminarin derivatives should be less sensitive to the variation of the basicity character of the solvent. These latter considerations are in agreement with the measured signals in the LC of labelled luminarin derivatives [1,2,6,7]. The best fluorescence performance in LC, defined in term of intrinsic fluorescence sensitivity (IFS), was observed in moderately polar, hydrogen-bond acceptor and non-hydrogen bonding solvents (i.e., dimethylsulfoxide and methylene chloride). These results suggest the selection of ethyl acetate, tetrahydrofuran, methylene chloride, dimethylsulfoxide and dimethylformamide (DMF) to sensitize the fluorescence of the luminarin derivatives. These solvents have the further advantage of dissolving high concentrations of luminarin derivatives, and

Table 9
Equations incorporating solvatochromic parameters (π^*, α and β) and ν'_{ex} values for the luminarins studied in various solvents

Compounds	$Y(\nu'_{ex}, \text{in cm}^{-1}) = a\pi^* + b\alpha + c\beta + e$	r/P
C.102	$Y = -1350.82\pi^* - 340.62\alpha - 544.97\beta + 27338.65$	0.783/0.046
C.102HS	$Y = -193.87\pi^* - 465.71\alpha + 233.18\beta + 25787.55$	0.629/0.236
Lu.OH	$Y = -1189.19\pi^* - 410.82\alpha + 208.59\beta + 26637.38$	0.739/0.084
Lu.A134	$Y = -378.80\pi^* - 406.41\alpha + 376.87\beta + 25895.38$	0.626/0.241
Lu.3	$Y = -1279.25\pi^* - 624.80\alpha + 19.96\beta + 26552.91$	0.940/< 0.001
Lu.4	$Y = -1051.33\pi^* - 373.08\alpha + 203.12\beta + 26199.86$	0.874/0.007
Lu.8	$Y = -764.41\pi^* - 420.99\alpha + 380.25\beta + 25936.91$	0.935/0.001
Lu.11	$Y = -1539.91\pi^* - 734.07\alpha - 196.19\beta + 27221.66$	0.924/0.001
Lu.12	$Y = -1093.06\pi^* - 608.18\alpha + 22.42\beta + 26582.27$	0.977/< 0.001
Lu.NPROH	$Y = -787.87\pi^* - 289.95\alpha + 353.75\beta + 25898.67$	0.845/0.014
Lu.NNACR	$Y = -966.62\pi^* - 282.69\alpha + 189.83\beta + 26179.81$	0.853/0.022

Table 10
Equations incorporating solvatochromic parameters (π^*, α and β) and ν'_{0-0} values for the luminarins studied in various solvents

Compounds	$Y(\nu'_{0-0}$, in $cm^{-1}) = a\pi^* + b\alpha + c\beta + e$	r/P
C.102	$Y = -1523.99\pi^* - 987.82\alpha - 513.50\beta + 25830.22$	0.968/ < 0.001
C.102HS	$Y = -1945.11\pi^* - 1386.36\alpha - 331.39\beta + 25236.56$	0.995/ < 0.001
Lu.OH	$Y = -1843.19\pi^* - 1488.64\alpha - 28.96\beta + 25289.50$	0.994/ < 0.001
Lu.A134	$Y = -1767.15\pi^* - 1171.50\alpha - 453.58\beta + 25735.84$	0.979/ < 0.001
Lu.3	$Y = -1860.69\pi^* - 1504.24\alpha - 152.42\beta + 25282.22$	0.994/ < 0.001
Lu.4	$Y = -1898.24\pi^* - 1410.59\alpha - 132.54\beta + 25284.61$	0.991/ < 0.001
Lu.8	$Y = -1845.38\pi^* - 1348.83\alpha - 73.70\beta + 25099.31$	0.991/ < 0.001
Lu.11	$Y = -1798.77\pi^* - 1387.82\alpha - 506.67\beta + 25842.66$	0.992/ < 0.001
Lu.12	$Y = -1865.73\pi^* - 1425.74\alpha - 415.88\beta + 25172.10$	0.995/ < 0.001
Lu.NPROH	$Y = -1703.73\pi^* - 1394.29\alpha - 2.87\beta + 25034.69$	0.996/ < 0.001
Lu.NNACR	$Y = -1529.81\pi^* - 846.14\alpha - 167.00\beta + 25058.22$	0.957/ < 0.001

can be used in postcolumn reactions enhancement after normal or reversed phase LC [2–8].

3.3. Relationship between the structure of the side chain at position 9 and the selected dependent parameters

Because of the common quinolizinocoumarin nucleus, the observed spectroscopic variations as a function to the solvent must be due to the structural difference of the side chain only. To validate this assumption, an attempt to correlate the structural variation of the chain with the observed ν'_{0-0}, ν'_{ex}, $\nu'_a - \nu'_f$ and ν'_{em} values were carried out for each solvent. As in the former case, MLRA was used to achieve this goal. First of all, it was necessary to define the regressors involved in MLRA. Owing to the number of studied luminarins ($n = 11$), no more than five regressors could be chosen (the $2n$ rule) [24]. After careful analysis of the structure of the eleven side chains (9-position), four groups of regressors (R_i) were selected and in each group a weight (w_i) was attributed to each selected regressor as a function of its estimated contribution to the solvent–solute interactions according to the LSER model (Table 12). Using this approach, one can define the chemical solvent–solute interactions involved, the chemical nature of the regressor and the number of regressors involved in a side chain with position 9.

Table 13 reports the regression coefficient (r) and the associated probability (P) corresponding to the MLRA performed with ν'_{0-0}, ν'_{em}, $\nu'_a - \nu'_f$

Table 11
Equations incorporating solvatochromic parameters (π^*, α and β) and $\nu'_\alpha - \nu'_f$ values for the luminarins studied in various solvents

Compounds	$Y(\nu'_\alpha - \nu'_f$, in $cm^{-1}) = a\pi^* + b\alpha + c\beta + e$	r/P
C.102	$Y = 346.04\pi^* + 1015.73\alpha + 494.72\beta + 2821.76$	0.895/0.004
C.102HS	$Y = 1799.27\pi^* + 863.42\alpha + 964.67\beta + 2321.84$	0.880/0.006
Lu.OH	$Y = 1121.44\pi^* + 959.25\alpha + 733.37\beta + 2821.94$	0.926/0.001
Lu.A134	$Y = 841.54\pi^* + 954.83\alpha + 914.01\beta + 2129.22$	0.958/ < 0.001
Lu.3	$Y = 750.78\pi^* + 988.76\alpha + 596.64\beta + 2565.13$	0.938/ < 0.001
Lu.4	$Y = 916.07\pi^* + 1294.97\alpha + 761.97\beta + 2217.47$	0.925/0.001
Lu.8	$Y = 1198.56\pi^* + 1215.14\alpha + 597.47\beta + 2194.23$	0.935/0.001
Lu.11	$Y = 324.35\pi^* + 1057.53\alpha + 538.26\beta + 2680.92$	0.876/0.007
Lu.12	$Y = 748.66\pi^* + 1134.05\alpha + 1183.68\beta + 2906.95$	0.958/ < 0.001
Lu.NPROH	$Y = 1284.39\pi^* + 1134.95\alpha + 783.37\beta + 2028.82$	0.921/0.001
Lu.NNACR	$Y = 1110.91\pi^* + 1186.59\alpha + 699.00\beta + 2236.55$	0.959/ < 0.001

Table 12
Regressors (R_i), chemical functions and corresponding weights (w_i) describing the structure of the side chain for MLRA (general equation: $Y = e + aR_1 + bR_2 + cR_3 + dR_4$)

Regressor (R_i)	Chemical function	Weight (w_i)
R_1, 1st group:	-COOH	4
hydrogen donor	-OH	1
R_2, 2nd group:	$-NH_2$	2
hydrogen acceptor	$-NHNH_2$	1
R_3, spacer	$-(CH_2)_n-$	1
R_4, hydrogen acceptor and dipole center	-O-	2

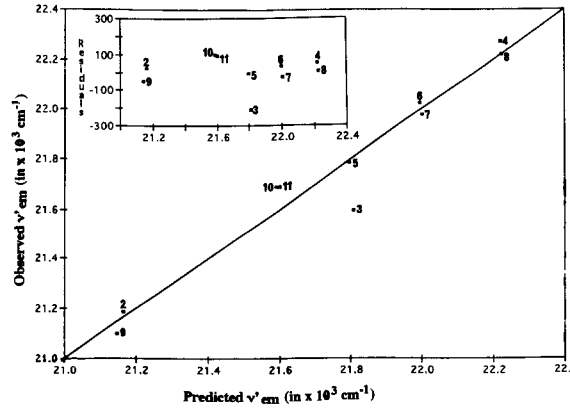

Fig. 2. Results of a multiple linear regression analysis using the weights of the selected regressors to predict the luminarin ν'_{em} in DMF. The predict ν'_{em} was calculated from the regression equation: $\nu'_{em} = 21676.04(\pm 118.68) + 209.30(\pm 28.06)R_1 + 198.14(\pm 64.82)R_2 + 141.37(\pm 44.48)R_3 - 108.72(\pm 19.16)R_4$ ($r^2 = 0.9498$, $P = 0.002$).The numbers in parentheses represent the standard deviations of the coefficients, and r^2 the square of the correlation coefficient, indicating the fraction of the variance of the dependent variable (ν'_{em}) predicted by the regression model. In the present case, 95% of the variance associated with ν'_{em} of derivatives is accounted by the multiple regression model. Inset: the corresponding residual analysis. For other details, see text. Compounds: 2, C.102 HS; 3, Lu.OH; 4, Lu.A134; 5, Lu.3; 6, Lu.4; 7, Lu.8; 8, Lu.11; 9, Lu.12; 10, Lu.NPROH; 11, Lu.NNACR.

and ν'_{ex} values. As can been seen, the best dependent parameters (Y) appear to be ν'_{0-0} and ν'_{em}, which globally show the best average correlation (0.855 and 0.888, respectively), and among all the tested solvents, the best correlations were obtained in DMF (0.964 and 0.975, respectively). This latter observation agrees with the importance of the dipole–dipole interaction and thus underlines the importance of the oxygen atom in the side chain. On the other hand, it should be pointed out that, as reported in Tables 8–11, the coefficient a of the π^* index is always predominant in comparison with the b and c coefficients. This indirectly corroborates the choice of the structural regressors (R_i) as well as their affected weights (w_i).

Finally, Table 13 shows clearly that the spectroscopic data related to the absorption (ν'_{ex}) and Stokes shift ($\nu'_a - \nu'_f$) are poorly correlated with the structure of the side chain, unlike ν'_{0-0} and ν'_{em}.

Table 13
Correlation coefficient (r) and probability (P) corresponding to the MLRA between the effects of the donor (COOH, OH), the acceptor (NH_2, $NHNH_2$), the spacer (CH_2) and the oxygen atom, of the side chain (position 9) of the studied luminarins, and the ν'_{0-0}, ν'_{em}, ν'_{ex} and $\nu'_a - \nu'_f$ values in various solvents

Solvents	ν'_{0-0}		ν'_{em}		ν'_{ex}		$\nu'_a - \nu'_f$	
	r	P	r	P	r	P	r	P
CycH.	0.825	0.241	0.850	0.189	0.911	0.076	0.927	0.054
DiisopE.	0.895	0.053	0.954	0.008	0.675	0.468	0.325	0.956
Chlorf.	0.765	0.272	0.819	0.167	0.376	0.924	0.600	0.624
Eth.Ac.	0.931	0.021	0.979	0.001	0.785	0.231	0.755	0.294
THF	0.960	0.006	0.975	0.002	0.773	0.257	0.848	0.117
Dichlm.	0.700	0.413	0.693	0.430	0.695	0.424	0.665	0.490
DMSO	0.942	0.013	0.894	0.055	0.764	0.274	0.830	0.146
DMF	0.964	0.004	0.975	0.002	0.609	0.606	0.843	0.125
ETOH	0.903	0.089	0.915	0.072	0.561	0.765	0.908	0.082
ACCN	0.881	0.070	0.868	0.087	0.590	0.642	0.800	0.202
MEOH	0.824	0.157	0.877	0.075	0.599	0.625	0.734	0.338
Water	0.672	0.474	0.853	0.109	0.743	0.319	0.823	0.159

Thus, the structure of the excited molecule appears to be essentially involved in the solvent–solute interactions, and the oxygen atoms located in the side chain, to play a crucial role. As an example, the regression analysis performed for the luminarin derivatives studied in DMF is depicted in Fig. 2.

In conclusion, the interest of the statistical tool of multiple linear regression analysis was to correlate the photophysical data of luminarins and their solvent–solute interactions via the LSER model, as well as to stress the role of the side chain structure in this interaction. In such a way, the drastic differences in the fluorescence signals of the luminarin labelled derivatives analysed by LC can now be more clearly understood. More precisely, the very low LODs observed with moderately polar, (non-hydrogen and hydrogen bonding acceptor) solvents (i.e., dimethylsulfoxide and methylene chloride) used as a co-eluent in LC can be related to the limited solvent–solute interaction between the oxygen atoms of the side chain (at position 9) and the mobile phase. Consequently, an important increase in fluorescence emission can be observed in such conditions.

Acknowledgements

This work was supported by a grant-in-aid (Aguire Basualdo) for scientific research from the Chancellery of the University (Paris, France). We thank Dr. Joseph Chalom, Eurobio-Seratec Laboratory (Les Ulis, France) for supplying luminarin compounds.

References

[1] M. Tod, R. Farinotti, I. Gaury and G. Mahuzier, Anal. Chim. Acta, 217 (1989) 11.
[2] M. Tod, M. Prevot, M. Poulou, R. Farinotti, J. Chalom and G. Mahuzier, Anal. Chim. Acta, 223 (1989) 309.
[3] M. Tod, M. Prevot, J. Chalom, R. Farinotti and G. Mahuzier, J. Chromatogr., 542 (1991) 295.
[4] M. Tod, J.Y. Legendre, J. Chalom, H. Kouwatli, M. Poulou, R. Farinotti and G. Mahuzier, J. Chromatogr., 594 (1992) 386.
[5] H. Kouwatli, J. Chalom, M. Tod, R. Farinotti and G. Mahuzier, Anal. Chim. Acta, 266 (1992) 243.
[6] F. Traoré, M. Tod, J. Chalom, R. Farinotti and G. Mahuzier, Anal. Chim. Acta, 269 (1992) 211.
[7] F. Traoré, G.A. Pianetti, L. Dallery, M. Tod, J. Chalom, R. Farinotti and G. Mahuzier, Chromatographia, 36 (1993) 96.
[8] F. Traoré, R. Farinotti and G. Mahuzier, J. Chromatogr., 648 (1993) 111.
[9] C.A. Parker and W.T. Rees, Analyst, 85 (1960) 587.
[10] R.S. Becker, in Theory and Interpretation of Fluorescence and Phosphorescence, Wiley-Interscience, New York, 1969.
[11] M.J. Kamlet, J.L.M. Abboud and R.W. Taft, J. Am. Chem. Soc., 99 (1977) 6027.
[12] R.W. Taft and M.J. Kamlet, J. Am. Chem. Soc., 98 (1976) 2886.
[13] M.J. Kamlet and R.W. Taft, J. Am. Chem. Soc., 98 (1976) 377.
[14] M.J. Kamlet, J.L.M. Abboud, M.H. Abraham and R.W. Taft, J. Org. Chem., 48 (1983) 2877.
[15] M.L. Vazquez, A. Cepeda, P. Prognon, J. Blais and G. Mahuzier, Anal. Chim. Acta, 255 (1991) 343.
[16] H.F. Herbrandson and F.R. Neufeld, J. Org. Chem., 31 (1966) 1140.
[17] R.L. Reeves, M.S. Maggio and L.F. Costa, J. Am. Chem. Soc., 96 (1974) 5917.
[18] C.J. Seliskar and L. Brand, J. Am. Chem. Soc., 93 (1971) 5405, 5414.
[19] E.M. Kosower and H. Dodiuk, J. Am. Chem. Soc., 100 (1978) 4173.
[20] L. Coosemans, F.C. De Schryver and A. Van Dormael, Chem. Phys. Lett., 65 (1979) 95.
[21] V. Masilamani and B.M. Sivaram, J. Luminesc., 27 (1982) 147.
[22] M.J. Kamlet, C. Dickinson and R.W. Taft, Chem. Phys. Lett., 77 (1981) 69.
[23] C. Reichardt, in Solvents and Solvent Effects in Organic Chemistry, 1st reprint of the 2nd edn., VCH, Weinheim, 1990, p. 339.
[24] R. Tomassone, E. Lesquoy and C. Millier, in la Régression, Masson, Paris, 1983.

ELSEVIER

Analytica Chimica Acta 294 (1994) 85–94

ANALYTICA CHIMICA ACTA

Infrared sample preparation and interpretation using a knowledge based system

Denise S. Moore *, J. Sterling White, B. Allen Harbin

R.J. Reynolds Tobacco Company, Bowman Gray Technical Center, Winston-Salem, NC 27102, USA

(Received 28th October 1993; revised manuscript received 1st March 1994)

Abstract

A knowledge based system has been developed to advise and assist in infrared sample preparation and interpretation. Advice for sample preparation of various types of materials including liquids, solids, gases, semisolids, spots and stains on paper, and pigments and dyes is included. Sample identification is approached in three ways. The main approach is done by searching major bands in the unknown sample against a database of band positions of known structures. Access to known spectral-structural correlations, and common materials with their major bands, are also included. The system captures a glimpse of some techniques developed from thirty years of infrared sample preparation and interpretation for industrial research and problem solving.

Key words: Infrared spectrometry; Sample preparation; Knowledge based system

1. Introduction

In the early days of artificial intelligence (AI) in chemistry, the primary focus of knowledge based system development was in the area of spectroscopic recognition of molecular structure. Since these beginnings and with the development of the personal computer (PC) and good software products, knowledge based systems have demonstrated their usefulness in a wide variety of areas in analytical chemistry [1–19]. The original goal of this system development effort was to capture some of the knowledge about preparation and interpretation of infrared samples acquired via thirty years experience in infrared (IR) analysis. The system would then serve as a tool to assist a less experienced spectroscopist.

In addition to the original goals, it was decided to add other sections to the system to provide useful information that the expert refers to daily. In this way the system also assists the more experienced spectroscopist. The current system, serving as an advisor and as an assistant, is a much more useful tool than was envisioned at the start of the system development cycle. This system provides useful information in an easy-to-access format along with the capability to easily add new information or modify existing information to address new techniques and equipment.

* Corresponding author.

SSDI 0003-2670(94)00128-9

2. Equipment and procedures

The expert system runs on a personal computer (any DOS based system), and is user-friendly. The program was developed using 1st Class, an Expert System Shell product from Trinzic Co. (Waltham, MA). Once the system is started, response to the first question gives access to one of four sections. These sections are: (i) Sample Preparation for Scanning, (ii) Band Identification, (iii) Quick Chart (gives major spectral-structural correlations by spectral regions), (iv) Common Materials (lists major bands for known common materials).

Two modes of operation are used. Sample Preparation and Band Identification are operated by a question and answer mode. The user moves through the system by selecting possible answers to a series of questions about the sample. The answers direct the user to each successive question until a conclusion is reached. The knowledge in this mode is structured as a decision tree. The expert decided how the underlying rules were connected to each other. With use, the system also allows the user to understand the logic used by the expert in deriving the conclusion. The second mode (including Quick Chart, and Common Materials) gives information from which to peruse and draw possible general conclusions such as compound type, or, match major bands with those of known common materials.

A choice is made from the possibilities using the up and down arrow keys on the PC keyboard. The selection depends on where the spectroscopist is in the problem solving process. The user can (at any time) back up any number of questions to redirect a session. Useful information can be accessed from numerous positions in the program by soft keys. Information, such as a description of microsampling techniques as well as tests to assist in confirming that the sample is a mixture, is available in this manner. This information is kept in the background to avoid forcing known information on more experienced spectro-

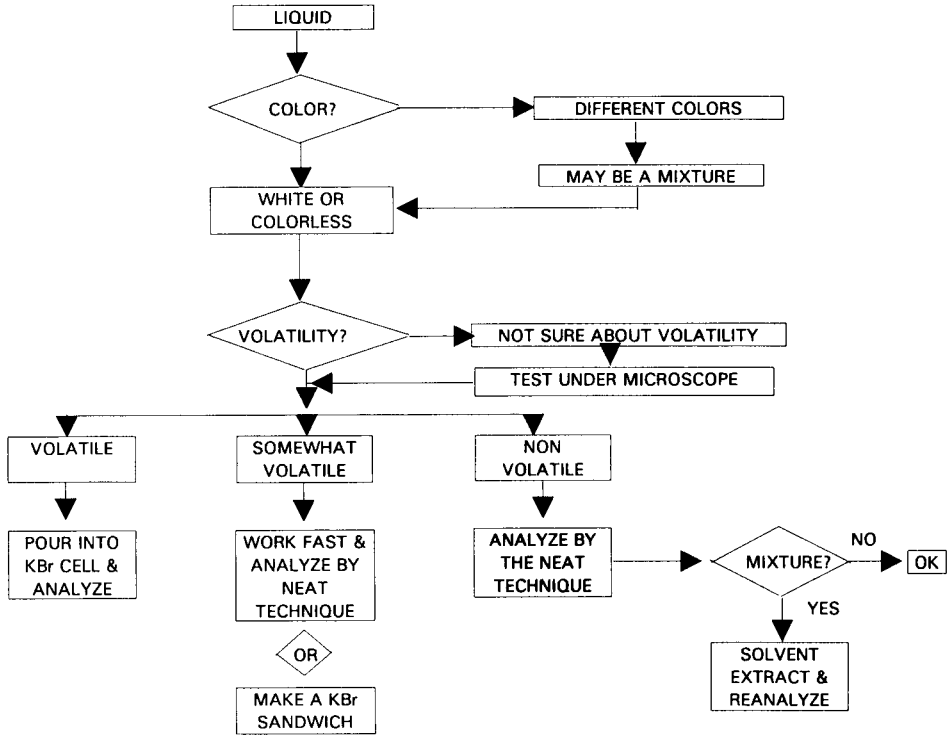

Fig. 1. Flow chart of FTIR sample preparation for liquids.

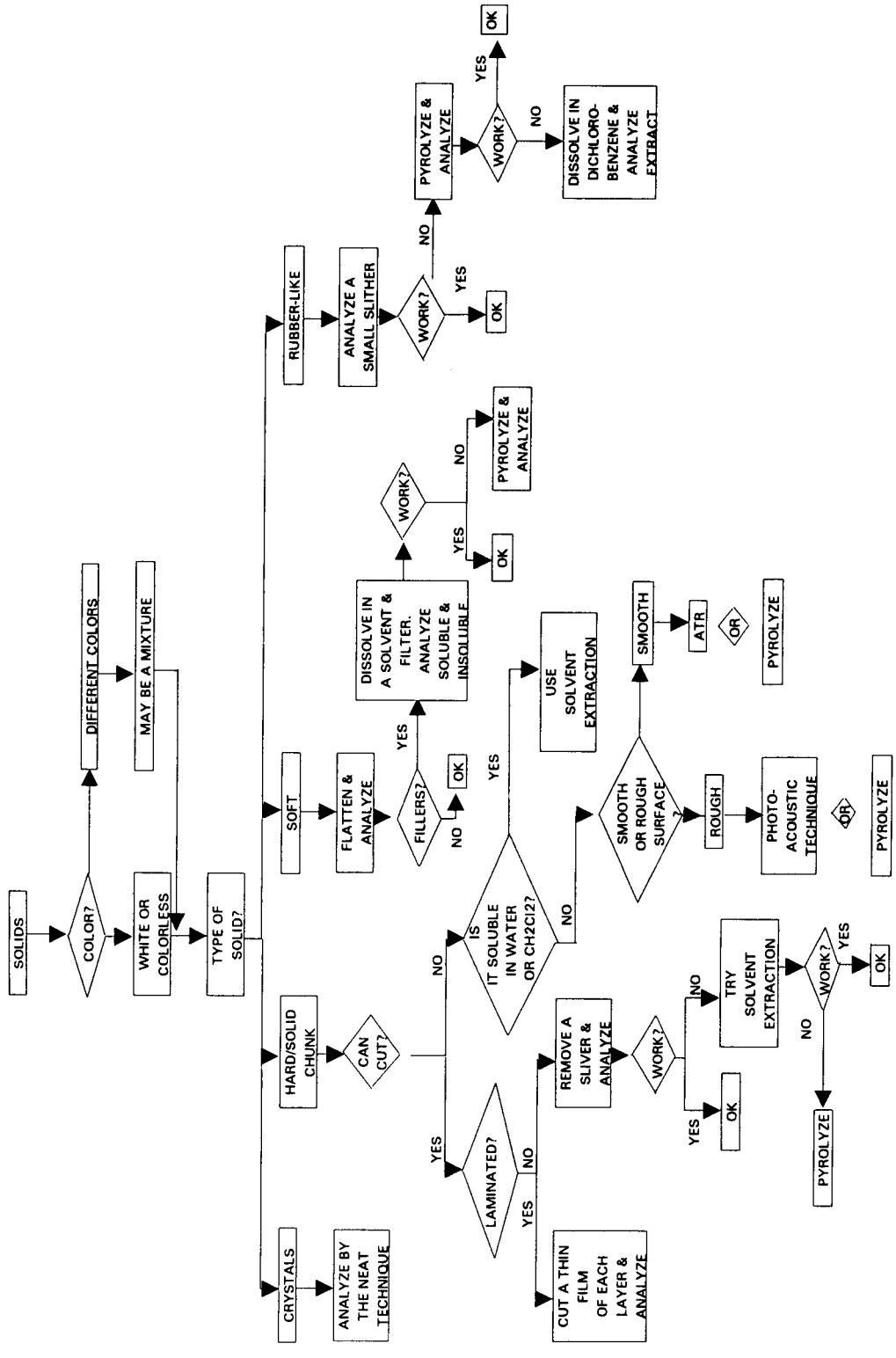

Fig. 2. Flow chart of FTIR sample preparation for solids.

scopists, and yet have it available for the less experienced.

2.1. Sample preparation for scanning

Sample preparation is a very important part of infrared spectroscopy. Without good sampling, it is almost impossible to get a single component or relatively pure spectrum without separation. It is up to the chemist to decide which sampling technique will work best. The Fourier transform infrared (FTIR) knowledge based system for sample preparation is set up to quickly guide the user to the best technique by answering a series of questions about the sample. Decision trees have been created depending on if the sample is a liquid, solid, gas, semisolid, or more specifically, a spot or stain on paper, or a pigment or dye.

Liquids

The decision tree for liquids starts by asking the color of the sample (Fig. 1). This question alerts the spectroscopist of the possibility of the sample being a mixture. Although colorless liquids can also be a mixture, the color alone (such as green) can sometimes be a clue that two or more colors (blue and yellow) or compounds, have been mixed together. Next, the volatility is requested. The volatility of the sample dictates the best sampling technique. The system suggests checking for the volatility of a liquid by placing a small amount of the sample on a disc under an optic microscope and observing if the sample size continues to grow smaller. Three possible sampling techniques are given depending on volatility. Samples that are volatile are analyzed in a potassium bromide (KBr) cell. Nonvolatile samples are analyzed by the neat technique. Solvent extraction is recommended if the sample is a mixture. Samples that are "somewhat volatile", may be analyzed by the neat technique, if done quickly, or, the sample may be sandwiched between two KBr discs.

Solids

The session for solids, including polymers (Fig. 2), also begins by asking the color of the sample. This response would also be used to determine the possibility of a mixture. The next question specifically asks for the type of solid sample-crystals, hard solid chunk, soft, or rubber-like? Depending on the response to this question, four different avenues of sampling are given.

The neat technique is recommended for all crystals. The Advisor cautions about large sized crystals which can distort the spectra. It the crystals are large, grinding is suggested before analysis. The sample may also be mixed with a mineral oil such as Nujol and analyzed. This consists of adding a drop of oil to the sample, mixing thoroughly, and analyzing on a KBr disc.

More questions are asked if the sample is a hard solid chunk. Can the sample be cut? Is it laminated? If the sample can be cut and it is laminated, small slithers of each layer, including adhesives, should be taken and analyzed by the neat technique. If the sample is not laminated, a small slither is to be removed, flattened, and analyzed by FTIR. If the sample is so hard that it is impossible to get a good sample, or it can not be cut, then solvent extraction is recommended. If the spectroscopist is at a loss as to which solvent to use, the program leads the viewer through a step by step process in selecting a solvent. This is done by first trying one polar and one non-polar solvent, water and methylene chloride. The object is to start with the least polar solvent if the sample is soluble in polar solvents and work down (extracting with the most polar solvents last) so that more information is given with each additional solvent extraction. The opposite route is taken with samples that easily dissolve in nonpolar solvents. The soluble extracts are analyzed by the neat technique and insoluble portions are smeared onto a KBr disc and analyzed. Pyrolysis may also be performed, if the sample is small enough or a small enough piece can be removed. If the sample cannot be cut and it is not soluble in organic solvents, the Advisor tells the spectroscopist that the sample must be an inorganic compound. If the outside surface of the sample is smooth, then the attenuated total reflectance (ATR) technique or pyrolysis is recommended. If the outside surface of the sample is rough, the photoacoustic technique or pyrolysis

is recommended. A soft key explains the pyrolysis procedure.

Soft samples require little sample preparation. The sample is flattened and analyzed. However, the spectroscopist is alerted to the fact that soft samples are often polymers, and polymers contain 95–98% inorganic fillers which often mask very important bands. If this is the case, the Advisor suggests that the sample be dissolved in a solvent, filtered, and both extracts analyzed. If all else fails, pyrolysis is recommended.

Two recommendations are given if the sample is rubber-like. First try to get a small enough sliver on the KBr disc to analyze. If this is not possible, then pyrolysis is recommended. If all else fails, the system advises the spectroscopist to dissolve the sample in dichlorobenzene and analyze the concentrated extract on a micro disc.

Gases

All gas samples should be analyzed in a gas cell.

Semisolids

Samples that are classified as semisolids are divided between those that are tacky and those that are not. If the sample is tacky, the Advisor asks what color the sample is, to alert the user to the possibility of a mixture. The sample should be smeared on a KBr disc and analyzed. The sample is then heated, rescanned, and compared to the first spectra to see if any water was present. A soft key explains some possible problems with tacky samples and what to do such as drying the sample using gentle heating on a hot plate, or if the sample is water absorbing, the sample should be flushed with dry air. Another soft key gives a list of common adhesives and their major bands.

If the sample is not tacky, it should be dried before scanning in case it is hydrous or hydroscopic. Again, samples with different colors could indicate that the sample is a mixture.

Specific materials

Spots or stains on paper. Spots and stains on paper are included in this program because the manufacturing of cigarettes often involves accessing the cause of spotted paper. Samples that are classified as spots or stains on paper are divided into two categories: cigarette paper and other paper such as wrapping materials. If the contaminated compound can be scraped off the paper, it should be analyzed by microscopic FTIR. Generally, spots on cigarette paper should be cut out and the area under the spot should be examined for unusual material that might contribute to spotting. A spot away from the adhesive seam should be chosen if possible. The cut out spot should be handled with tweezers.

The Advisor then asks the color of the spot. The color of the spot links the problem to specific sources often seen before and suggests the solvent that should be used. Next, the Advisor asks that the solvent of choice be entered, and the neat technique is recommended for analysis. The proper solvent should be added drop by drop using a microliter syringe to the cut spotted paper. The tip of the paper should be in contact with the KBr window, letting the solvent flow to the KBr window. If the contaminated compound could not be isolated, the ATR technique is recommended. A warning about accidentally picking up some adhesive from the analysis of spots on wrapping materials is given.

Pigment or dye. The Advisor informs that pigments and dyes are sometimes very difficult to isolate and suggests that a pigment solubility test be done. If the sample is soluble, repeated extractions are advised until all color is removed. The next steps involve evaporating the solvent, drying the residue, and analyzing the residue by FTIR.

The Advisor also informs that sometimes two or more colors or powders may be mixed together, and that they may, or may not be soluble in the same solvent. It suggests examining the residue under the microscope for two colors. If two colors are present, it tells the user to separate them manually under the microscope if possible, and to analyze each color using the FTIR instrument. If two colors cannot be seen under the microscope, and the IR spectrum suggests a mixture, more solvent extraction with different solvents is recommended.

If the sample is not soluble in any solvent, the Advisor suggests heating the sample in a furnace at a high temperature, or with a blow torch, and analyzing any inorganic pigment that is left.

2.2. Sample identification

This route provides assistance with band identification by searching a data base of band positions with position windows that the band is expected to fall within. These regions of interest are known to correlate to specific structural features (aliphatic CH, carbonyl, etc.) and hence help to identify the type of compound searched. A band position is entered into the system to begin the search and the system requests additional information as possible matches are found. The system is designed to expect the highest band (closest to 1700 cm^{-1}) of reasonable intensity as the band to key the search. The system inquires about other bands. An answer is highlighted using the up and down arrow key on the PC keyboard. It is possible that the system will ask if two bands at the same intensity with different $\pm$values are present. This indicates two bands within this range. Since pyrolysis condensate will look different from unpyrolyzed data, the system asks if the sample is pyrolyzed or not. The default value for the search window is set to ± 10 cm^{-1}. The band width can be changed to a larger number if an alcohol or an inorganic compound is suspected. After the search, types of compounds are then suggested and listed. The underlying schematic for the identification of compounds was structured by the expert from various published charts of IR interpretation.

Appendix 1 shows an example of a user interfacing the knowledge-based system for sample identification. The infrared spectrum used to answer the questions, a methylene chloride extract of a stain on paper, is shown in Fig. A1. Before the Advisor was consulted, the two broad bands at wavelengths 3350 and 3190 cm^{-1} were recognized as major bands of a common contaminant from plastic bags in which samples are often stored in (*cis*-13-docosenamide or erucamide). Erucamide is an agent used to prevent adhesion of surfaces of plastic films to each other. Eru-

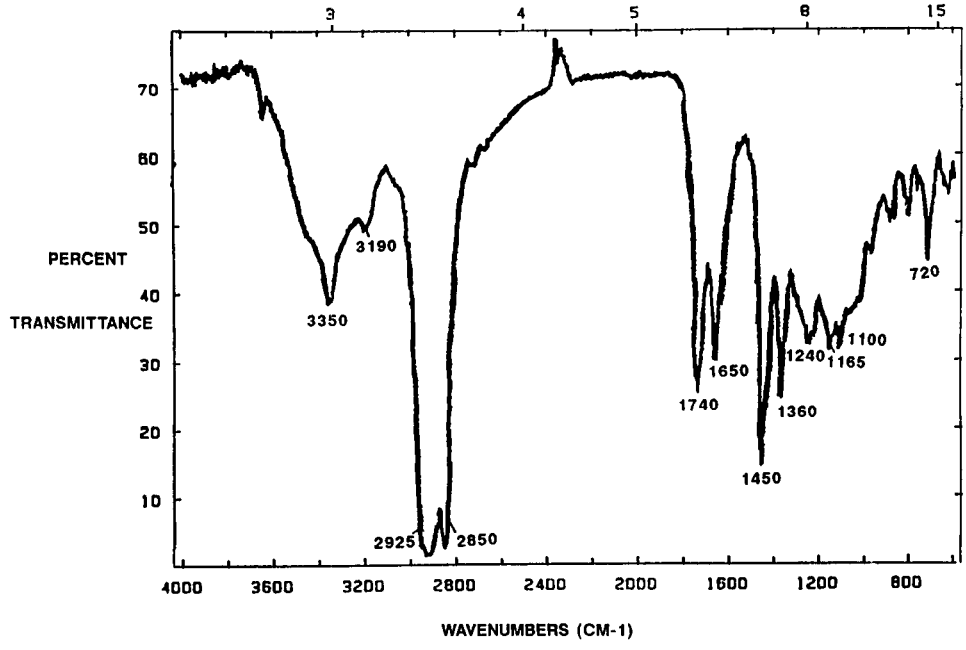

Fig. A1. FTIR spectrum of CH_2Cl_2 extract of spot on paper. (Transmission spectrum taken at 32 scans per minute and a resolution of 4.)

camide is listed as a contaminant in the Common Materials section. The band at 1650 cm^{-1} is a prominent band also present in erucamide. The remaining bands at wavelengths 2925, 2850, 1740, 1450, 1360, 1240, 1165, 1100, and 720 cm^{-1} are noted, and the Advisor is consulted. By answering the questions asked by the Advisor, the system suggests a ketone, several types of esters, or a carbonate. The unknown compound was identified as a fatty ester or type of cooking oil such as corn oil (Fig. A2). This compound is also listed in the Common Materials section under Common Spots/Stains.

2.3. Quick chart

Quick Chart gives major spectral-structural correlations of compounds by spectral regions. A quick overview of the types of compounds that may be present help narrow the possibilities to a few chemical structures. Reference files can then be checked by compound classes (Table 1).

Table 1
Quick chart [major spectral-structural correlations by spectral regions (in cm^{-1})]

OH, NH, C≡CH, NH_2	3700–3100
Aryl, olefinic, 3-membered ring CH	3100–3000
Aliphatic CH	3000–2700
Acidic, strongly bonded H (end), N–X	3100–2400
SH, BH, PH, SiH	2600–2100
C≡N, C≡C, O≡C–metal, –X=Y=Z	2300–1900
Aryl and olefinic overtones (C=C weak)	2000–1700
C=O (carbonyls)	1900–1550
C=C	1680–1600
C=N	1690–1630
N=O	1660–1450
NH_2, NH_3^+, C–NH, OH (hydrate)	1660–1500
Aromatic, heteroaromatic rings	1620–1420
CH_3, CH_2	1500–1230
B–O, B–N, NO_3^-, CO_3^-, NH_4^+	1470–1310
SO_2, SO_3^-, SO, SO_4^{2-}	1400–1000
P=O	1300–1140
CF_3, CF_2	1350–1120
CH_2, CH	1350–1150
C–O	1300–1000
Si–O, P–O	1100– 830
Olefinic C=CH	1000– 600
Aromatic=CH	900– 700
C–Cl, C–Br, C–I	830– 500

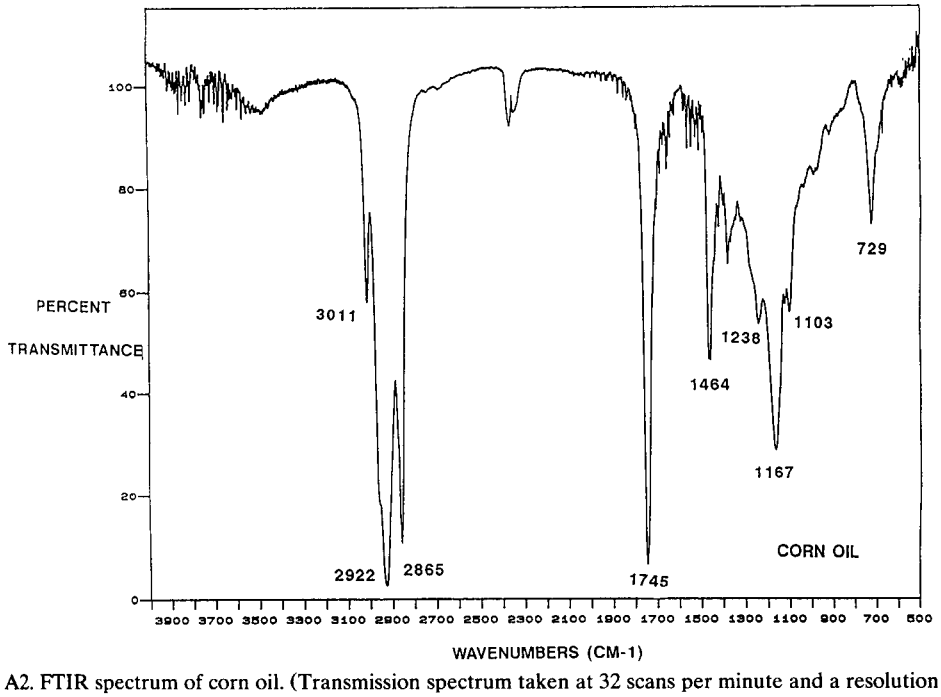

Fig. A2. FTIR spectrum of corn oil. (Transmission spectrum taken at 32 scans per minute and a resolution of 4.)

Table 2
Common adhesives (major bands, transmission spectra)

Material	Wavelength (cm^{-1})
Polyvinylacetate	740, 1240, 600
Poly-2-ethylhexyl acrylate	1740, 1240, 1170
Polystyrene/butadiene	965, 760, 700
Benzoflex	710
Polytetramethylene terephthalate	1720, 1270, 1100, 730
Silicone rubber	1260, 1100–1000(b), 800
Bisphenol-A epoxy resin	1600, 1500, 1240, 830
Polyurethane	3300, 1720, 1530, 1220, 815, 700
Natural rubber (polyisoprene)	840
Styrene/butadiene/isoprene	965, 830, 760, 700
Polycy anoacrylate	2220, 1740, 1250, 860
Polyvinylacetate/ethylene	1740, 1240, 720
Polyvinylacetate/acrylate	1740, 1240, 1160

(b) = Broad band.

2.4. Common materials

The Common Materials section of the software includes eight tables of similar types of materials in each table. They include common adhesives, coatings, elastomers, fibers, fillers, plastics, pigments and dyes, and spots/stains. The major bands from the infrared spectra of each compound are listed in each table. Compounds that occur frequently can easily be accessed in Common Materials for comparison. It saves time looking for spectral matches. Table 2, Table 3 and Table 4 show three of these tables. Common mixtures are also included. This is especially helpful since mixtures often combine overlapping bands and smaller and sometimes important bands get masked.

3. Conclusion

An expert system has been developed to assist in the sampling and interpretation of infrared

Table 3
Common coatings (major bands, transmission spectra)

Material	Wavelength (cm^{-1})
Polyacrylate	1270, 1240, 1193, 1149
o-Phthalic alkyd	2900 ± 100, 1735, 1640, 1275, 1130, 1075, 740, 710,
Epoxy resin	3400, 1600, 1500, 1360(2), 1240, 1040, 830
Polyamide	3300, 2900 ± 100, 1640, 1560, 1250, 720
Melamine formaldehyde	1560, 1490, 1390, 1090, 1020, 920, 815, 630
Urea formaldehyde	3280, 1670, 1530, 1270, 1080
Silicones	1260, 1100–1000(b), 800
Fatty acid	3400–2400(b), 3050 ± 50, 2900 ± 100, 1710, 1295, 950, 720(2)
Polyglycols	3600–3200(b), 1100, 1250

(b) = Broad, (2) = 2 bands.

Table 4
Common elastomers (pyrolyzed) (major bands, transmission spectra)

Material	Wavelength (cm^{-1})
Polyisoprene	887, 970, 990
Polychloroprene [a]	900–700(3)
Ethylene/propylene/diene	1461, 1375, 909, 720
Silicone rubber	1260, 1100–1000(b), 800
Polyvinyl chloride [a]	1735, 1280, 1120, 1080
Poylbutadiene \ styrene	965, 760, 700
Polybutadiene \ styrene \ natural rubber	990, 970, 887, 760, 700, 725, 775
Acrylonitrile \ butadiene \ styrene	2240, 965, 760, 700
Polyurethane	1730, 1530, 1230, 1100, 820, 770

[a] Can do a copper wire test to test for presence of chlorine. (b) = Broad, (3) = three bands.

spectra of organic and inorganic compounds. The principal motives were (1) to capture the available knowledge of an in-house expert and (2) document the knowledge in an accessible way.

At present the system is being validated in practice. The system is periodically improved and updated. Its usefulness is threefold. Not only does it inform and guide the spectroscopist through the sampling and interpretation of a particular sample, it also serves as a reference for common materials, and teaches the inexperienced spectroscopist the logic that a more experienced spectroscopist goes through in the FTIR sampling and identification process.

4. Appendix 1. Example of the IR band identification route.

(The answers to the questions are underlined.)

1. Is the sample a–
   non – pyrolyzate pyrolyzate
2. Enter BAND to search for– 1740cm^{-1}. The system is designed to expect the highest band (closest to 1700 cm^{-1}) of reasonable intensity as the band to key the search.
3. The default value for the search window is set to +10, do you want to change this value or leave it at this setting?
   Leave the setting at +10 Change the setting
   (For the following questions– Due to the design of the system and the methodology used in entering the bands into the databases; "yes" should be chosen even if the band is very small. This increases the possibility that the correct compound will be in the list.)
4. Do you have BANDS at: 2720 ± 30, 2820 ± 10?
   Yes No
5. Do you have a BAND at: 1225 ± 175?
   Yes No
6. Do you have a BAND at 1240 ± 10?
   Yes No
7. Do you have a BAND at 1190 ± 10?
   Yes No
8. Do you have a BAND at 1180 ± 10?
   Yes No
9. Do you have a BAND at 1165 ± 10?
   Yes No
10. Do you have a BAND at 1650 ± 10?
    Yes No
11. Do you have a BAND at 1160 ± 10?
    Yes No

The following computer matches were found.

KETONE, 5-membered (1745 ± 10).
KETONE, alpha-halogen (1750 ± 10).
ESTER, CO–O– (1735 ± 10, 1225 ± 175).
ESTER, acetate (1735 ± 10, 1240 ± 10).
ESTER, methyl ester (1735 ± 10m 1165 ± 10).
ESTER, Ar–CO–O–Ar (1735 ± 10).
ESTER, alpha, keto ester (1730 ± 10).
ESTER, cycloester, 6-member (1735 ± 10).
ESTER, alpha, lactone (1750 ± 10).
ESTER, alpha-pyrones, coumarins, iso coumarins, 6-membered lactones (1730 ± 10).
ESTER, fatty, –CO–O– (saturated) (1740 ± 10, 1160 ± 10).
CARBONATE, –O–CO–O (saturated) (1750 ± 10).

References

[1] M. Farkas, J. Markos, P. Szepesvary, I. Bartha, G. Szalontai and Z. Simon, Anal. Chim. Acta, 133 (1981) 19.
[2] G. Szalontai, Z. Simon, Z. Csapó, M. Farkas and G. Pfeifer, Anal. Chim. Acta, 133 (1981) 31.
[3] B. Debska, J. Duliban, B. Guzowska-Swider and Z. Hippe, Anal. Chim. Acta, 133 (1981) 303.
[4] L.A. Gribov, M.E. Elyashberg, V.N. Koldashov and I.V. Pletnjov, Anal. Chim. Acta, 148 (1983) 159.
[5] J. Seil, I. Köhler, C.W. v. D. Lieth, and H.J. Opferkuch, Anal. Chim. Acta, 188 (1986) 219.
[6] K. Janssens and P. Van Espen, Anal. Chim. Acta, 184 (1986) 117.
[7] M. Bos, E. Hoogendam and W.E. van der Linden, Anal. Chim. Acta, 211 (1986) 61.
[8] J. Klaessen, L. van Beysterveldt, T. Saris, B. Vandeginste, and G. Kateman, Anal. Chim. Acta, 222 (1989) 1.
[9] J. Klaessen, J. Sanders, B. Vandeginste and G. Kateman, Anal. Chim. Acta, 222 (1989) 19.
[10] H.J. Luinge and J.H. van der Maas, Anal. Chim. Acta, 223 (1989) 135.
[11] J.A. van Leeuwen, B.G.M. Vandeginste and G. Kateman, Anal. Chim. Acta, 228 (1990) 145.
[12] H. Hong and X. Xin, Anal. Chim. Acta, 262 (1992) 179.

[13] M. Esteban, I. Ruisánchez, M.S. Larrechi and F.X. Rius, Anal. Chim. Acta, 268 (1992) 95.
[14] B. van den Bogaert, J.B.W. Morsink and H.C. Smit, Anal. Chim. Acta, 270 (1992) 107.
[15] C.L. Guillemin, Lab. Inf. Manage., 17 (1992) 201.
[16] W. Penninckx, J. Smeyers-Verbeke, D.L. Massart, L.G.C.W. Spanjers and F. Maris, Lab. Inf. Manage., 17 (1992) 193.
[17] L. Buydens, P. Schoenmakers, F. Maris and H. Hindriks, Anal. Chim. Acta, 272 (1993) 41.
[18] B. Adler, P. Schütze and J. Will, Anal. Chim. Acta, 271 (1993) 287.
[19] R.A. Olivero, S. Seshadri and S.N. Deming, Anal. Chim. Acta, 277 (1993) 441.

ELSEVIER

Analytica Chimica Acta 294 (1994) 95–102

ANALYTICA CHIMICA ACTA

Experimental design approach to the optimisation of the analysis of non-conducting materials using a glow discharge source

S.J. O'Gram [a], J.R. Dean [a,*], W.R. Tomlinson [a], J. Marshall [b]

[a] *Department of Chemical and Life Sciences, University of Northumbria at Newcastle, Ellison Building, Newcastle Upon Tyne NE1 8ST, UK*

[b] *ICI Materials, Wilton Research Centre, PO Box 90, Wilton, Middlesbrough, Cleveland TS6 8JE, UK*

(Received 18th October 1993; revised manuscript received 7th February 1994)

Abstract

Optimisation of the analysis of a non-conducting material in a copper matrix by glow discharge atomic absorption spectroscopy was undertaken. The optimum copper content and glow discharge sputter conditions were determined using experimental design. The chosen design detected a threshold value for burn conditions above which conditions should be maintained. Using post-threshold burn conditions, the iron content of two certified reference materials (CRMs) was determined (BCS-CRM 395 bauxite and NIST-CRM 1645 river sediment).

Key words: Experimental design; Atomic absorption spectrometry; Glow discharge source; Non-conductor analysis; Certified reference materials

1. Introduction

The direct analysis of samples without any pretreatment would reduce sample analysis time and avoid sample dissolution problems. In 1953, Price [1] developed a technique for spectrographic analysis of slags and ores involving briquetting the sample with graphite. Several authors [2–4] have also described the analysis of non-conducting samples by glow discharge atomic spectroscopy by incorporation of the non-conductor into a conducting matrix, usually copper [5–8], and pelletisation of the resultant mixture into a disc. The method would prove particularly useful for samples not easily dissolved, e.g. refractories and some plastics. Alternatively, but not the subject of this paper, is the use of a new ion source based on a r.f. discharge for the direct analysis of non-conductors. Early results [9,10] have indicated the potential of this method of analysis.

The fundamental sample requirement for analysis by d.c. glow discharge is electrical conductivity. Analysis of metal samples using a glow discharge as the source is relatively simple since samples already have this prerequisite [11,12]. However non-conducting samples do require some pre-treatment before they are suitable for glow discharge analysis. Matrixing the non-conducting sample with a conductor, copper powder in this case, introduces the problem of homogeneous mixing and analyte dilution into the sample

* Corresponding author.

SSDI 0003-2670(94)00116-4

preparation process. The mixture must then be pressed into a disc to be in a suitable form for the subsequent analysis.

There are several important variables affecting the production of sample discs which must be considered in order to provide accurate and reliable measurements. The pressure and duration of pressing has an effect on the robustness of the disc [6], and also the surface composition [8]. The size of sample discs (and hence the mass of conductor and sample) is limited to the requirement of the glow discharge atomization apparatus [13]. The conditions under which the sample is sputtered and the composition of the disc with regards to non-conductor content are also significant factors and are considered here.

Discs containing Fe_2O_3 and Al_2O_3, the non-conducting portion of the sample, matrixed with copper powder as the conductor, have been studied. While other workers have also considered the use of Fe_2O_3 and Al_2O_3 [2,8,14] no group has yet undertaken a systematic study of their use. In this study a rigorous experimental design approach has been implemented to elucidate the optimum non-conductor to conductor ratio and other analytical parameters. The analyte chosen for investigation in this study was Fe. The Al_2O_3 was used as a filler to allow representative variation of the total non-conductor content. Two certified reference materials (CRMs) were analysed for Fe under the conditions established.

2. Experimental

The instrumentation and its mode of action has been fully described elsewhere [15]. However, the main features are described here for convenience. The Atomsource (Analyte Co., Medford, OR) workhead was mounted in the optical path of a Perkin Elmer Model 1100 atomic absorption spectrometer (Perkin Elmer, Beaconsfield). Samples are held, using a torque screw, against the external face of a water-cooled cathode plate. The sampling orifice is 0.8 cm in diameter. Located within the orifice is the uniquely designed accelerator. This consists of six grooves at equidistant intervals around its diameter through which argon gas flows. The unique sputtering pattern produced by the accelerator has been previously shown [15]. To prepare discs for calibrating the instrument response pre-calculated amounts of Cu powder, Fe_2O_3 (Aldrich, Gillingham) and Al_2O_3 (BDH, Poole) powders, (particle diameters < 60 μm [6]) were mixed in a micronising mill (McCrone, London) for 30 min (3 min per g of sample). The same procedure was implemented for the two reference materials, bauxite, British Chemical Standard – Certified Reference Material 395, obtained from the Bureau of Analysed Samples (Middlesbrough) and river sediment, National Institute of Science and Technology – Standard Reference Material 1675 (U.S. Department of Commerce, Washington, DC). Each component was weighed out directly into the mill since small particles readily adhere to surfaces. Approximately 1 g portions of the mixture, (1.00 g) were pressed for approximately 2 min under a pressure of 6020 kg cm^{-2} in a die of 13 mm diameter.

It was not possible to use the same conditions to sputter pressed disc samples as those used to analyse solid metals [15] since their robustness and heat and electrical conductivities are quite different. This limits the number of sputters appropriate for representative sampling. For the analysis of the CRMs two full sputter cycles were run for bauxite with the measurements taken over a 40 s period during the burn sequence of the second cycle, while for the river sediment sample measurements were taken over only one sputter cycle during the last 40 s of the burn sequence. The preburn sequence was used at low power to prepare the sample surface (Table 1).

2.1. Experimental design

The variables to be optimised were burn current, burn pressure and non-conductor content of the sample disc. Rather than have three variables in the design, which can complicate the interpretation of results, the current and pressure factors were studied at various non-conductor contents [16]. Therefore the experimental procedure, varying burn current and burn pressure, was repeated for four different non-conductor concentrations,

Table 1
Operating conditions

Parameter	Setting
HCL current	8 mA
HCL wavelength	248.3 nm
Number of sputters	2
Burn time	70 s
Integration time	5 s
Burn stablization time	30 s
Burn pressure	To be optimised
Burn current	To be optimised
Preburn time	25 s
Preburn pressure	(933 Pa)
Preburn current	20 mA
No. of sputter cycles	2
Measurement time	40 s
	(2nd run)

HCL = Hollow cathode lamp.

with the Fe concentration in the discs remaining the same. Four sets of discs were prepared containing 5, 10, 15 and 20% non-conducting portion. (19:1, 9:1, 5.67:1 and 4:1 ratios of copper to non-conductor). The Fe analyte (in the form of Fe_2O_3) was at a level of 0.56% in each disc.

The experimental design was chosen to accommodate possible quadratic effects. These might be expected since analyte concentration is directly proportional to the amount of non-conductor in the disc but the sputter rate will decrease as the electrical conductivity of the sample decreases [8]. Therefore there is a region where an optimum non-conductor content should yield the best sensitivity. Consequently, the amount of conducting material mixed with the sample will be a compromise between achieving maximum sample loading whilst still exhibiting sufficient electrical conductivity. The designs able to analyse curvature in the response are '3^k' factorial designs and central composite designs [17]. The latter are more efficient when k (the number of factors) $\geqslant 3$. However, for this work ($k = 2$), a central composite design was chosen because of the more detailed interrogation of the factor-response space made possible by utilising a larger number of variable levels. Central composite designs comprise 'cube' points, 'star' points, and centre points. Cube points equate to those of a 2-level factorial design, and are at a coded distance 1.0 from the centre point. Star points are extended from the centre point to a coded distance 'a' where $a > 1.0$. Central composite designs allow determination of all the coefficients (b) of the parametric model

$$Y = b_0 + b_1 v_1 + b_2 v_2 + b_3 v_1^2 + b_4 v_2^2 + b_5 v_1 v_2$$

where Y is the response (absorbance), v_1 and v_2 are the variables burn current and burn pressure, b_1–b_5 the parametric coefficients and b_0 the intercept.

It is desirable that the design should confer both orthogonality and rotatability. Such designs, however, include a large number of centre points. The difficulty in producing replicates for this work suggested that a smaller number of centre points be utilised. One course of action is to fix the axial (star point) spacing for rotatability and then to add as many centre points as possible to approach orthogonality. This compromise is recommended [18] because a small average standardised variation is achieved. To confer rotatability, then, the star points were at a coded level 'a' calculated from

$$a^2 = \sqrt{n_c}$$

where n_c refers to the number of cube points (equal to 4 for $k = 2$. Hence $a = 1.414$).

The number of centre points to confer orthogonality is calculated from

$$a^2 = \left\{ \left[(n_a + n_c + n_o) n_c \right]^{1/2} - n_c \right\} / 2$$

where n_c is the number of factorial or cube points, and n_o is the number of centre points. This gives a value of $n_o = 8$. However, for the reasons stated above, four centre points were used in this study.

The range of the levels of each factor (factor space) was predetermined during preliminary investigations, principally to obtain the experimentally accessible high and low values. In this case for the two factors and corresponding levels, these values are given in Table 2.

The run order of the design matrix was randomised using statistical software.

3. Results and discussion

3.1. Optimisation

In order to avoid sample heating which results in an unstable signal, the number of sputters and their duration are an important factor in obtaining accurate signals with acceptable relative standard deviations. If sputtering time is too long, sample heating occurs. If sputtering time is too short, the signal does not have time to stabilize and very poor R.S.D. values are exhibited for absorbance readings. (This is not such a problem for metal samples where their ability to rapidly conduct heat alleviates the problem.) The possibilities include a single sputter over a reasonable length of time with measurements taken after the signal has stabilized, or sputtering the sample consecutively and taking measurements after a few sputters.

Sputtering conditions are also more significant for a disc containing a non-conductor. If conditions are too vigorous sample heating again will occur but there is the added problem of plasma breakdown resulting in an erratic signal. Also because the sample has been prepared by pressing there may be surface contaminants present (water, oxygen) on the disc surface [8]. To remove these contaminants it was necessary to include a pre-sputter step in the overall sputtering cycle.

Table 2
Experimental equivalents of coded values

Coded value	Burn current (mA)	Burn pressure (Pa)
+1.414	68.3	1493
+1	60	1333
0	40	933
−1	20	533
−1.414	11.7	373

The signal obtained with a disc of particular analyte concentration is dependent on the non-conductor content and the operating parameters of the glow discharge (Table 1). Consideration must also be made of matrix matching and the diluent effect of the Al_2O_3 filler and the copper powder content. Analyte concentration must be of a level to ensure detection, irrespective of the above effects. This was not a problem here where the Fe_2O_3–Al_2O_3 mixture has a high Fe content, but problems may arise for samples of very low analyte concentrations.

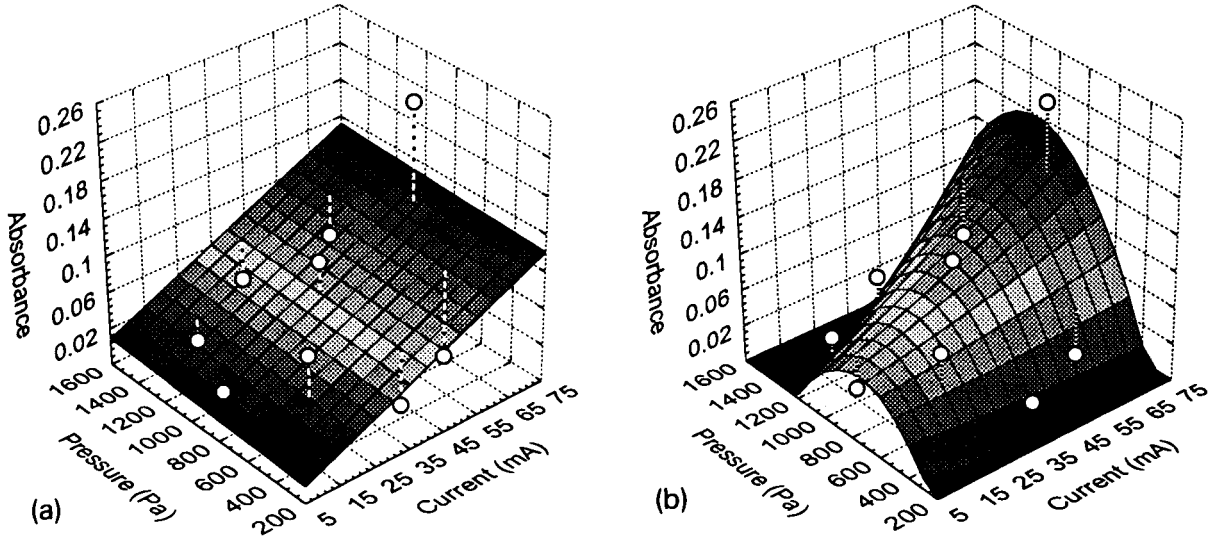

Fig. 1. (a) Response surface plot for first order fitting of all data, for discs containing 5% w/w non-conductor. (b) Response surface plot for quadratic fitting of all data, for discs containing 5% w/w non-conductor.

Table 3
Results of experimental design

Expt. No.	Burn current (mA)	Burn pressure (Pa)	Iron absorbance, % non-conductor			
			5%	10%	15%	20%
1	20	533	0.073	0.053	0.023	0.024
2	40	933	0.099	0.054	0.041	0.032
3	68.3	933	0.223	0.087	0.088	0.046
4	40	933	0.100	0.057	0.041	0.032
5	40	933	0.096	0.064	0.039	0.033
6	60	533	0	0	0	0
7	40	1493	0.025	0.015	0.010	0.008
8	20	1333	0.007	0.005	0.002	0.002
9	40	933	0.099	0.061	0.044	0.029
10	11.7	933	0.007	0.004	0.005	0.001
11	40	373	0	0	0	0
12	60	1333	0.056	0.043	0.029	0.022

3.2. Selection of a model

Considering the results of the blocked experimental design, Table 3, it is apparent that the discs containing the lower non-conductor content of 5% gave the highest absorbance values. Multiple linear regression (using statistical software [19]) was applied to these results and for the disc containing 5% non-conductor, both first order, including main and interaction terms, and quadratic parametric models were fitted to the data (Table 4). Perusal of the values of the correlation coefficients in Table 4, and comparison of the response surface plots for the two models (Fig. 1a and b), suggests that the quadratic model gives rise to lower residuals. However, the fitting of the results to the quadratic model cannot be regarded as satisfactory. Scatter is evident in the 'predicted versus observed' plot of Fig. 2.

Perusal of Table 3 suggests that absorbance readings at the lower pressure values (373 and 533 Pa), and corresponding high current values are erratic, perhaps implying the existence of a limiting or "threshold" pressure value, below which unstable behaviour occurs.

If the results corresponding to "sub-threshold" pressure values are removed from the regression analysis, a considerable improvement results in the correlation coefficients (r^2) for both first order and quadratic models (Table 4) and the response surface plots exhibit much less scatter, especially in the case of the quadratic model (Fig. 3a and b). The "predicted versus observed" absorbance plot (Fig. 4) supports the applicability of this modified quadratic model above the threshold pressure. The statistical significance (deduced from P values) of the standardized regression weights for the modified quadratic model are also much greater (Table 5). The response (absorbance) behaviour is therefore dependent of main and interaction effects of pressure and current, and on a quadratic pressure term.

Table 4
Correlation coefficients for the applied models

Model	Data	Correlation coefficient [a]
First order	All	0.5199
Quadratic	All	0.7116
First order	"Sub-threshold" values removed	0.9784
Quadratic	"Sub-threshold" values removed	0.9950

[a] $n = 12$ for $r^2 = 0.5199$ and 0.7116; $n = 9$ for $r^2 = 0.9784$ and 0.9950.

Low pressure and high current combinations result in high discharge power which can lead to unstable sputtering. This is likely to be the cause of the erratic absorbance values and justifies the removal of such results from the statistical analysis.

It should be noted that removal of sub-threshold values from the regression analysis leads to an ill-conditioned matrix. If an accurate repre-

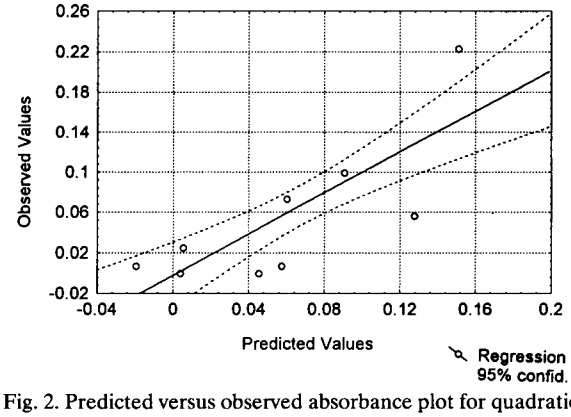

Fig. 2. Predicted versus observed absorbance plot for quadratic fitting of all data, for discs containing 5% w/w non-conductor.

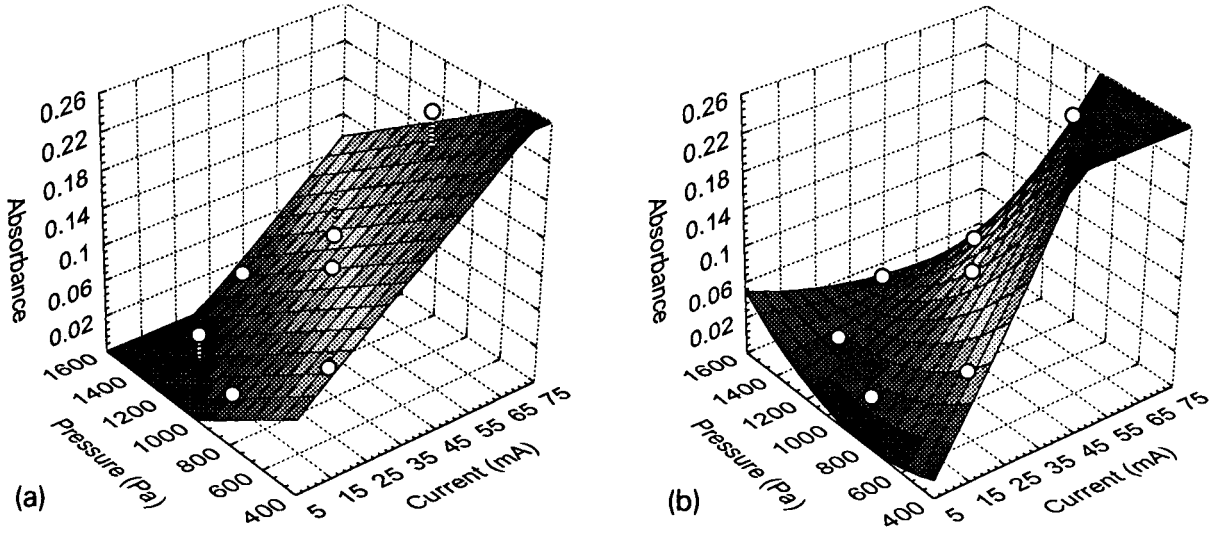

Fig. 3. (a) Response surface plot for first order fitting of data with sub-threshold data not included for discs containing 5% w/w non-conductor. (b) Response surface plot for quadratic fitting of data with sub-threshold data not included, for discs containing 5% w/w non-conductor.

sentation of the response surface were to be required, then the design should be reconstructed (or further samples run) avoiding the unstable region. However, for the purposes of this work, the analysis was continued with the statistical significance levels for the regression tightened.

3.3. Selection of sputter conditions

It is interesting to note the considerable difference in response surface for the original and modified quadratic models. The response surface for the modified quadratic model appears to adequately represent the experimental system and implies that, provided the threshold pressure value is exceeded, analysis conditions should be those of minimum pressure and maximum current. However, in practice sample heating effects limit the current level.

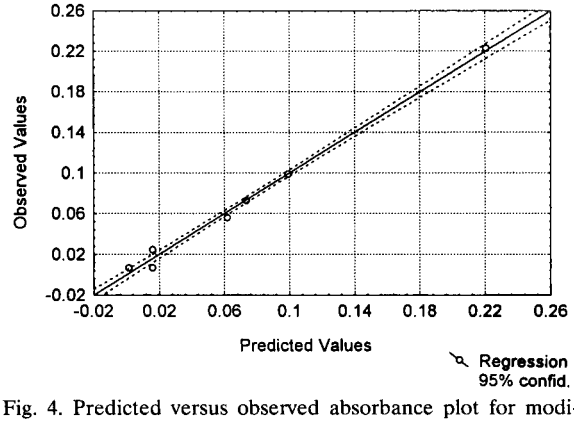

Fig. 4. Predicted versus observed absorbance plot for modified quadratic model for discs containing 5% w/w non-conductor.

3.4. Analysis of Certified Reference Materials

Three discs of each CRM were prepared with copper in the ratio 19:1, mixed and pressed according to the method described previously. The bauxite disc contained 0.2504 g bauxite which corresponded to a Fe percentage of 0.57% w/w

Table 5
Results of multiple linear regression for the modified and original quadratic models

Term	Original model		Modified model	
	Beta value	*P* level	Beta value	*P* level
Burn current (I)	−2.1176	0.1863	3.8006	0.0002
Burn pressure (p)	3.4092	0.0519	−1.4386	0.0093
I^2	0.4300	0.7015	0.3220	0.0859
Ip	2.3905	0.0652	3.1206	0.00025
p^2	−3.5140	0.0256	1.3543	0.0092

in the disc while the river sediment disc contained 0.2511 g river sediment corresponding to 0.585% w/w Fe. For the analysis of the CRMs, a calibration graph was generated over the range 0–1% for bauxite and 0–0.8% Fe for the river sediment, using the appropriate amounts of Fe_2O_3 with the total amount of non-conductor being made up with Al_2O_3. To maintain the linear dynamic range and to further minimise sample heating, a burn current of 40 mA for bauxite and 30 mA for the river sediment was used at a pressure value of 933 Pa. This allowed the threshold values previously determined using experimental design to be comfortably exceeded. The correlation coefficients (r) for the calibration plots obtained were 0.9930 for bauxite analysis and 0.9968 for the river sediment analysis (six datapoints were used to construct each calibration plot; each of the six datapoints was an average reading of nine values). The R.S.D. values ($n = 9$) for the absorbances of the samples used in the generation of the calibration plot varied between 1.99–5.06% for bauxite and 1.67–6.00% for river sediment. The results of the analysis of the three discs containing the CRMs are given in Table 6. The average Fe content in bauxite and river sediment CRMs was found to be 0.61% (Table 6a) and 0.49% (Table 6b), respectively (average of 3 sets of 9 measurements); whereas the certificate values of $16.29 \pm 0.08\%$ Fe_2O_3 and $11.3 \pm 1.2\%$ Fe, correspond to an Fe content in the disc of 0.57% w/w and 0.585% w/w for bauxite and river sediment, respectively. The agreement of the results indicate the potential of the method for quantitative analysis. The R.S.D. values for the absorbance values obtained for the three sample discs of bauxite were 0.81, 2.38 and 1.28% while for the river sediment discs 7.15, 5.42 and 4.08%. This greater imprecision reported for the river sediment discs is probably due to the greater inhomogeneity of this sample type.

Table 6a
Analysis of Bauxite Reference Material (BCS-CRM 395)

Disc	Response (absorbance)	%Fe (95% confidence limits) [a] ($n = 9$)
1	0.082	0.638 ± 0.004
2	0.077	0.599 ± 0.011
3	0.078	0.607 ± 0.006
		Average = 0.61% Fe

[a] Expected value in disc was 0.57% (certificate value = $16.29 \pm 0.08\%$ Fe_2O_3).

Table 6b
Analysis of River Sediment Reference Material (NIST-CRM 1643)

Disc	Response (absorbance)	%Fe (95% confidence limits) [a] ($n = 9$)
1	0.061	0.472 ± 0.0263
2	0.066	0.511 ± 0.0213
3	0.062	0.480 ± 0.0152
		Average = 0.49% Fe

[a] Expected value in disc was 0.585% Fe (certificate value = $11.3 \pm 1.2\%$Fe).

4. Conclusions

The application of experimental design has provided a large amount of information concerning the factor-response behaviour of this analytical method at high efficiency and a with a minimum of preparatory procedure. The central composite design identified threshold conditions without compromising the derivation of a model of the factor-response behaviour. Low gas pressures result in erratic measurements and assays should be conducted above a threshold pressure. The model involves main and interaction effects for current and pressure, and a quadratic term in pressure.

The highest sensitivity was obtained for discs of only 5% non-conductor content. This was due to improved electrical conductivity resulting in increased sputtering. Analysis of two CRMs with adequate accuracy indicates the potential of the method for quantitative analysis.

Acknowledgements

We acknowledge the Trustees of the Analytical Chemistry Trust Fund of The Royal Society of Chemistry for the award of an Industrial SAC

Studentship in association with ICI plc, Wilton Research Centre.

References

[1] W.J. Price, Spectrochim. Acta, 6 (1953) 26.
[2] M.R. Winchester and R.K. Marcus, Appl. Spectrosc., 42(6) (1988) 941.
[3] D. McDonald, Anal. Chem., 49(9) (1977) 1336.
[4] M. Dogan, K. Laqua and H. Massmann, Spectrochim. Acta, 40B (1972) 65.
[5] S. El Alfy, K. Laqua and H. Massmann, Fresenius' Z. Anal. Chem., 263 (1973) 1.
[6] G. Ehrlich, U. Stahlberg and V. Hoffmann, Spectrochim. Acta, 46B (1991) 115.
[7] H. Nickel, D. Guntur, M. Mazurkiewicz and A. Nauomidis, Spectrochim. Acta, 46B (1992) 125.
[8] M.R. Winchester, S.M. Hayes and R.K. Marcus, Spectrochim. Acta, 46B (1991) 615.
[9] D.L. Donohue and W.W. Harrison, Anal. Chem., 47 (1975) 1528.
[10] D.C. Duckworth and R.K. Marcus, Anal. Chem., 61 (1989) 1879.
[11] A.E. Bernhard, Spectroscopy, 2 (1987) 24.
[12] C.L. Chakrabarti, K.L. Headrick and P.C. Bertels, J. Anal. At. Spectrom., 3 (1988) 713.
[13] S.J. O'Gram, J.R. Dean and J. Marshall, Anal. Proc., 30 (1993) 135.
[14] J.C. Woo, N. Jakubowski and D. Steuwer, J. Anal. At. Spectrom., 8 (1993) 881.
[15] S.J. O'Gram, J.R. Dean, J. Marshall and W.R. Tomlinson, J. Anal. At. Spectrom., 7 (1992) 229.
[16] S.N. Deming and S.L. Morgan, Experin ental Design, a Chemometric Approach, Elsevier, Amsterdam, 1987.
[17] J.A. Palasota and S.N. Deming, J. Chem. Educ., 69 (1992) 560.
[18] C.K. Bayne and I.B. Rubin, Practical Experimental Designs and Optimisation Methods for Chemists, VCH, Deerfield Beach, FL, 1986.
[19] CSS: Statistica, Release 3.0F, Statsoft UK, Letchworth, UK.

ELSEVIER

Analytica Chimica Acta 294 (1994) 103–111

ANALYTICA CHIMICA ACTA

Copper–amine speciation: an electrochemical investigation of the selection of volatile amines for steam generator water

A.G. Kumbhar, S.V. Narasimhan, P.K. Mathur *

Water and Steam Chemistry Laboratory, Applied Chemistry Division (BARC), Indira Gandhi Centre For Atomic Research Campus, 603 102 Kalpakkam, Tamil Nadu, India

(Received 15th June 1993; revised manuscript received 31st January 1994)

Abstract

Addition of volatile amines for pH control to steam generator water of power plants to protect the steam water system from corrosion is called all volatile treatment (AVT) of steam generator water. Metal ion concentrations in steam generator water will generally be in the $\mu g\ l^{-1}$ range. Pseudopolarography in combination with differential pulse anodic stripping voltammetry copper speciation studies (at 50 $\mu g\ l^{-1}$ copper concentration) were carried out in aqueous media containing four important amines, viz. 3-methoxypropylamine (3MPA), 1-dimethylamino-2-propanol (DMPA), 2-dimethylaminoethanol (DMAE) and piperidine (Pip), all having a large potential for use as AVT reagents. The copper–amine complexes were identified and their log stability constants (log K) values were as follows: $[Cu(I)(3MPA)_2]$: 10.47; $[Cu(II)(OH)_2(DMPA)_2]$: 20.33; $[Cu(II)(OH)_2(DMAE)_2]$: 20.51; [Cu(I)(Pip)]: 8.29; $[Cu(I)(Pip)_2]$: 9.89; $[Cu(I)(OH)_2(Pip)_2]$: 16.67. Electroreduction mechanisms of these identified species at a hanging mercury drop electrode were studied. The ability of some of the amines to influence the stepwise reduction/oxidation of copper results in impeding its transport in dissolved form in the steam generator water. Hence it is recommended that only those amines that do not stabilize Cu(I) in solution be selected for use as AVT reagents for ensuring better performance of steam water circuits in power industries.

Key words: Anodic stripping voltammetry; Differential pulse polarography; Differential pulse voltammetry; Polarography; Amines; Complexation; Copper speciation; Corrosion

1. Introduction

Volatile amines are added to steam generator (SG) water of a power station to raise the pH to a desired level and thereby reduce corrosion. These amines volatilize and provide the entire steam water circuit with protection against corrosion. Hence the treatment is called all volatile treatment (AVT), and the amines used are called AVT reagents [1]. 3-Methoxypropylamine (3MPA), 1-dimethylamino-2-propanol (DMPA), 2-dimethylaminoethanol (DMAE) and piperidine are amines with a potential for use as better performing AVT reagents [2].

Copper is one of the major alloying elements

* Corresponding author.

SSDI 0003-2670(94)00122-3

of Monel 400 SG tubing material used in Indian pressurized heavy water reactors (PHWRs) and hard copper deposits and metallic suspensions have been observed in some of the SGs [3]. Therefore, copper was selected for the present speciation studies with the above four amines. The nature of the ligand (AVT reagent) is decisive for the mode of electroreduction of the metal–amine complex. Cu^{2+} ions exhibit stepwise reduction: Cu(II) → Cu(I) → Cu(0), in the presence of ammonia and a number of organic amines and nitrogen-containing heterocyclics. Single-step reduction Cu(II) → Cu(0) is also observed in the presence of a number of amines [4]. The structure of the ligand containing a nitrogen atom, the basicity of amines, and the electron density on the nitrogen atom determine the reduction behaviour of the Cu–amino complex [5]. The amines that did not stabilize Cu(I) may inhibit the disproportionation route to the formation of metallic copper in either a reducing atmosphere or at local electrical potentials. Cu^{2+} ions will then be retained in solution as a complex and will be removed by blow down from the SG, thus providing minimal chance for deposition on metallic heat-transfer surfaces. Hence identification of copper–amine complexes and a study of their electroreduction characteristics is important from the point of view of selecting a suitable amine as an AVT reagent. The purpose of this investigation is to identify those amines which can stabilize the Cu^{+} state of copper in solution. This will enable us to avoid the usage of such amines for SG water treatment. Metal ion concentration in SG waters is in the range of 10–100 $\mu g\ l^{-1}$. Pseudopolarography [6] in combination with differential pulse anodic stripping voltammetry (DPASV) was used for speciation studies.

2. Experimental

All polarographic measurements were carried out with 20 ml deoxygenated solution under inert atmosphere and potentiostatic control using an EG&G PARC Model 174 A polarographic analyser in a thermostated cell (25 ± 0.2°C). For all experimental purposes an ionic strength of 1 M using KNO_3 was maintained. For cyclic voltammetry (CV) experiments an EG&G 175 universal programmer was combined with the 174 A polarographic analyser. A dropping mercury electrode (DME) with a mercury flow-rate of 1.5 mg s^{-1} in 1 M KNO_3 in open circuit was used as a working electrode, a saturated calomel electrode (SCE) as a reference electrode and a platinum electrode as a counter electrode. For CV and DPASV experiments, a Metrohm E410 hanging mercury drop electrode (HMDE) with drop area of 0.0218 cm^2 was used as working electrode. Drop time: 1 s; scan rate: 5 mV s^{-1}; and DPP pulse amplitude: 50 mV were kept constant for all experimental purposes. At a constant copper concentration of 7.87×10^{-7} M, DPASV experiments were performed for various combinations of pH (8.5–12) and free amine concentrations (0.001–0.5 M). At the HMDE, copper was deposited from the solution having a certain amine concentration for a fixed cathodic deposition time of 3 min while the sample was stirred. Subsequently, a copper peak obtained by anodic stripping in the differential pulse mode with a scan rate of 5 mV s^{-1} was recorded. Repeating this measurement at a chosen amine concentration over a sufficient range of cathodic deposition potentials and using the dependence of anodic peak heights on cathodic deposition potential yielded the corresponding pseudopolarographic wave [7]. The half-wave potential ($^*E_{1/2}$) corresponding to each concentration of amine and pH were then computed. All polarographic and pseudopolarographic waves were processed using a three-parameter non-linear least square fit program [8] to get the electron transfer coefficient (α), $E_{1/2}$ and i_d values.

The pseudopolarographic half-wave potential $^*E_{1/2}$ is more cathodic than the d.c. polarographic half-wave potential [9]. For the computation of $^*\Delta E_{1/2} = [^*E_{1/2(\text{simple})} - ^*E_{1/2(\text{complexed})}]$, $^*E_{1/2}$ values for simple (uncomplexed) Cu^{+} and Cu^{2+} were obtained by addition of the experimentally observed cathodic shifts of 0.092 V for one-electron transfer and of 0.051 V for two-electron transfer vs. SCE to the respective DPP peak potential values E_p. Thus for Cu(I), the E_p value for uncomplexed Cu^{+} of +0.159 V [10] was com-

bined with a cathodic shift of 0.092 V for one-electron reduction resulting in a value of 0.067 V (+0.159–0.092). This value was taken as $^{*}E_{1/2}$ for simple Cu(I). For Cu(II) the observed E_p value for uncomplexed Cu(II) of +0.035 V was combined with a cathodic shift of 0.051 V for single-step two-electron reduction resulting in a value of −0.016 V. This value was taken as $^{*}E_{1/2}$ for simple Cu^{2+}.

The ligand mixtures (buffer) were prepared by mixing the theoretically computed quantities of amine and amine–nitrate required for the desired amine and pH combination using the respective K_b values of the amine. The pK_b values for 3MPA: 3.67; Pip: 2.88; DMPA: 4.50 and for DMAE: 4.52 were determined by pH metric titrations.

3. Results and discussions

In amine-treated SG water, amine and hydroxyl ions are the only competiting ligands for complexation of the metal ion. The possible copper complexation in this media is given by:

$$xL + yOH^- + M^{n+} \rightleftharpoons [ML_x(OH)_y]^{(n-y)} \quad (1)$$

where M is a metal ion, and L and OH^- are ligand and hydroxide forming the metal complex.

The relation between the shift of the pseudopolarographic half-wave potential ($^{*}E_{1/2}$) for reduction of the above complex, ligand (amine) concentration, hydroxyl ion concentration (pH), and stability constant of the complex is given by the following equation:

$$^{*}\Delta E_{1/2} = \frac{RT}{nF}\ln K + x\frac{RT}{nF}\ln L + 2.303\frac{RT}{nF}y(\mathrm{pH} - 14) \quad (2)$$

where x and y are the number of ligands and hydroxide ions, respectively, contributing to the complexation in Eq. 2. The above equation is similar to that derived by Brown and Kowalski [11] and is analogous to the Lingane equation and the equation used in classical polarography to determine stability constants and coordination numbers of metal complexes [12].

3.1. Copper–3MPA system

Fig. 1 shows the results of Cu–3MPA speciation studies. The distinctly well defined current plateau observed at higher deposition potentials in the pseudopolarographic wave (Fig. 1a) and "log plot" slope value of 65 mV for this wave show that the complex undergoes a reversible one-electron-transfer electrode reaction Cu(I) → Cu(0). The full width at half maximum (FWHM) value of 110 mV for the DPP anodic stripping peak is also in support of the one-electron-transfer reversible reaction. The linear nature of $^{*}\Delta E_{1/2}$ vs. log[3MPA] with a slope of 132 mV (Fig. 1b) shows the absence of higher order complexes and an association of two 3MPA molecules with each copper atom. At constant concentration $^{*}\Delta E_{1/2}$ did not show any dependence on pH, indicating the absence of the OH^- group in the complex.

The cyclic voltammogram of Cu–3MPA at 20 mV s^{-1} scan rate shows two well defined cathodic and anodic peaks (Fig. 1c), indicating that copper in a 3MPA medium stabilizes both Cu(I) and Cu(II) species and undergoes a stepwise one electron-transfer reaction. Since the pseudopolarographic wave corresponding to the reduction reaction Cu(II) → Cu(I) was merged with the mercury oxidation wave, Cu(II) complexation studies could not be performed. In the studied range (pH: 10–11 and amine concentration: 0.05–0.50 M), a Cu(I) complex $[Cu(3MPA)_2]^+$ with log stability constant (log K) value of 10.47 ± 0.16 was identified.

3.2. Copper–piperidine system

Fig. 2 shows the results of copper–piperidine speciation studies. The pseudopolarographic wave shows a shift with increasing current to more negative peak potentials (Fig. 2a) and the "log plot" slope of ca. 60 mV shows that the Cu–Pip complex undergoes a one-electron-transfer electrode reaction with decrease in reversibility. The observed electron-transfer coefficient of 0.763 and DPP anodic stripping peak FWHM value of 110 mV are also in support of this. In piperidine media, depending on piperidine concentration

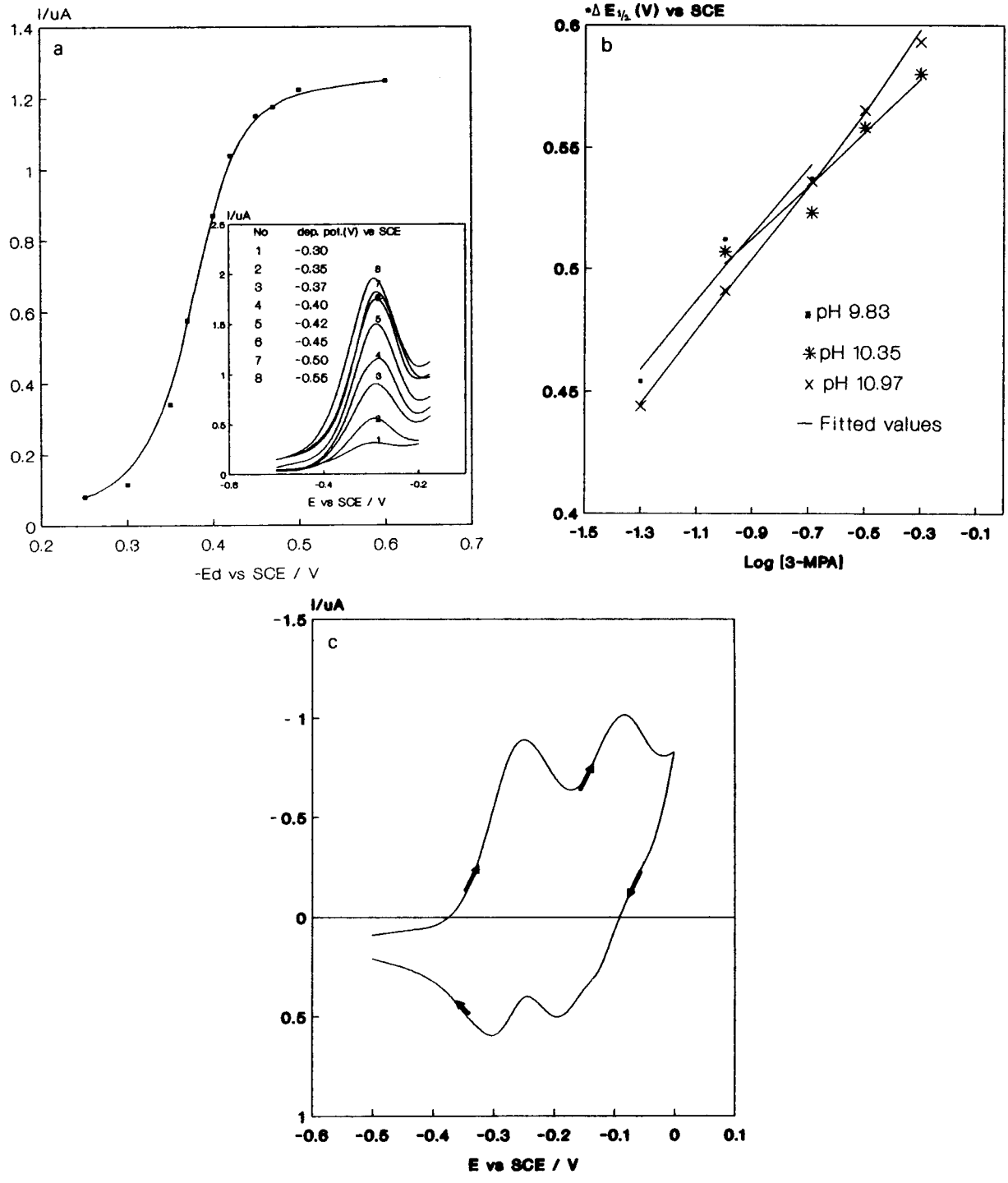

Fig. 1. Cu–3MPA speciation results. (a) Pseudopolarographic wave with (inset) stripping current profile for various deposition potentials; 3MPA = 0.05 M, pH = 10.92, scan rate = 5 mV s^{-1}. (b) Variation of $^{*}\Delta E_{1/2}$ as a function of 3MPA concentration. (c) Cyclic voltammogram of Cu–3MPA system; 3MPA = 0.05 M, pH = 10.87, scan rate = 20 mV s^{-1}.

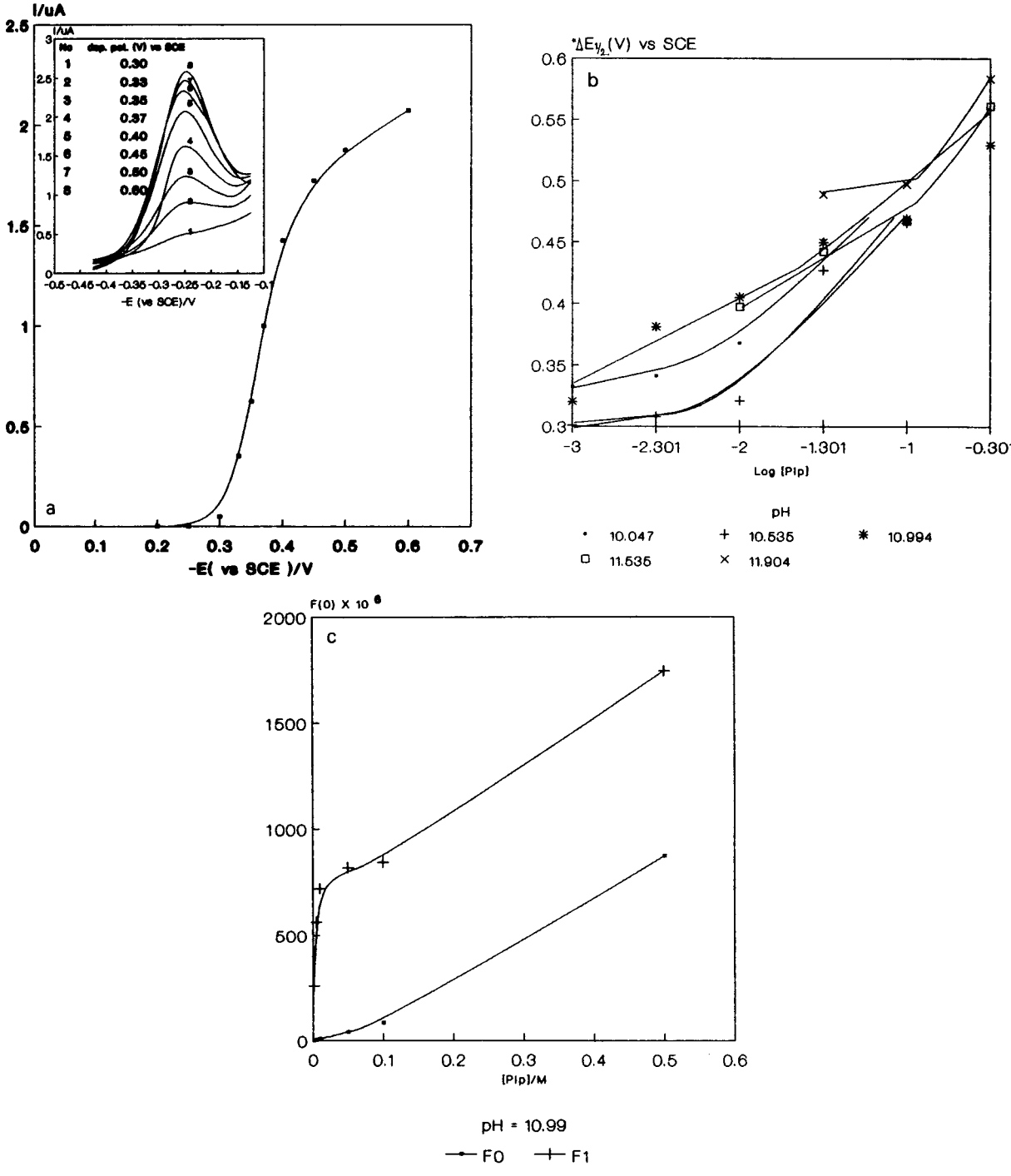

Fig. 2. Cu–piperidine speciation results. (a) Pseudopolarographic wave with (inset) stripping current profile for various deposition potentials; Pip = 0.05 M, pH = 11.02, scan rate = 5 mV s^{-1} (b) Variation of $^{*}\Delta E_{1/2}$ as a function of piperidine concentration. (c) Plot of $F(0)$ and $F(1)$ fuction vs. piperidine concentration at pH 10.994.

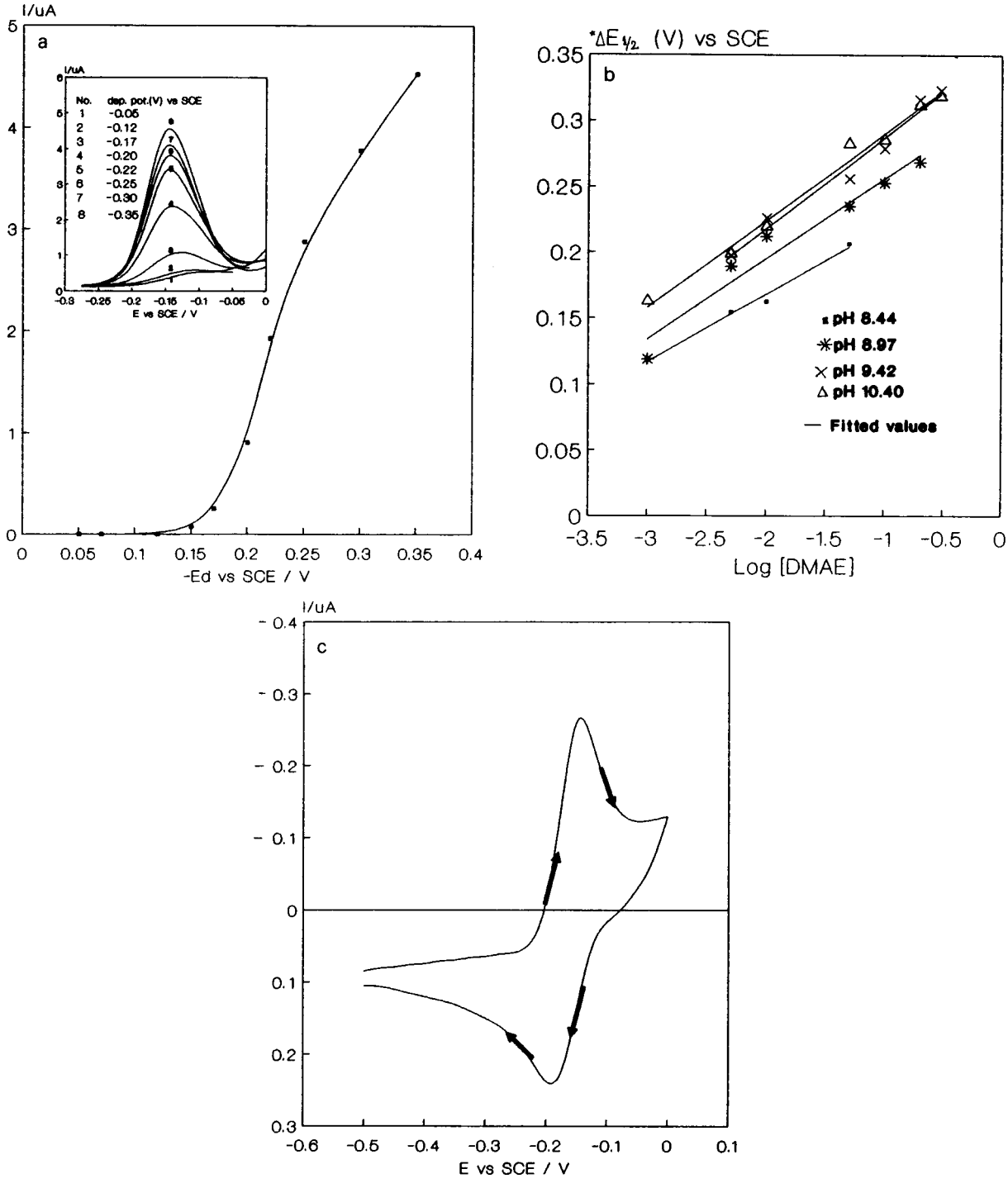

Fig. 3. Cu–DMAE speciation results. (a) Pseudopolarographic wave with (inset) stripping current profile for various deposition potentials; DMAE = 0.005 M, pH = 9.8, scan rate = 5 mV s^{-1}. (b) Variation of $^{*}\Delta E_{1/2}$ as a function of DMAE concentration. (c) Cyclic voltammogram of Cu–DMAE system; DMAE = 0.005 M, pH = 9.89, scan rate = 20 mV s^{-1}.

and pH, both Cu(I) and Cu(II) are stabilized. Due to insufficient shift of Cu(I) and Cu(II) reduction waves, d.c. polarography cannot be used for speciation studies. With the DPP polarographic technique, however, it was possible to study both Cu(II) and Cu(I) complexes. In DPASV, due to the cathodic shift of $E_{1/2}$ values, the Cu(O) → Cu(I) oxidation peak is being separated from the Cu(I) → Cu(II) oxidation peak. However, the latter gets merged with the high-current mercury oxidation peak and hence only Cu(I) species could be used for interpretation. The non-linear nature of the plot of $^{*}\Delta E_{1/2}$ vs. log[Pip] indicates a stepwise complex formation (Fig. 2b). $^{*}\Delta E_{1/2}$ did not show any dependence on pH at constant piperidine concentrations indicating the absence of the OH^- contribution towards the complexation. $F(0)$ analysis of the data (Fig. 2c) using the DeFord Hume method [12] shows that a [Cu(I)(Pip)] complex with a log K value of 8.29 ± 0.47 and a [Cu(I)(pip)$_2$] complex with a log K value of 9.89 ± 0.24 are formed.

3.3. Copper–DMAE and DMPA system

Fig. 3 shows the results of copper speciation study with DMAE. Absence of the typical sigmoidal shape and absence of a well defined current plateau even at high applied potentials in peudopolarographic waves (Fig. 3a) indicate an irreversible oxidation process and complexation. The processings of these waves were carried out using a three-parameter non-linear least square fit programme [8]. Under the same experimental conditions and taking into account all possible errors, a standard deviation of 10 mV was observed in the estimation of $^{*}E_{1/2}$ values. Electron-transfer coefficients in the range of 0.3–0.6 support the irreversibility. The presence of single anodic and cathodic peaks in higher scan rate (20 mV s^{-1}) cyclic voltammogramms confirms a single-step two-electron reduction (Fig. 3c). The linear nature with a ca. 60 mV slope of the plot of $^{*}\Delta E_{1/2}$ vs. log[DMAE] (Fig. 3b) indicates association of two DMAE molecules and absence of

Table 1
Electrochemical speciation studies of copper–amine complexes

Amine	Conc. range (M)	pH range	Complex type	Reduction mode	Electron transfer coefficient (α)		log K [a]
					d.c.	DPASV	
3MPA	0.01–0.5	10.0–11.0	$[Cu(I)L_2]$	One electron	0.5–0.7	0.8–1.0	d.c.: 9.49 d.p.: 9.71 d.p.a.: 10.47
DMPA	0.001–0.30	8.5–10.5	$[Cu(II)(OH)_2L_2]$	Direct; two electron	0.8–1.0	0.4–0.7	d.c.: 17.89 d.p.: 18.24 d.p.a.: 20.33
DMAE	0.001–0.30	8.5–10.5	$[Cu(II)(OH)_2L_2]$	Direct; two electron	0.7–1.0	0.5–0.7	d.c.: 19.86 d.p.: 20.39 d.p.a.: 20.51
PIP	0.001–0.50	10.0–12.0	[Cu(I)L]	One electron	–	0.4–1.0	d.p.: 7.66 d.p.a.: 8.29
			$[Cu(I)L_2]$		–		d.p.: 9.24 d.p.a.: 9.89
			$[Cu(II)(OH)_2L_2]$	Direct; two electron	–	–	d.p.: 16.67

d.c.: log K values from d.c. polarography; d.p.: log K values from d.p. polarography; d.p.a.: log K values from DPASV pseudopolarography.
[a] Ref. 4.

higher order complexes. Similarly, a plot of $^{*}\Delta E_{1/2}$ vs. pH at constant ligand concentration shows association of two hydroxyl ions in the complex. In the range of study (pH 8.5–10.5 and DMAE concentration 0.001–0.5 M) a copper complex species $[Cu(DMAE)_2(OH)_2]$ with log $K = 20.51 \pm 0.49$ was identified.

Copper speciation studies with DMPA showed a pseudopolarographic wave corresponding to a single-step two-electron reduction process and which was similar to that observed for DMAE copper speciation studies. In the range of study (pH 8.5–10.5 and DMPA concentration 0.001–0.5 M), on the basis of the $^{*}E_{1/2}$ dependence analysis on log[DMPA] and pH, a $[Cu(DMPA)_2(OH)_2]$ species with a log K value of 20.33 ± 0.49 was identified.

Table 1 shows stability constants obtained by various techniques and electron-transfer coefficients. The essential difference between direct current polarographic (DCP) techniques and pseudopolarography is that the species undergoing reduction at the electrode surface need different times in crossing the diffusion layer to reach the electrode surface. In a stirred solution, the diffusion layer thickness is different from that of an unstirred solution. While making a study of the reduction behaviour of labile complexes, variation in diffusion layer thickness may contribute to changes in electron transfer coefficients.

The variation observed in the electron-transfer coefficients is expected due to the following reasons:

Since each current measurement in pseudopolarography arises from deposition followed by stripping, the uncertainty in the current measured is larger than that present in DCP. Hence pseudopolarography is considered less accurate than classical DCP. While processing a pseudopolarogram this effect has to be included. The d.c. polarographic data was processed using a non-linear least square fit programme with fixed errors in potential and current data. Similar processing was also done for pseudopolarographic data. However, better fitting could have been obtained if the uncertainty in each of the current measurements was also used for curve fitting. Since this information was not available the forced fit of the programme resulted in lower α values in case of pseudopolarograms. This explanation could account for a larger error in α values rather than a decrease in α values.

The variations in electron-transfer coefficients given in this paper can be explained as follows:

(i) In case of DCP for the Cu(I)–3MPA complex, the α value is lower in comparison with DPASV because the uncertainty in the current computation is more due to interference of the Hg oxidation wave. With DPASV this interference is removed due to the log linear deposition time dependent cathodic shift of $E_{1/2}$ of the pseudopolarographic wave.

(ii) In the case of DMPA, DMAE and Pip, lower α values in DPASV in comparison with DCP can be partly attributed to kinetic effects of the electrode reaction due to the steric hindrance of the bulkier ligands, if one considers contribution of metal (due to the metal complex dissociation) to the electrode during the deposition in addition to the back diffusion of ligands and the static nature of the diffusion layer in DPASV. Shuman and Woodword [13] have reported a decrease in the stripping current of Cd at higher concentrations of EDTA. Reduction of reversibility by addition of ethylenediamine during Cu(II) analysis is also reported by Zirino and Kounaves [14]. In view of the fact that DCP waves have shown α values close to 1.0 and the deviation in the 3MPA case being due to overlapping with the Hg wave, the computations with pseudopolarographic waves were done without giving special weight to α. It is considered only as an apparent change. These two articles cited above are in support of the observations given in this paper. It is tacitly assumed that the reversibility of the electrode reaction is not compromised except for the apparent behaviour either due to the overlapping wave/peak in DCP/DPP and/or due to the inherent uncertainty in current measurements in DPASV.

4. Conclusions

Copper speciation studies with 3MPA, Piperidine, DMAE and DMPA using DCP and DPP techniques were performed by us earlier at 0.047

mM copper concentration [4]. The necessary conditions for complexation study, namely ligand concentration ≫ metal concentration, could not be met for the OH^- concentration in these studies. However, in the present study the metal concentration at the time of deposition was 0.8×10^{-3} mM, well below the OH^- concentration. The present study proved conclusively that speciation has not changed due to this variation. The good agreement between log K values obtained from three different techniques (Table 1) reconfirms the earlier work at higher copper concentration. Speciation studies at copper concentration of 10^{-7} M are of direct practical relevance to the investigations pertaining to reactor water and steam generator water samples. Higher stability of Cu–DMAE and Cu–DMPA complexes shows their much better ability to keep the corroded metal ion in solution over that of the Cu–3MPA and Cu–Pip complexes. Moreover, 3MPA and piperidine stabilize Cu(I) complexes, further providing an easier path for reduction of copper and its deposition on SG surfaces. Hence from the point of view of electroreduction and deposition, DMAE and DMPA can be preferred over 3MPA and piperidine as AVT reagents for SG water treatment.

Acknowledgements

The authors are thankful to Dr P.N. Moorthy, Head of Applied Chemistry Division, BARC, Bombay, for his continued support and encouragement during this work. This work is a part of the fulfillment of the Ph.D. thesis of A.G.K., submitted to the University of Madras.

References

[1] J.W. Cobble and P.J. Turner, EPRI project 1571-3, Report NP-4209, Interim Report, August 1985.
[2] J.W. Cobble and P.J. Turner, in Proceedings of JAIF International Conference on Water Chemistry in Nuclear Power Plants, JAIF, Tokyo, Vol. 1, 1988 p. 485.
[3] C.M. Loucks, in J.A. Ayres (Ed.), Decontamination of Nuclear Reactors and Equipments, Ronald Press, New York, 1970, pp. 17–18.
[4] S.V. Narasimhan, A.G. Kumbhar and S. Rangarajan, in Proceedings of JAIF International Conference on Water Chemistry in Nuclear Power Plants, JAIF, Fukui City, Japan, April 1991, pp. 492–496.
[5] V.P. Persiantseva, Sov. Sci. Rev. B. Chem., (1987) 1.
[6] S. Bubic and M. Branica, Thalassia Jugosl., 9 (1973) 47.
[7] M. Branica, D.M. Novak and S. Bubic, Croat. Chem. Acta, 49 (1977) 539.
[8] S.V. Narasimhan, G. Visalakshi and K.S. Venkateswarlu, Report BARC-1236, BARC, Bombay, 1984.
[9] (a) A. Zirino and S.P. Kounaves, Anal. Chem., 49 (1977) 56; (b) A. Zirino and S.P. Kounaves, Anal. Chem., 51 (1979) 592.(correction).
[10] J.F. Fisher and J.L. Hall, Anal. Chem., 39 (1967) 1550.
[11] S.D. Brown and B.R. Kowalski, Anal. Chem., 51 (1979) 2133.
[12] D.R. Crow, Polarography of Metal Complexes, Academic Press, London, 1969.
[13] S. Shuman and G.P. Woodward, Anal. Chem., 45 (1973) 2032.
[14] A. Zirino and S.P. Kounaves, Anal. Chim. Acta, 113 (1980) 79.

Time-of-Flight Mass Spectrometry and its Applications

Edited by **E.W. Schlag**, Institut für Physicalische und Theoretische Chemie, Universität München, Germany

Previously published as a special issue of the journal
International Journal of Mass Spectrometry and Ion Processes, Volume 131 (1994)

The present set of contributions attempts to give a survey of current applications from many of the active groups in the field. A variety of new applications are considered which are no doubt just the beginning of large new areas of application.

Contents: Laser assisted reflectron time-of-flight mass spectrometry (B.A. Mamyrin). How to specify the ion optical system of a time-of-flight mass spectrometer (T. Bergmann, T.P. Martin). The application of ion optics in time-of-flight mass spectrometry (D. Ioanoviciu). Design considerations in energy resolved time-of-flight mass spectrometry (A.E. Giannakopulos *et al.*). Laser ion sources for time-of-flight mass spectrometry (U. Boesl *et al.*). Photoemission electron impact ionization in time-of-flight mass spectrometry: an examination of experimental consequences (S.M. Colby, J.P. Reilly). High-resolution mass spectrometry in a linear time-of-flight mass spectrometer (J.M. Grundwürmer *et al.*). The design and performance of an ion trap storage-reflectron time-of-flight mass spectrometer (B.M. Chien *et al.*). Pulse amplitude analysis: a new dimension in single ion time-of-flight mass spectrometry (P.V. Bondarenko *et al.*). Mass analyzed threshold ionization: structural information for a mass spectrum and mass information for ionic spectroscopy (P.M. Johnson, L. Zhu). Decay energetics of molecular clusters studied by multiphoton mass spectrometry and pulsed field threshold ionization (H.J. Neusser, H. Krause). Using reflectron time-of-flight mass spectrometer techniques to investigate cluster dynamics and bonding (S. Wei, A.W. Castleman, Jr.). The one dimensional photofragment translational spectroscopic technique: intramolecular clocking of energy redistribution for molecules falling apart (H.J. Hwang *et al.*). Quantitative determination of kinetic energy releases from metastable decomposition of sputtered organic ions using a time-of-flight mass spectrometer with a single-stage ion mirror (D.F. Barofsky *et al.*). Kinetic energy analysis in time-of-flight mass spectrometry: application of time of flight methods to clusters and pyrolysis studies in supersonic expansions (J.S. Riley, T. Baer). Photodissociation of magnesium ion-molecule complexes in a refectron time-of-flight mass spectrometer (C.S. Yeh *et al.*. Resonance-enhanced two-photon ionization time-of-flight spectroscopy of cold perfluorinated polyethers and their external and internal van der Waals dimers (D.S. Anex *et al.*). Time-of-flight mass spectrometry of DNA laser-ablated from frozen aqueous solutions: applications to the Human Genome Project (P. Williams). Factors affecting the resolution in matrix-assisted laser desorption-ionization mass spectrometry (A. Ingendoh *et al.*). Sequencing of peptides in time-of-flight spectrometer: evaluation of post-source decay following matrix-assisted laser desorption-ionization (MALDI) (P. Kaufmann *et al.*). Energy-isochronous time-of-flight analyzers (H. Wollnik). Author index. Subject index.

©1994 422 pages Paperback
Price: Dfl. 215.00 (US$122.75)
ISBN 0-444-81875-8

ELSEVIER
An imprint of Elsevier Science

ORDER INFORMATION
ELSEVIER SCIENCE B.V.
P.O. Box 330
1000 AH Amsterdam
The Netherlands
Fax: +31 (20) 5862 845
For USA and Canada
P.O. Box 945
Madison Square Station
New York, NY 10159-0945
Fax: +1 (212) 633 3680

PUBLICATION SCHEDULE FOR 1994

	J	F	M	A	M	J	J	A	S	O	N	D
Anal. Chim. Acta	284/3 285/1–2 285/3	286/1 286/2 286/3	287/1–2 287/3 288/1–2	288/3 289/1 289/2	289/3 290/1–2 290/3	291/1–2 291/3 292/1–2	292/3 293/1–2 293/3	294/1 294/2 294/3	295/1 295/2 295/3	296/1–2 296/3 297/1–2	297/3 298/1 298/2–3	299/1 299/2–3 300/1
Vib. Spec.	6/2		6/3		7/1		7/2		7/3		8/1	

INFORMATION FOR AUTHORS

Detailed "Instructions to Authors" for *Analytica Chimica Acta* was published in Volume 289, No. 3, pp. 381–384. Free reprints of the "Instructions to Authors" of *Analytica Chimica Acta* and *Vibrational Spectroscopy* are available from the Editors or from: Elsevier Science B.V., P.O. Box 330, 1000 AH Amsterdam, The Netherlands. Telefax: (+31-20) 5862459.

Manuscripts. The language of the journal is English. English linguistic improvement is provided as part of the normal editorial processing. Authors should submit three copies of the manuscript in clear double-spaced typing on one side of the paper only. *Vibrational Spectroscopy* also accepts papers in English only.

Rapid publication letters. *Letters* are short papers that describe innovative research. Criteria for letters are novelty, quality, significance, urgency and brevity. Submission data: max. of 2 printed pages (incl. Figs., Tables, Abstr., Refs.); short abstract (e.g., 3 lines); *no* proofs will be sent to the authors; submission on floppy disc; *no* revision will be possible.

Abstract. All papers and reviews begin with an Abstract (50–250 words) which should comprise a factual account of the contents of the paper, with emphasis on new information.

Figures. Figures should be prepared in black waterproof drawing ink on drawing or tracing paper of the same size as that on which the manuscript is typed. One original (or sharp glossy print) and two photostat (or other) copies are required. Attention should be given to line thickness, lettering (which should be kept to a minimum) and spacing on axes of graphs, to ensure suitability for reduction in size on printing. Axes of a graph should be clearly labelled, along the axes, outside the graph itself. All figures should be numbered with Arabic numerals, and require descriptive legends which should be typed on a separate sheet of paper. Simple straight-line graphs are not acceptable, because they can readily be described in the text by means of an equation or a sentence. Claims of linearity should be supported by regression data that include slope, intercept, standard deviations of the slope and intercept, standard error and the number of data points; correlation coefficients are optional.

Photographs should be glossy prints and be as rich in contrast as possible; colour photographs cannot be accepted. Line diagrams are generally preferred to photographs of equipment. Computer outputs for reproduction as figures must be good quality on blank paper, and should preferably be submitted as glossy prints.

Nomenclature, abbreviations and symbols. In general, the recommendations of IUPAC should be followed, and attention should be given to the recommendations of the Analytical Chemistry Division in the journal *Pure and Applied Chemistry* (see also *IUPAC Compendium of Analytical Nomenclature, Definitive Rules*, 1987).

References. The references should be collected at the end of the paper, numbered in the order of their appearance in the text (*not* alphabetically) and typed on a separate sheet.

Reprints. Fifty reprints will be supplied free of charge. Additional reprints (minimum 100) can be ordered. An order form containing price quotations will be sent to the authors together with the proofs of their article.

Papers dealing with vibrational spectroscopy should be sent to: Dr J.G. Grasselli, 150 Greentree Road, Chagrin Falls, OH 44022, U.S.A. Telefax: (+1-216) 2473360 (Americas, Canada, Australia and New Zealand) or Dr J.H. van der Maas, Department of Analytical Molecular Spectrometry, Faculty of Chemistry, University of Utrecht, P.O. Box 80083, 3508 TB Utrecht, The Netherlands. Telefax: (+31-30) 518219 (all other countries).

0003-2670/94/$07.00